

THESIS

EVALUATION OF PARATHYROID HORMONE AND ZOLEDRONIC ACID IN PROMOTING BONE
HEALING AFTER STEREOTACTIC RADIATION THERAPY FOR LOCAL CONTROL OF OSTEOSARCOMA
IN AN ORTHOTOPIC RAT MODEL

Submitted by

Ryan C. Curtis

Department of Microbiology, Immunology & Pathology

In partial fulfillment of the requirements

For the Degree of Master of Science

Colorado State University

Fort Collins, Colorado

Fall 2014

Master's Committee:

Advisor: Sue VandeWoude

Co-Advisor: Seth Donahue

Jamie Custis

Nicole Ehrhart

EJ Ehrhart

Copyright by Ryan Christopher Curtis 2014

All Rights Reserved

ABSTRACT

EVALUATION OF PARATHYROID HORMONE AND ZOLEDRONIC ACID IN PROMOTING BONE HEALING AFTER STEREOTACTIC RADIATION THERAPY FOR LOCAL CONTROL OF OSTEOSARCOMA IN AN ORTHOTOPIC RAT MODEL

Clinical studies using definitive-intent stereotactic radiation therapy (SRT) for the local treatment of canine osteosarcoma (OSA) have achieved similar median survival times in patients as the current standard of care (amputation and adjuvant chemotherapy). Despite this, there remains an unacceptably high risk of pathologic fracture following radiation treatment. Zoledronic acid (ZA) and parathyroid hormone (PTH) are therapeutic candidates for decreasing this fracture risk post-irradiation. Due to differing mechanisms, we hypothesized that the combined treatment with ZA and PTH would significantly improve bone healing more than ZA or PTH treatment alone. Using an orthotopic model of canine osteosarcoma in athymic rats, we evaluated bone healing following clinically-relevant doses of radiation therapy (12Gy x 3 fractions, 36 Gy total). Groups included 36 Gy SRT only, 36 Gy SRT plus ZA, 36 Gy SRT plus ZA and PTH, 36 Gy SRT plus PTH, and 36 Gy SRT plus localized PTH treatment. Our study showed significant increases in bone volume and polar moments of inertia within the region of interest (distal femoral metaphysis) 8 weeks after radiation in the combined (ZA/PTH) treatment group as compared to radiation treatment alone. Histomorphometric analysis revealed evidence of active mineralization at study endpoint as well as successful tumor-cell kill across all treatment groups. This work provides further evidence for the expanding potential indications for ZA and PTH therapy, including post-irradiated bone disease due to canine osteosarcoma.

TABLE OF CONTENTS

Chapter 1 Introduction

1.1 Osteosarcoma	1
<i>Canine Osteosarcoma – overview, current treatment methodology</i>	
<i>Human Osteosarcoma – overview, current treatment methodology</i>	
<i>Research Models</i>	
<i>Biological Mechanisms of Disease</i>	
1.2 Stereotactic Radiation Therapy.....	9
<i>Radiation Biology</i>	
<i>Evolution/Applications</i>	
<i>Radiation Effect on Bone</i>	
<i>SRT for Primary Bone Tumors/Osteosarcoma</i>	
1.3 Parathyroid Hormone	19
<i>Endocrinology/Physiologic effects of PTH</i>	
<i>Clinical applications of PTH administration</i>	
<i>Safety Concerns/Side Effects</i>	
<i>PTH and Radiation</i>	
<i>bbPTH</i>	
<i>Local Delivery</i>	
1.4 Bisphosphonates	27
<i>Mechanism of Action/Physiologic effects of bisphosphonates</i>	
<i>Clinical Applications of Bisphosphonate administration</i>	
<i>Zoledronic Acid</i>	
1.5 Hypothesis and Specific Aims.....	31

Chapter 2 Methods

2.1 Animals	34
2.2 Osteosarcoma Cells	34
2.3 Drug Therapies.....	35
2.4 Osteosarcoma Cell Inoculation.....	35
2.5 Experimental Design.....	36
2.6 Bioluminescence Imaging.....	37

2.7 Radiography	38
2.8 Stereotactic Radiation Therapy	40
2.9 Micro-CT	42
2.10 Histology	43
2.11 Statistical Analysis	44
Chapter 3 Results	
3.1 Tumor Development.....	45
3.2 Response to Stereotactic Radiation Therapy	45
<i>Bioluminescence</i>	
<i>Radiography</i>	
3.3 Micro-CT.....	49
<i>Whole Bone Analysis - BMD, BV and pMOI</i>	
<i>Trabecular and Cortical Analysis</i>	
<i>Control Analysis</i>	
3.4 Histology	56
<i>Dynamic Histomorphometry</i>	
<i>Static Histomorphometry</i>	
Chapter 4 Discussion.....	68
References	76
Appendix I – SOPs	82
Appendix II - bbPTH release profile in Vetrigel.....	108

Chapter 1

Introduction

1.1 Osteosarcoma

Canine Osteosarcoma

Canine osteosarcoma is the most prevalent primary bone tumor of dogs accounting for over 90% of malignancies of bone origin (Withrow and Khanna 2009). It primarily affects the appendicular skeleton, with the axial skeleton and even soft tissues being implicated much less frequently as sites of primary tumor growth. The metaphyseal regions of long bones at the proximal humerus, distal radius, and distal femur are most commonly affected (Gorman, Barger et al. 2006). The tumor itself is locally aggressive, with a high rate of metastasis. Metastasis occurs mainly to the lungs via hematogenous spread, but also to other bones, the brain, subcutaneous tissues, liver, spleen, and the skin (Lane, Black et al. 2012). It is well established that osteosarcoma shows an increased prevalence among middle-aged to older, large or giant breed dogs. Only 5% of osteosarcomas occur in dogs weighing less than fifteen kilograms (Gorman, Barger et al. 2006).

Clinical cases of osteosarcoma present with a varied degree of lameness and swelling at the primary site of the tumor (Morello, Martano et al. 2011). The lameness may be mild at first but typically progresses over time. The mass may also be palpably painful on manipulation. In severe cases, a presentation of an acute, non-weight bearing lameness may be the result of a pathologic fracture due to the tumor. Pathologic fractures account for less than 3% of all fractures (Gorman, Barger et al. 2006).

A diagnosis of a primary bone tumor is often presumed from the collection of information gained from a complete history, clinical examination and radiographic findings. Many other diagnostic tools are available to confirm the diagnosis including fine needle aspiration and cytology as well as multiple bone biopsy techniques (Morello, Martano et al. 2011). Diagnostic imaging is used for complete staging and may include radiography, nuclear scintigraphy, computed tomography (CT), positron emission tomography (PET/CT), and magnetic resonance imaging (MRI). At the time of presentation, less than 5% of patients show radiographic evidence of lung metastasis (Morello, Martano et al. 2011). Despite this low number, approximately 90% of dogs with osteosarcoma are expected to have microscopic metastasis at the time of initial presentation (Withrow and Khanna 2009).

Treatment is dependent upon whether palliative or curative-intent therapy is initiated. Palliative-intent therapy aims solely at controlling pain. Methods utilized include radiation, anti-inflammatory, and bisphosphonate medical therapy (Morello, Martano et al. 2011). Curative-intent therapy aims to control the local tumor through either amputation or limb-sparing procedures, and metastasis is delayed through adjuvant chemotherapy. Following this standard of care various protocols have produced median survival times between 235 and 413 days. Ongoing research aims to improve the outcome of current therapies as well as providing new treatment approaches. Included in these approaches are stereotactic radiation therapy for local control, molecular targeting of metastasis, and immunostimulatory agents (Mueller, Fuchs et al. 2007; Withrow and Wilkins 2010).

Human Osteosarcoma

Human osteosarcoma is the most frequently diagnosed primary cancer of bone (Bielack, Carrle et al. 2008). Its incidence is most prevalent in the adolescent age group (15-19 yrs.) with 8–11/1000 000/year (Bielack, Carrle et al. 2008). This time period coincides with a period of rapid bone turnover suggesting a correlation with rapid bone proliferation. Osteosarcoma is generally fatal, due to its ability to consistently metastasize to the lungs. These traits, as well as many others, make it very similar to osteosarcoma in canine patients. It is also similar in its presentation. Human patients typically present with localized bone pain, swelling, and limited movement around the affected joint area. The most common areas affected include the metaphyses of long bones with the most common sites being the distal femur, proximal tibia, and proximal humerus (Ritter and Bielack 2010).

A diagnostic work up for suspected cases of osteosarcoma begins with a full history, physical examination, and radiographs. Advanced imaging techniques are also utilized to assess local tissue involvement and metastatic disease. This would include magnetic resonance imaging for local tissue involvement and a CT scan of the thorax for lung metastasis. Baseline assessments of heart, liver and kidney function are usually carried out as well due to the likely chemotherapeutic treatment plan. These therapies can have a significant effect on other organs and it is important to assess these systems prior to initiation of any therapy. Due to the broad spectrum of appearances histologically it is strongly recommended for biopsies to be collected and evaluated by an experienced pathologist. The various tumor grades have shown some correlation to metastatic potential however the full prognostic significance has yet to be established.

A multidisciplinary treatment approach is essential as 80-90% of all patients with seemingly localized disease will eventually develop metastasis (Ritter and Bielack 2010). Current standard of care treatment includes preoperative chemotherapy (neoadjuvant), limb salvage surgery and/or amputation, and post-operative (adjuvant) chemotherapy. Doxorubicin, cisplatin, methotrexate and ifosfamide are the most active agents against osteosarcoma however ideal combinations utilized for treatment are yet to be defined (Ritter and Bielack 2010). Standard of care treatment strategy results in a 60% overall survival at 5 years (Mueller, Fuchs et al. 2007)

Despite improvements in surgical techniques, overall survival rates for osteosarcoma patients have largely unchanged in the last thirty years. Due to this, a number of novel treatment modalities are being studied. These aim to identify various molecular pathways which could help us find new targets for therapy. Many of these are molecular targets for metastasis or chemoresistance markers and also immunomodulatory agents (Mueller, Fuchs et al. 2007).

Research Models

The complete pathogenesis of osteosarcoma remains to be discovered, however it is clear that a combination of genetic, environmental and other predisposing factors play a role. Due to this complexity, a priority has been to create reliable animal models to study various aspects of the disease. Although a single model has not been recognized as the gold standard, the most revealing model would include a spontaneous primary bone tumor and pulmonary metastases in an immunocompetent host. Current models include the use of mice, rats and dogs and each model has its own unique strengths depending on the aims of the study at hand.

Osteosarcoma models are either syngeneic or xenogeneic. Syngeneic means genetically identical or immunologically compatible allowing for successful transplantation whereas xenogeneic allows for immunologically non-compatible but accepted transplantation. An example of a xenogeneic model would involve the inoculation of human or canine osteosarcoma cells into immunodeficient murine models. Xenogeneic models allow for the study of human or canine osteosarcoma biology but they fail to model important host cell interactions. Many models of osteosarcoma rely on inoculation or transplantation of tumor cells or tissues directly into bone sites. Although controlled as far as tumor burden and site location these models do not accurately simulate the true process of primary tumorigenesis. An alternative to this would be endogenous models whereby osteosarcoma originates from resident mesenchymal cells. Several murine knockout models have been established that generate spontaneous development of osteosarcoma with as high as 100% penetrance; however, anatomic location of tumor cannot be predicted. This introduces the concept of orthotopic versus heterotopic animal models of osteosarcoma. Orthotopic models study the growth and development of tumors within the bone environment whereas heterotopic models develop tumors at non-osseous sites. Although convenient, heterotopic models fail to illustrate true phenotype outside of the normal bone matrix.

A number of human, canine and rat xenogeneic models have been described. The KRIB and 143B models are transformed human osteosarcoma cell lines that show great capacity for primary tumor formation and pulmonary metastases (Fan 2010). The SaOS-2 model originated from an 11-year-old Caucasian girl with primary osteosarcoma and has been used to study many chemotherapeutic agents (Fan 2010). A canine xenogeneic model was recently described

in athymic rats using the Abrams osteosarcoma line to study the effects of stereotactic radiation therapy (SRT) on appendicular osteosarcoma (Schwartz, Custis et al. 2012). The K7M2 model is a mouse syngeneic model that has been thoroughly characterized to mimic a natural disease course in humans (Fan 2010). The DLM8 luciferase transfected mouse syngeneic model was developed to study various treatment effects on metastasis in immunocompetent mice (Sottnik, Duval et al. 2010).

Besides orthotopic osteosarcoma models, there are a number of genetically engineered mouse models that manipulate specific genes known to spontaneously generate osteosarcoma. Knowledge of these genetically associated cancers comes from a few rare hereditary human disorders including Li-Fraumeni syndrome, familial retinoblastoma and RecQ helicase disorders. These disorders involve germ-line mutations of P53, RB, and RECQL4 respectively (Ng, Mutsaers et al. 2012). A number of mouse models with genetically modified P53 and Rb have increased incidence of osteosarcoma. One report described a 92% incidence of osteosarcoma in mice with a compound deletion of one Rb allele with homozygous p53 deletion (Ng, Mutsaers et al. 2012). There has been a number of other genes implicated in osteosarcoma pathogenesis. Examples of these include c-fos, p16INK4a, and WWOX (Ng, Mutsaers et al. 2012).

Mice and rats provide substantial knowledge in understanding the pathogenesis, biology, and therapeutic potential against osteosarcoma, but the companion canine population provides another unique model for many reasons. Both human and canine osteosarcoma share a number of similarities including clinical presentation, biology, treatment, complications and outcomes (Withrow and Wilkins 2010). There is a tenfold increase in prevalence for canine osteosarcoma providing a large population of patients seeking treatment. Other advantages of

studying osteosarcoma in the dog include the spontaneous nature of disease, larger animal size and concomitant weight bearing load, immunocompetency of the host, and similar genetic aberrations found in both dogs and humans (Withrow and Wilkins 2010). The canine model will thus be crucial not only for translational research, but investigation of this system will result in the improved care of our canine patients as well.

Biological Mechanisms of Disease

The cell of origin for osteosarcoma has been widely researched. At this time, there is evidence that the cell of origin is either a mesenchymal stem cell or an osteoprogenitor cell (Siclari and Qin 2010). Data from a number of sources strongly suggests that the cell of origin is derived from a committed osteoblast lineage. Osteosarcoma seems to be “differentiation defective” in that no terminally differentiated osteoblastic cells are found (Ng, Mutsaers et al. 2012). There are also biological similarities between osteosarcoma cells and osteoblasts in their ability to produce osteoid. Deletion of p53 in pre-osteoblasts and osteoblasts progenitors resulted in a significantly higher incidence of osteosarcoma than cells with multi-lineage potential (Ng, Mutsaers et al. 2012). There is also evidence that osteosarcomas, at least in part, are composed of more primitive cells capable of differentiating into all three dermal layers. One study showed that both a rat and human osteosarcoma cell line, cultured in conditions specific for multipotent stem cells, displayed markers indicative of mesodermal, endodermal, and ectodermal phenotypes (Russinoff, Miran et al. 2011).

Despite an incomplete understanding of the molecular pathogenesis of osteosarcoma there are a number of risk factors that have been identified. Human osteosarcoma has an increased incidence of development during the rapid bone growth experienced during puberty

(Broadhead, Clark et al. 2011). The male:female ratio of disease is 1.5 :1 for osteosarcoma and patients with the disease are taller compared to the age-matched normal population (Longhi, Pasini et al. 2005). Fifty-six percent of all cases are located around the knee, in the region of the metaphysis of the femur or tibia (Vigorita 2008). Human patients with Paget's disease also have an increased predilection for osteosarcoma (Broadhead, Clark et al. 2011). Canine osteosarcoma patients have similar predisposing features, however the canine disease tends to occur in middle-aged or older dogs (Mueller, Fuchs et al. 2007). A number of environmental factors have been suggested as risk factors for osteosarcoma including physical trauma, chemical, and biological agents. The most readily accepted of these is ionizing radiation, although this does not play a major role in pediatric disease, as it would take 10-20 years between exposures for observation of tumor (Broadhead, Clark et al. 2011).

There are a number of human genetic disorders that have been linked to the development of osteosarcoma including Li-Fraumeni syndrome, familial retinoblastoma and RecQ helicase disorders such as Rothmund-Thomson Syndrome. These disorders involve germline mutations of p53, RB, and RECQL4 respectively. P53 and Rb are tumor suppressor genes that when mutated result in loss of their protective function. This allows for accumulating mutations and ultimately cancer. P53 is found to be mutated in 50% of all cancers and 22% of osteosarcomas (Broadhead, Clark et al. 2011). Recent work showed that p53 expression correlated with lower grade tumors, improved survival and reduced metastatic disease (Hu, Yu et al. 2010). The Rb gene is critical in coordinating the G1-S phase cell cycle progression and mutations of it result in osteosarcoma in nearly half of those affected (Ng, Mutsaers et al. 2012). RecQL4 is a DNA helicase that when mutated due to a familial disorders causes

osteosarcoma with a 30% frequency (Ng, Mutsaers et al. 2012). This mutation has not been shown in sporadic osteosarcoma and its association with familial disease may separate it from the true disease course. Further work is necessary to clarify its correlation to risk.

Many proto-oncogenes have been found to be overexpressed in both canine and human osteosarcoma. In dogs, erB-2, which encodes for human epidermal growth factor receptor 2 (HER-2) was overexpressed in 86% of cell lines and 40% of tissue samples tested (Flint, U'Ren et al. 2004). In human osteosarcomas, erB-2 expression profiles are varied. Hepatocyte growth factor and its receptor, cMET, have been shown to be overexpressed in both canine and human cell lines and may indicate correlation with malignant phenotype of disease (MacEwen, Kutzke et al. 2003) C-myc, c-fos, c-sis, and insulin-like growth factor-1 are other oncogenes that have demonstrated higher expression in canine and human osteosarcoma (Mueller, Fuchs et al. 2007).

1.2 Stereotactic Radiation Therapy

Radiation Biology

Radiobiology is the study of the action of ionizing radiation on living things. Ionizing radiation has sufficient energy to eject one or more orbital electrons from an atom or molecule. The importance of this process is the energy released can break chemical bonds leading to biological effects on tissue. Three outcomes are cell killing, carcinogenesis, or mutation. Our focus here will be on cell killing, and the benefits of using ionizing radiation in the treatment of cancer.

Ionizing radiation can be classified as either electromagnetic or particulate radiation. Electromagnetic radiation includes radio waves, microwaves, infrared, visible light, ultraviolet

light, x-rays, and y-rays. These types of radiation are indirectly ionizing. This means that they do not produce damage themselves, but when absorbed, these forms of radiation transfer energy to other charged particles that ultimately produce damage. Particulate radiation includes electrons, protons, neutrons, α -particles, and heavy charged ions. These particles are directly ionizing in that they themselves can disrupt and damage atomic structure (Hall and Giaccia 2012).

The principle target for the biological effects of radiation is deoxyribonucleic acid (DNA). Once irradiated, the double-stranded molecule breaks in either a single or double stranded fashion. Single-strand breaks are of little significance and can be readily repaired. It is closely positioned double-strand breaks that can result in cell killing. Cell death, in regard to radiation, is usually defined by loss of its reproductive integrity. Most cells will undergo a mitotic cell death while trying to divide although other mechanisms can occur.

Long before mechanisms were understood, radiation was used to treat different diseases, including cancer. Following the discovery of x-rays in 1895 by Rontgen, a case of breast cancer was treated a year later (Linz 2012). The early lack of knowledge resulted in poor clinical outcomes and high morbidity due to exposure of normal tissues. By 1922, Henri Coutard, a French radiologist, observed that the same radiation dose that would produce severe side effects could be fractionated over the course of days. Given in fractions the dose would remain effective but limit the skin and tissue destruction. This process of fractionation remains the basis of most current radiation techniques today.

A number of different radiation techniques are utilized today including conventional external beam radiation, stereotactic radiation, intensity-modulated radiation therapy,

brachytherapy, and particle therapy. Each of these techniques is utilized for very specific treatment aims depending on the type, severity and location of a given cancer. Ionizing radiation therapy, or radiotherapy, is used in approximately two-thirds of cancer patients today with solid malignancies (Chandra, Lan et al. 2013). It is imperative to strive for the continued improvement of treatment techniques in tumor control as well as normal tissue sparing.

Evolution/Applications of Stereotactic Radiation Therapy (SRT)

Stereotactic Body Radiation Therapy (SBRT) is a novel radiation treatment technique where higher doses per fraction (10-20 Gy) are administered over a course of five or fewer fractions. This is much different from the more conventional external beam radiation protocols by which a lower dose per fraction (typically around 2 Gy) is administered over many treatments ultimately providing a higher total dose of radiation. In the past, these higher doses were largely dismissed due to limitations of providing the higher dose without being able to spare normal tissues to such doses. Today, due to technological advances made in patient immobilization, image guidance, and treatment planning and delivery clinicians are able to provide a safe and effective delivery of this amount of radiation (Arcangeli, Scorsetti et al. 2012).

In the 1950's, a Swedish neurosurgeon delivered a single ablative dose intra-cranially with the use of an external head frame used to fix the skull. Using this technique, now known as stereotactic radiosurgery (SRS), he was able to accurately and effectively deliver a single high dose to brain tumors (Chang and Timmerman 2007). Later on, there were a number of techniques developed for SBRT using rigid immobilization devices largely used for treatment of spinal lesions (Chang and Timmerman 2007). Before applying this treatment to tumors of the

thoracic and abdominal cavity, a similar body immobilization device was developed to dampen the inherent movement of respiration. This technology has mostly been utilized in the treatment of lung and liver tumors. With the vast increase in technology over the past twenty years, systems capable of delivering SBRT now have advanced on-board imaging modalities. Some examples of these include near diagnostic quality, digital, x-ray systems and CT scanners which can be used to get real time image guidance to ensure proper positioning throughout the entire procedure.

Much of the clinical experience with SBRT has been gained by treating either primary or metastatic disease of the liver and lungs. Diseases of the pancreas, prostate, kidneys, and spine stand to gain from utilizing this new treatment modality. The liver is a common site of metastasis and SBRT offers a noninvasive alternative to many treatments (surgery, chemotherapy, thermo-therapy). In treating the lungs, SBRT seeks ultimately to prove equivalent to surgical resection which now has a 65% survival rate at 5 years (Chang and Timmerman 2007). This is for Stage I lung cancers and pulmonary metastases. Currently, overall survival rates for pancreatic cancer have not shown improvements with SBRT but overall systemic treatments need to be improved for this local treatment to be more important. Initial studies on SBRT for metastatic renal cell carcinoma and for inoperable primary renal carcinoma appear promising; however, prospective work is needed to establish appropriate protocols. SBRT has been utilized to treat primary or metastatic spinal tumors since early in its development. Doses utilized are limited due to sensitivity of the spinal cord but palliative treatments have been shown to drastically reduce pain without myelopathy or other major complications.

Risks of SBRT are similar to those apparent for all other types of radiation treatments. Side effects are typically divided into acute and late term effects. Acute side effects occur during or right after treatment and typically resolve in a few weeks to months. Late effects can occur months to years later. Some of the most common acute effects of radiation include fatigue, skin swelling, mucositis, moist desquamation, erythema, dryness, diarrhea, nausea, vomiting, and headaches. Late effects can include specific organ changes (lung, kidney, brain), colon/rectal toxicity, secondary cancer, as well as bone pathology and fracture. Acute side effects are reversible while long term side effects are irreversible. All of these effects vary depending on the treatment administered, location, dose, protocol, and disease status.

SBRT allows for delivery of ablative doses of radiation to tumors for local control only due to a high degree of confidence in tumor location and treatment capability. Further risks of delivering such doses is best illustrated by noting the risks associated with the two most frequently treated sites; liver and lung. In conventionally fractionated radiation therapy the predominant dose-limiting toxicity has been radiation pneumonitis. Typical clinical signs include cough, fever, chest pain and shortness of breath that usually occurs weeks to months after treatment. SBRT can result in this typical pneumonitis as well as an increase in bronchial injury. Tumor location is an important factor in determining risk, as higher doses may affect normal surrounding tissue. Besides the main-stem bronchi and bronchioles, the esophagus is also at risk for stricture as a late effect. Precise knowledge and planning based on tumor location must take place and early recognition of toxicity is essential for proper management to take place and continued treatment to occur (Kavanagh and Timmerman 2005).

In the 1960's, a syndrome was observed following whole liver irradiation that was described with symptoms including increased liver enzymes, hepatomegaly, and ascites. It is now more commonly referred to as radiation induced liver disease (RILD). Outcomes varied from asymptomatic to death. Fortunately, RILD is a rare occurrence that strongly correlates to the volume of liver irradiated (Kavanagh and Timmerman 2005). This allows for SBRT in that high doses can still be administered as long as areas of normal liver receive an acceptable low risk dose for RILD (Kavanagh and Timmerman 2005).

In general, the largest benefit of SBRT comes from enhanced tumor control. Large doses of radiation are able to be delivered while only exposing normal tissue to a steep dose reduction gradient outside of the tumor and target volume. Another patient benefit of SBRT results from the reduction in number of treatments needed. More conventional protocols require a number of treatments that typically result in stress to our patients. This may be due to proximity to treatment centers, cost, and age-related factors (Arcangeli, Scorsetti et al. 2012). SBRT may provide a more beneficial treatment while not causing further stress or cost burdens to our patients. Many studies are currently ongoing and planned for the continued study of SBRT for various tumors. Retrospective studies performed at individual institutions inhibits comparisons between protocols and results in smaller numbers of patients enrolled, providing a strong rationale for development of multicenter clinical trials utilizing well defined radiation therapy protocols.

Radiation Effect on Bone

Acute radiation effects result from the loss of large numbers of cells in a relatively short amount of time. Tissues that typically show acute effects are rapidly dividing tissues, including

the skin, gastrointestinal tract, and the hematopoietic system. Radiation-induced DNA damage leads to cell death in the first cell division after irradiation or within the first few divisions. Reproductive cell death (mitotic death) is usually caused by unrepaired or improperly repaired chromosomal damage (Stone, Coleman et al. 2003). Late radiation effects appear in tissues that are typically slowly proliferating or not proliferating at all. Examples of these include the lung, kidney, liver, nervous system, and bone. The biological mechanism for late effects is not yet well understood as a number of complex interacting processes are likely involved. One of the major differences between early and late affected tissues is their ability to repair. Much of the time acute damage is completely reversible, however late responding tissues may improve but rarely completely repair (Hall and Giaccia 2012).

Bone exposure to radiation most commonly occurs during treatment of nearby malignancies. Irradiation of normal bone can lead to significant morbidities including fracture and loss of bone marrow function (Chandra, Lan et al. 2013). One study revealed a three-fold increase in hip fractures following radiation for cervical, rectal and anal cancers (Baxter, Habermann et al. 2005). A study of prostate cancer patients revealed an increased risk of 76% for hip fractures following radiation treatment (Elliott, Jarosek et al. 2011). Bone is also exposed to significant radiation following metastasis typically for management of cancer related pain. This occurs commonly with metastatic breast and prostate cancer and radiation is the treatment of choice (Hess, Barlev et al. 2012).

Various components of bone respond quite differently in their radio-sensitivity. Mineralized bone is considered the least sensitive part of bone to radiation. According to one study, osteopenia occurs between 8% and 23% of the time following irradiation and changes in

bone mineral content were found after single doses of >20 Gy (Hopewell 2003). Other work demonstrated alterations in the composition of apatite and that these changes may be correlated with changes in mechanical properties (Hubner, Blume et al. 2005). Although some changes in mineralized bone have been observed, it is the non-mineralized elements of bone that are more radiosensitive (Jegoux, Malard et al. 2010). This includes the growth plate, marrow cells, and osteogenic cells. Bone marrow has been shown to tolerate fractionated doses of radiation more readily, however; a reduction in hematopoietic cells is observed and essentially the entire bone marrow can be destroyed at high doses (Jegoux, Malard et al. 2010). Osteoclasts and osteoblasts are reduced following radiation and differentiation of precursor cells is also inhibited (Jegoux, Malard et al. 2010). Radiation results in reduced alkaline phosphatase (ALP) activity and expression of mRNA encoding ALP and collagen type 1 (Jegoux, Malard et al. 2010). Another important impact of radiation on bone is the subsequent reduction of blood flow. This effect appears to be dose related with doses up to 20 Gy (Jegoux, Malard et al. 2010). The different components of bone are highly variable in their response to radiation and they continue to be studied.

SRT for Bone Tumors/Osteosarcoma

Stereotactic radiation therapy is not part of the current standard of care for human osteosarcoma patients. It is mainly used for palliation for non-resectable or incompletely resected tumors (Morello, Martano et al. 2011). With improved radiation capabilities, SRT may play a role in certain smaller non-resectable tumors and treatment regimens are tailored on a case by case basis (Federman, Bernthal et al. 2009). Much more common than the treatment of primary bone tumors with radiation is the treatment of metastatic bone tumors from tissues

such as prostate, breast, lung and kidneys. The most common sites of metastasis include the spine, pelvis and ribs due to their vast blood supply. The advantages of stereotactic radiation for these tumors include a shortened treatment course, less exposure to normal tissue volume, longer duration of pain relief, and better local control (Jhaveri, Teh et al. 2008). Disadvantages would include prolonged pre-treatment planning, the potential for high dose exposure to normal tissues, fracture, and severe skin and soft tissue reactions for bony lesions that lie close to adjacent skin (Jhaveri, Teh et al. 2008). Stereotactic radiation therapy is a safe and effective treatment modality for the relief of bone pain due to metastatic lesions and continued work is underway to find the most effective treatment plans for various tumors.

Curative intent therapy of canine appendicular osteosarcoma with fractionated external beam protocols has been attempted with limited success, and has not yet demonstrated significant improvement over palliative protocols (Coomer, Farese et al. 2009). In vitro work has revealed a relative radioresistance of canine OSA cell lines with a high survival fraction at 2 Gy (Coomer, Farese et al. 2009). Work has shown that this is due to a low alpha:beta ratio, similar to late responding tissues. It is reasonable to expect that larger doses per fraction are needed to increase cell killing. Farese et al. described a curative intent SRT protocol for canine OSA combined with chemotherapy that resulted in a mean survival time of 363 days for 11 dogs (Farese, Milner et al. 2004). Adverse effects included alopecia, desquamation, hyperpigmentation, and pathologic fracture in four of the eleven total dogs. This protocol included 30-35 Gy to the periphery of the tumor with the central part receiving 40-50 Gy. Following this study, the technique was modified to cover the whole tumor with a 30-35 Gy isodose line. This work has been promising for a nonsurgical limb-sparing treatment for canine

OSA. Patients with metastatic disease, advanced osteolysis, and large tumor volumes are not considered good candidates for curative-intent SRT (Coomer, Farese et al. 2009).

Work at Colorado State University's Flint Animal Cancer Center has revealed another curative-intent SRT protocol as a nonsurgical limb-sparing technique for treatment of canine OSA. This radiation protocol utilizes 12 Gy/tx for 3 consecutive days for a total dose of 36 Gy. Complete staging is carried out prior to radiation which includes bloodwork, biopsy, lesion radiographs, three-view chest radiographs, and CT scan. Pamidronate, a bisphosphonate, is administered intravenously at 1mg/kg prior to the first radiation treatment. Chemotherapy includes 4 cycles of Carboplatin given intravenously at 300 mg/m² every three weeks starting at the first or second day of radiation treatment. Serial radiographs are taken to monitor for lesion progression and metastasis (Custis 2014).

Complete analysis of the results from 75 canine OSA patients treated with this protocol is underway. This treatment is able to achieve great local tumor with minimal acute radiation effects. Overall survival was 30% at 365 days with a median survival time of 247 days (Custis 2014). The most common complication of the treatment was subsequent pathologic fracture which occurred in approximately one-third of those treated with this protocol. Pathologic fracture ultimately led to either surgical repair or limb amputation. It is the goal of those involved in this research to decrease this risk of pathologic fracture thereby improving the quality of life for these patients and increasing survival time. The objective of the studies described here was thus to evaluate therapeutics that may reduce this risk and improve the mechanical strength of bone following bone cancer irradiation. The rationale and proposed mechanism of action of these therapeutics is described below.

1.3 Parathyroid Hormone

Endocrinology/Physiologic Effects of PTH

Parathyroid hormone (PTH) is synthesized and secreted by the parathyroid gland in response to changes in serum calcium levels. In its biologically active form it is an 84 amino acid sequence, although N-Terminal fragments (PTH 1-31 and 1-34) retain many of the biological functions of the intact peptide. Regulation of PTH occurs when a calcium receptor within the parathyroid cell plasma membrane senses changes in the extracellular calcium concentrations. Once secreted, PTH acts directly in bone tissue to stimulate calcium resorption and in the kidney to stimulate calcium reabsorption in the distal tubules. In bone, PTH binds to preosteoblasts through its PTH receptor PTHr1 stimulating them to mature into bone-forming osteoblasts (Rosen 2013). Stimulated osteoblasts increase their expression of RANKL and decrease their expression of Osteoprotegerin (OPG). RANKL is then free to bind RANK, facilitated by the decrease in OPG, which also binds RANK. This binding stimulates osteoclast precursors to fuse, forming new osteoclasts, ultimately enhancing bone resorption (Coetzee and Kruger 2004). This indirect mechanism, causing increased resorption, occurs with chronic exposure to high PTH concentrations. Intermittent exposure of PTH has been shown to result in relatively more bone formation than resorption (Rosen 2013). There are a number of genes induced by intermittent PTH exposure including IGF-1, amphiregulin, Runx2, TGF-beta, RANKL, and M-CSF (Rosen 2013). Work continues to fully elucidate the seemingly paradoxical mechanism by which PTH stimulates resorption in chronic exposure but bone formation with intermittent exposure.

Primary hyperparathyroidism is defined by a loss of calcium homeostasis due to excessive PTH secretion resulting in hypercalcemia. Approximately 85% of cases of this condition result from parathyroid chief cell adenomas. Remaining cases are caused by hyperplasia (Pallan, Rahman et al. 2012). Women seem to be twice as likely to be affected by the disease and it is typically diagnosed between 50 and 60 years of age. The majority of patients are discovered with an asymptomatic hypercalcemia found at routine screening. A minority present with clinical signs consistent with increased serum calcium levels including fragility fractures, nephrolithiasis, nephrocalcinosis, polyuria and renal insufficiency. Parathyroidectomy is the treatment of choice for symptomatic hyperparathyroidism. Patients with hyperparathyroidism experience preferential bone loss at sites rich in cortical bone however the association between bone mineral density and fracture risk has not fully been defined in asymptomatic disease (Pallan, Rahman et al. 2012). Secondary hyperparathyroidism is the overproduction of PTH secondary to chronic renal disease and vitamin D deficiency. As opposed to primary hyperparathyroidism, it is usually managed medically with either vitamin D supplementation or various treatments for renal disease.

Hypoparathyroidism is a disorder defined by hypocalcemia with low or absent PTH. It is most commonly seen following neck surgery with few much rarer genetic causes. Regardless of etiology, the standard treatment is supplementation with oral calcium and vitamin D with the aim of maintaining low normal serum levels without hypercalciuria (Cusano, Rubin et al. 2012). This is the only endocrine disorder for which the missing hormone, PTH, is not yet an approved therapy. A number of studies have shown promising results for both PTH 1-34 (teriparatide) and PTH 1-84 (the full-length molecule). Results included a reduction or complete cessation of

supplemental treatment, stable serum calcium levels, and normal skeletal dynamics (Cusano, Rubin et al. 2012). Long term studies are needed to more completely assess skeletal features including bone mineral density (BMD), bone quality, and quality of life measures. This is essential as PTH therapy for this treatment would most likely become a long-term therapeutic option. Most recently, a report of safe and effective treatment with PTH 1-84 was utilized for up to four years (Cusano, Rubin et al. 2013).

Clinical Applications of PTH Administration

Osteoporosis is characterized by a loss of bone mass and deterioration of bone tissue that results in increased bone fragility and susceptibility to fracture. A mainstay for osteoporosis treatment includes antiresorptive agents such as bisphosphonates. Although bisphosphonates have been shown to increase bone mineral density by 4-8%, patients typically suffer a 25% or greater loss of their skeletal mass (Cheng and Gupta 2012). The so called “osteoblastic” agents, which include PTH, have shown a more potent increase in bone mineral density. Anabolic agents have enhanced our therapeutic potential against osteoporosis. They act directly to stimulate bone formation, improve bone mass and quality, and reduce fracture risk.

PTH 1-34 (teriparatide) is currently approved in the United States for the treatment of severe osteoporosis in both men and women while PTH 1-84 is only approved in Europe (Rosen 2013). It is dosed daily, for up to two years, leading to increases in osteoblastic activity, improved bone mass and skeletal architecture (Neuprez and Reginster 2008). The limit of two years of use comes from the discovery in preclinical work indicating an increased incidence of bone tumors, including osteosarcoma, over a two year period of treatment (Vahle, Sato et al.

2002). Also, there is a finite period of time where PTH promotes relatively more bone formation than resorption. This period of time where the anabolic activity of PTH is maximized is referred to as the “anabolic window” (Rubin, Cosman et al. 2002). Significant increases in bone mineral density and a reduction of fractures has been reported in numerous studies. One large trial showed a 13% and 6% increase in BMD in the lumbar spine and femoral neck, respectively, following 18 months of PTH 1-34 treatment (Neer, Arnaud et al. 2001). It also showed a significant fracture risk reduction of 65 to 75% for vertebral fractures following 8 months of treatment (Neer, Arnaud et al. 2001). PTH has proved effective as an anti-osteoporosis drug but its high cost, route of injection, and safety concerns have hindered its use as a first-line treatment (Rosen 2013).

Given its proven success in anabolic bone therapy there have been a number of studies evaluating other applications of PTH, including its use as an adjunct therapy for fracture healing, hypoparathyroidism treatment, and periodontal disease. Pre-clinical studies evaluating PTH’s impact in fracture healing and spinal fusion have indicated that therapy may result in increased fracture site strength, callus quality, and greater mineralization at the fracture site (O’Loughlin, Cunningham et al. 2009). Many case reports have shown improved callus formation, union, and resolution of pain (Aspenberg and Johansson 2010; Rubery and Bukata 2010; Schalin-Jantti, Mornet et al. 2010).

Hypoparathyroidism can become difficult to treat with high doses of supplemented calcium and vitamin D. One trial indicated a possible superiority of PTH to calcitriol (Winer, Yanovski et al. 1996). Another showed twice daily dosing of PTH resulted in less fluctuation in serum calcium levels (Winer, Yanovski et al. 1998). Periodontal disease is a major cause of

morbidity world-wide characterized by a loss of supportive tissues including alveolar bone. One trial, following 40 patients after periodontal surgery, resulted in greater radiographic resolution and improved wound healing (Bashutski, Eber et al. 2010).

Safety Concerns/Side Effects

Both PTH 1-34 (teriparatide) and 1-84 are well tolerated at recommended doses. The two most common short term adverse effects are hypercalcemia and hypercalciuria. In one trial, only 11% of women receiving teriparatide at recommended doses had an elevated serum calcium and only 3% were persistent requiring a dose reduction (Neer, Arnaud et al. 2001). In the same trial there were no reported cases of nephrocalcinosis. Despite this, PTH is not recommended for those with a history of kidney stones or hypercalciuria. PTH 1-84 has shown to cause hypercalcemia in approximately 10% of subjects after retesting (Hodsman, Hanley et al. 2003). Nausea and headache were reported but were not significantly different from those who received placebo (Neer, Arnaud et al. 2001).

PTH 1-34 and 1-84 are rarely associated with long-term side effects. The most significant theoretical risk reported is an association between teriparatide and osteosarcoma formation in rats (Vahle, Sato et al. 2002). A follow up study revealed a dose and time-dependent relationship to risk that was highest in rats treated with high doses of PTH over the course of nearly 80% of their lifespan (Vahle, Long et al. 2004). Jolette et al. worked on another long term rat study this time with PTH-184. This work revealed a non-carcinogenic dose for PTH at 10ug/kg/day dosed over a 2 year period, a dose that is 4.6 times the recommended clinical dose for humans (Jolette, Wilker et al. 2006). The approval of PTH for treatment of osteoporosis came with an FDA mandated “black box” warning for the potential side effect of

osteosarcoma as well as a company sponsored surveillance program for osteosarcoma. The Osteosarcoma Surveillance Study is ongoing, but a 2012 report indicates that no osteosarcoma patients included in this study had a history of teriparatide treatment (Andrews, Gilsenan et al. 2012). A causal association between osteosarcoma and teriparatide has not been detected in humans.

Two additional published reports describe osteosarcoma patients with a history of PTH treatment. The first was a postmenopausal woman in her 70's with a complicated medical background. She was treated with PTH 1-34 at the recommended dose for osteoporosis and subsequently died during her second year of treatment due to metastatic cancer. Although the primary cancer site was never identified, a bone pathologist was able to identify biopsy material as osteosarcoma. Causality was never established for this particular case. At the time over 250,000 people had been treated with PTH 1-34 in the US and this case posed no greater risk for osteosarcoma than in the general population (Harper, Krege et al. 2007). A second case of potential teriparatide-induced osteosarcoma was reported by Subbiah et al. Given this patient's history of radiation exposure investigators reported it unlikely that PTH played a predominant role in the cause for the osteosarcoma for a number of reasons (Subbiah, Madsen et al. 2010). They did recommend that certain contraindications should be considered prior to initiating therapy, including previous radiotherapy (Subbiah, Madsen et al. 2010).

PTH and Radiation Therapy

Bone is the most common normal tissue exposed to significant doses of radiation during the treatment of solid malignancies in nearby tissues (Chandra, Lan et al. 2013). It is also exposed to radiation following primary bone irradiation in specific conditions previously

mentioned. Although the benefits of radiation therapy typically outweigh the risks well documented effects of radiation on bone have been seen. These include the potential for delayed healing, vascular depletion, osteonecrosis, increased fracture risk, and in rare circumstances neoplasia itself (Brown, Pelker et al. 1991; Mitchell and Logan 1998; Shaheen, Deheshi et al. 2006; Conill, Tomas et al. 2007; Kang, Deshpande et al. 2013). Due to the anabolic effect of intermittent PTH therapy it has been studied recently with the goal of protecting bone from radiation induced damage.

One study utilized an orthotopic model of metastatic breast cancer in nude mice that received radiation therapy of 20 Gy. Following radiation, the supplemental use of PTH increased bone mineral density and bone mass significantly in comparison to those groups with bisphosphonate therapy alone and untreated mice (Arrington, Fisher et al. 2010). Focal radiation in the tibiae of rats with concomitant PTH administration resulted in increases in trabecular number, thickness, connectivity, structure model index and stiffness (Chandra, Lan et al. 2013). A radioprotective effect of PTH was also shown in a murine model of distraction osteogenesis. Kang et al. demonstrated a reversal of radiation induced hypovascularity with increases in vessel volume fraction, vessel thickness, vessel number, and a decrease in vessel separation (Kang, Deshpande et al. 2013). Koh et al. was able to show that an irradiated bone marrow microenvironment actually increased the anabolic capabilities of PTH in comparison to nonirradiated mice (Koh, Novince et al. 2011). Despite these promising results, both PTH and radiation remain as independent risk factors for the development of osteosarcoma. A clearer mechanistic understanding is necessary for best determining risks of both treatments utilized in combination (Subbiah, Madsen et al. 2010).

bbPTH

Reduction of mechanical stress to bone results in accelerated osteoclast mediated resorption and is termed disuse osteoporosis. Common causes of this in humans include prolonged bed rest, immobilization, and the application of a cast to treat fractures (Takata and Yasui 2001). It has been shown in certain hibernating species, such as black bears, that extended periods of hibernation and disuse do not change their bone properties. One study revealed that although bone turnover did decrease during hibernation, a balance of formation and resorption is maintained preserving bone strength thus preventing osteoporosis (McGee-Lawrence, Carey et al. 2008). Similar work demonstrated that trabecular bone resorption and formation indices remained balanced in hibernating grizzly bears. There were no differences in bone volume fraction or tissue mineral density between hibernating or active bears (McGee-Lawrence, Wojda et al. 2009). Continued work led to the implication of black bear parathyroid hormone (bbPTH) in preserving bone during disuse. A positive correlation was shown between bone formation markers, including bbPTH, during periods of hibernation (Donahue, Galley et al. 2006; Donahue, McGee et al. 2006; McGee-Lawrence, Wojda et al. 2009). Further support for the role of black bear PTH is a study demonstrating greater anabolic effects on trabecular bone in dystrophin-deficient mice than wild type mice. This included increased bone volume fraction, trabecular number, and osteoblast area (Gray, McGee-Lawrence et al. 2012). Work utilizing the same model showed that bbPTH was more potent than hPTH at increasing trabecular bone volume. Approximately half of the required hPTH dose was needed to achieve wild-type values of femoral bone volume (Gray 2012).

Local Delivery of PTH

Systemic administration of parathyroid hormone requires daily subcutaneous self-injections that result in the exposure of non-targeted tissues. This is less than ideal for the optimization of localized bone regeneration. Local therapy has the potential to create a number of advantages over systemic administration. These include a possible reduction in side effects from systemic use, a decrease in dose and number of treatments, and the ability to tailor dosages to the level needed locally (Chan and McCauley 2013). There are few publications on locally administered parathyroid hormone. In vivo work at the Musculoskeletal Research Unit in Zurich revealed rapid filling of drilled defects (13 x 8 mm) in sheep bone following treatment with a fibrin-based hydrogel and PTH 1-34 (Kemper 2003). Fuerst et al. described the successful treatment of a sub-chondral bone cyst in a warm blood filly. Following curettage and lavage, the cyst was filled with 1.5 ml of 1mg PTH 1-34/ml enriched hydrogel resulting in improved healing time without complications (Fuerst, Derungs et al. 2007). Jung et al. demonstrated that a hydrogel containing PTH was effective at achieving bone regeneration in a dental implant model. More bone was formed in comparison to vehicle treated and empty defects however they could not detect significant differences between their PTH groups and those implants using autogenous bone (Jung, Cochran et al. 2007). Arrighi et al. showed in vivo success treating humeral and femoral defects in a sheep model with a parathyroid hormone fusion protein (TGpPTH1-34)-derivatized fibrin. They found a dose-dependent improvement in percent bone formation in defects without evidence of an immunological response (Arrighi, Mark et al. 2009).

1.4 Bisphosphonates

Mechanism of Action/Physiologic Effects of Bisphosphonates

Bisphosphonates are derivatives of inorganic pyrophosphate, which is a naturally occurring compound released as a by-product of a number of the body's synthetic reactions (Russell 2006). Early work demonstrated pyrophosphate's ability to inhibit calcification by binding to hydroxyapatite crystals (Fleisch, Russell et al. 1966). Bisphosphonates share this extremely high affinity for mineral in binding to hydroxyapatite crystals. Once bound they effectively inhibit bone resorption through two different mechanisms. Non-nitrogen containing bisphosphonates (etidronate, clodronate, and tiludronate) are metabolized in osteoclasts to compounds that replace the terminal pyrophosphate moiety of ATP. This forms a nonfunctional molecule in osteoclasts leading to apoptosis and cell death (Frith, Mönkkönen et al. 1997). Nitrogen-containing bisphosphonates (including alendronate, risedronate, ibandronate and zoledronate) inhibit the enzyme farnesyl pyrophosphate synthase in osteoclasts. This enzyme is important in the mevalonate pathway and disrupts the ability of cellular proteins to attach to the cell membrane. This ultimately creates non-functional osteoclasts thereby inhibiting resorption (Russell, Xia et al. 2007). Bisphosphonates not bound to bone mineral are rapidly excreted through renal clearance. This mechanism has led to the common use of bisphosphonates as primary therapy for a number of disorders characterized by imbalances in bone remodeling.

Clinical Applications of Bisphosphonate Administration

The major applications for current bisphosphonate therapy include postmenopausal osteoporosis, glucocorticoid-induced osteoporosis, Paget disease of bone, osteogenesis imperfecta, hypercalcemia and malignancy metastatic to bone. Treatment for osteoporosis, a disease characterized by decreased bone strength with an increased fracture risk, is the most

common application of bisphosphonate therapy. Both alendronate and risedronate, oral bisphosphonates, reduce the number of vertebral and hip fractures, while slowing the progression of vertebral deformities and height loss in postmenopausal women (Lieberman, Weiss et al. 1995; Black, Cummings et al. 1996). Initial work consistently used daily dosing however more recent studies have shown similar results with bisphosphonates dosed at weekly or even monthly regimens. Paget disease of bone is characterized by disordered and poorly formed bone resulting in bone pain, fractures, and even deformities. Bisphosphonates ability to profoundly suppress bone resorption has made them the cornerstone for current treatment. Bone metastases are commonly found with breast and prostate cancer and bisphosphonates have been shown to substantially decrease bone pain and other complications. Osteogenesis imperfecta, a heritable skeletal disorder in children, responds to bisphosphonate therapy with increases in bone mineral density and reduces fracture risk (Akçay, Turan et al. 2008). Despite its broad use, it is important to understand the potential adverse effects of bisphosphonate therapy. Potential adverse effects include osteonecrosis of the jaw, atrial fibrillation, hypocalcemia, an acute inflammatory response, and gastro-esophageal irritation with oral administration (Drake, Clarke et al. 2008).

Zoledronic Acid

Zoledronic acid (zoledronate) is a third generation nitrogen containing bisphosphonate that is the only drug of its class developed exclusively for intravenous administration (Russell, Watts et al. 2008). It is used in a once-yearly infusion regimen which makes it attractive in comparison to more frequent oral administration of other bisphosphonates. Among similar drugs it has the most potent enzymatic inhibitory effect with a strong affinity for bone. Like

other bisphosphonates it is widely used in patients with bone metastases as well as the treatment of osteoporosis. It is marketed in the US as Reclast and Zometa for the treatment of osteoporosis and metastatic bone disease, respectively. Reclast is dosed as a 5mg once yearly infusion and Zometa is a 4mg monthly infusion. Like other bisphosphonates, Zoledronic acid has been shown to reduce the amount of skeletal related events (SREs) including pathologic fracture through its inhibition of osteoclastic bone resorption (Arrington, Fisher et al. 2010).

Although zoledronic acid is used for its anti-resorptive capabilities, a number of studies in recent years have demonstrated a variety of direct and indirect anticancer activities (Gnant and Clezardin 2012). Zoledronic acid has been extensively studied in a number of cancer cell lines. It induces apoptosis, inhibits proliferation, and directly prevents tumor cell invasion and adhesion (Clezardin 2011). It has also been shown to indirectly prevent angiogenesis in vivo. It does this by modulating endothelial cell proliferation, adhesion and migration as well as reducing levels of vascular endothelial growth factor (Winter, Holen et al. 2008; Green and Clezardin 2010; Clezardin 2011). In a mouse model of metastatic breast cancer, zoledronic acid prevented metastasis to bone, liver, and lung (Hiraga, Williams et al. 2004). Other work has shown improved antitumor characteristics when given following chemotherapeutic treatments (Gnant and Clezardin 2012).

Clinical trials have also supported the concepts studied in preclinical work. The addition of zoledronic acid to adjuvant therapy in hormone responsive breast cancer in 1803 premenopausal women resulted in a prolonged disease-free survival, recurrence-free survival, and a prolonged overall survival as compared to hormone therapy alone (Gnant, Mlineritsch et al. 2009; Gnant, Mlineritsch et al. 2011). Another trial, showed a significant increase in disease-

free interval among patients who were postmenopausal for greater than five years before initiating treatment. This suggests that the anticancer effects of zoledronic acid are most significant in a low-estrogen environment. Other work showed a positive effect in premenopausal women. Here, the addition of zoledronic acid improved disease-free survival in breast cancer patients taking anastrozole or tamoxifen. The data from this trial was interpreted to demonstrate persistent benefits of zoledronic acid administration as a chemotherapeutic agent, and authors recommended the addition of zoledronic acid to adjuvant therapy (Gnant, Mlineritsch et al. 2011). Zoledronic acid is currently undergoing clinical trials involving over 25,000 patients with various cancers (Gnant and Clezardin 2012).

1.5 Hypothesis and Specific Aims

Bone tissues are exposed to radiation during a variety of treatment strategies. These include exposure to nearby normal bone during treatment of adjacent tissues, during treatment of metastatic bone disease, and in few instances using new treatment methodology for primary bone tumors themselves. Research indicates a potential for adverse effects on the skeleton following irradiation including delays in healing, osteonecrosis, growth abnormalities, pathological fracture, and even neoplasia itself.

Specific to the treatment of canine osteosarcoma with stereotactic radiation therapy, a loss of mechanical integrity and a high rate of pathologic fracture limit the utility of radiation therapy. If a large number of patients experience fracture as a side effect of the SRT, this promising therapy will not provide advantages over the current standard of care. Thus therapies to restore bone strength and limit future fracture risk are needed. Promising compounds include the class of drugs known as bisphosphonates. Through their ability to

inhibit osteoclastic bone resorption, these drugs have demonstrated the potential to restore bone properties following radiation. Although promising, bisphosphonates may not stabilize lytic lesions and an agent that could stimulate bone formation could augment the effect of bisphosphonates alone. PTH is an osteoanabolic agent approved for use for postmenopausal osteoporosis. Its ability to stimulate bone formation over resorption makes it an attractive candidate to improve properties of bone following radiation and ultimately reduce fracture risk.

Central Hypothesis: Black bear parathyroid hormone combined with zoledronic acid therapy, administered systemically following bone cancer irradiation in a rat orthotopic model of canine osteosarcoma, will result in greater increases in bone volume, strength, and revitalization than those treated with PTH, bisphosphonate (zoledronic acid), or stereotactic radiation treatment alone.

Specific Aims:

- 1) Assess microstructural properties of bone in the distal metaphysis via uCT comparing treatment groups 8 weeks following stereotactic radiation therapy (36Gy).
- 2) Compare treatment groups via dynamic and static histomorphometry following 8 weeks of treatment using various histologic staining techniques including H&E, TRAP, VK, and calcein labeling. Static histomorphometric analysis will include % tumor necrosis, tumor recurrence, osteoclast number, osteoclast surface, TRAP surface, bone area, bone surface, osteoid thickness, osteoid surface, osteoid volume and osteoblast number. Dynamic histomorphometric analysis will include double labeled surface, interlabel width and mineral apposition rate.

3) Demonstrate a safe and effective method of delivering PTH locally via vetrigel (polymer hydrogel). Aim to decrease systemic effects of therapy while enhancing local bone regenerative properties.

Chapter 2

Methods

2.1 Animals

Forty immunocompromised, athymic, female nude rats (RH-*Foxn1^{rnu}*) that were 7 to 8 weeks of age were obtained from the National Institutes of Health and housed at a laboratory animal resources facility. Animals were housed 2 per cage with climate-controlled conditions and allowed free access to standard laboratory diet and water. Each rat was identified by an ear tag. Rats rather than mice were chosen for the model because their larger size allows for the use of image-guided SRT with clinically relevant total dose and fractionation schedules, which would not be feasible in mice. Rats were acclimated for one week prior to initiation of experiments with tumor inoculation. All animal procedures and experiments were carried out under an approved protocol by the Colorado State University Institutional Animal Care and Use Committee (Protocol ID: 12-3596A).

2.2 Osteosarcoma Cells

Abram's luciferase-expressing canine osteosarcoma cell line was generously provided by the Colorado State University's Flint Animal Cancer Center. Canine OSA cell validation was performed by multiplex PCR using mitochondrial DNA to ensure the cell line was from canine origin and free of contamination (O'Donoghue, Rivest et al. 2011). The cells were grown at 37°C with 5% CO₂ in Minimum Essential Media (MEM) supplemented with 10% fetal calf serum, 7.5% sodium bicarbonate, MEM essential amino acids, 10mM non-essential amino acids, L-glutamine and an antibiotic-antimycotic (penicillin-streptomycin). Cells were split as needed (~90%

confluency) by incubating in 0.25% Trypsin for 5 minutes, centrifugation at 1200 rpm for 10 minutes followed by re-suspension and plating in growth media. Luciferase activity was confirmed by exposing luciferase expressing OSA cells for 5 minutes to luciferin. Then expression was captured using a Xenogen IVIS 100 (Caliper, Hopkinton, MA) at a 30 second exposure with medium binning (Appendix A, Donahue Lab SOP 5-11).

2.3 Drug Therapies

Recombinant black bear parathyroid hormone 1-84 (bbPTH) was produced by Proteos (Kalamazoo, MI). bbPTH was stored lyophilized from PBS at -80°C. The bbPTH was reconstituted in acidic (0.15M NaCl and 0.001M HCl) saline solution to a concentration of 0.1 µg/µl before subcutaneous administration. For local administration, bbPTH was reconstituted in Vetrigel (Royer Biomedical, Frederick, MD) at a concentration of 2.264 µg/µl (Appendix A, Donahue Lab SOP 9-11). Zoledronic acid (ZA), provided by Novartis (Basel, Switzerland), was stored at room temperature and reconstituted in sterile normal saline prior to use (Appendix A, Donahue Lab SOP 9-12).

2.4 Osteosarcoma Cell Inoculation

Rats were anesthetized by gaseous chamber induction with isoflurane (4-5%) and oxygen. Rats were transferred to a heated surgery table and anesthesia maintained via isoflurane (1% to 3%) mixed with 100% oxygen administered via facemask and a non-rebreathing anesthesia circuit. As previously described by Schwartz et al., a 22-gauge needle was inserted into the femur at the level of the trochanteric fossa, advanced distally within the medullary canal with a rotating motion to the distal metaphysis, and then withdrawn. A 1ml syringe was then drawn up with 200 µl of MEM at a concentration of 1×10^6 cells per 50 µl. A

new 22-gauge needle is placed on the syringe and held upright for three minutes (needle down). This allows for settling of cells increasing percentage of tumor take. This needle and syringe (holding 200 μ l of MEM at a concentration of 1×10^6 cells per 50 μ l) was then advanced to the distal metaphyseal region through the track previously made. Approximately 90 μ l was slowly injected, greatly reducing the risk of embolization. This injection technique allows for approximately 40 μ l of solution to be injected at the level of the distal metaphysis (50 μ l in needle). Approximate estimation of cell number is between 1 and 3 million cells following settling in syringe (Appendix A Donahue Lab SOP 9-19).



(Image: Schwartz, 2013)

Fig. 1 Inoculation technique entering proximally at the level of the trochanteric fossa and depositing osteosarcoma cells at the distal metaphysis.

2.5 Experimental Design

Tumor-inoculated (Day 0) rats were randomly divided into one of five treatment groups: 36 Gy SRT only, 36 Gy SRT plus ZA, 36 Gy SRT plus ZA and bbPTH(1-84), 36 Gy SRT plus bbPTH(1-84), and 36 Gy SRT plus localized bbPTH treatment. Radiographs consistent with distal femoral osteosarcoma were confirmed on day 10 following inoculation and stereotactic radiation

therapy was administered on days 14, 15, and 16. Each fraction consisted of 12 Gy of radiation for a total treatment dose of 36 Gy. This protocol was used for all rats in the study (n = 40). The rats in the zoledronic acid group and the combined ZA/bbPTH group (each n = 8) were injected subcutaneously once weekly with ZA (12.5 µg/kg) beginning on day 13 (total ZA dose of 100 µg/kg). The rats in the bbPTH and ZA/bbPTH combined groups (each n = 8) were injected with bbPTH (100 µg/kg) subcutaneously daily (5 days per week) beginning on day 17. The localized bbPTH treatment group (n=8) received 100 µg via intramedullary inoculation utilizing the same technique described for tumor inoculation on day 17. The bbPTH was reconstituted in Vetrigel (hydrogel polymer) (Royer Biomedical, Frederick, MD) at a concentration of 2.26 µg/µl just prior to inoculation. To administer the dose of 100 µg, 44 µl of bbPTH reconstituted in Vetrigel was administered slowly over one minute prior to hardening of gel (Appendix B – bbPTH release profile from Vetrigel, Gookin S). All rats were imaged with radiography (every two weeks) and bioluminescence imaging (weekly until loss of expression, then again at Day 70 endpoint) throughout the experiment to monitor for any tumor progression. Animals were euthanized at day 70 following tumor inoculation or earlier if they developed severe lameness caused by tumor burden or fracture.

2.6 Bioluminescence Imaging

Rats were imaged on days 0, 4, and 10 and then weekly using a Xenogen IVIS 100 (Caliper, Hopkinton, MA). All rats were imaged until complete loss of expression and finally on the day of sacrifice (Day 70). Five minutes prior to imaging, rats were anesthetized by chamber induction (5% isoflurane with 2L/min O₂) and maintained by mask (1-3% isoflurane with 2 L/min O₂) and injected intraperitoneally with 150 µl/rat of luciferin (30mg/ml) (Caliper,

Hopkinton, MA). Rats were positioned in right lateral recumbency in the Xenogen machine and images of the left femur were taken at 3 minute time intervals at medium binning. The expression value (photons/sec) was recorded for each animal at each time point. Due to the inability to reproduce consistent numerical values for expression only a qualitative analysis was completed.

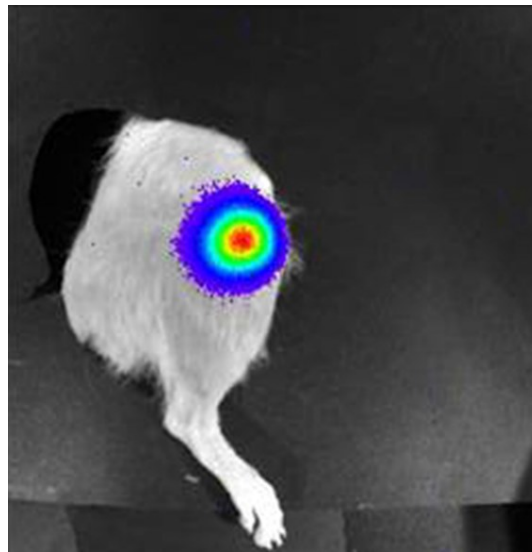


Fig. 2 Representative image illustrating bioluminescence at the distal metaphysis following tumor cell inoculation.

2.7 Radiography

While rats were anesthetized, digital radiography of the femurs was performed (every two weeks) to monitor the onset of tumor-associated osteolysis, tumor progression, and risk of pathological fracture. Rats were positioned in dorsal recumbency with both limbs down creating ninety degree angles at the knee and hip joints. Lateral radiographic views were obtained. Images were acquired with settings of 50 kV and 2.5 mA at 0.14 seconds, and stored electronically for comparison and analysis.



Fig. 3 Representative radiograph (lateral) of the left femur highlighting a lytic lesion shown at the distal metaphysis (arrow).

A scoring system was created to monitor the degree of lysis and progression of tumors prior to and throughout the treatment schedule. The evaluator was blinded to treatment group and comparisons were made between groups using ANOVA. A detailed description of the scoring can be seen below in Figure 4.

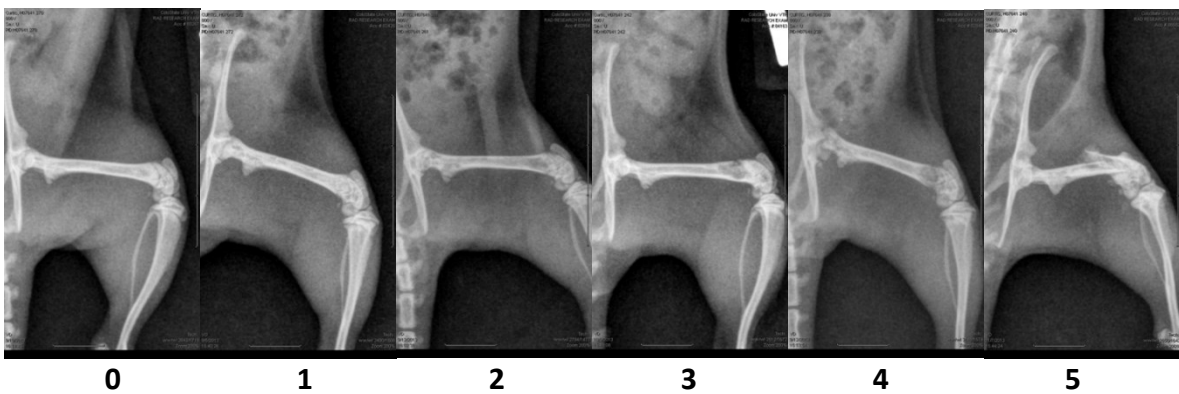


Fig. 4 Radiograph severity scoring on a scale from 0-5. 0 – No evidence of tumor osteolysis. 1 – Mild trabecular lysis apparent (less than 50% of the femur diameter affected). 2 – Moderate trabecular lysis apparent (>50% of the femur diameter affected). 3 – Severe osteolysis evident with 1 cortex involved. 4 – Severe osteolysis evident with both cortices affected. 5 – Fracture.

2.8 Stereotactic Radiation Therapy

Stereotactic radiotherapy was initiated 2 weeks after osteosarcoma cell injection and after confirmation of tumor cell engraftment via radiography and bioluminescence imaging. In preparation, rats assigned to receive SRT were individually anesthetized via the same protocols as previously described. Breathing was observed via closed circuit video monitors when personnel were required to be outside the radiation suite. Non-invasive immobilization was achieved by positioning each rat in dorsal recumbency within a customized bolus and cushion indexed to the couch of the linear accelerator via the baseplate. Any space between the rat and bolus was ablated with petroleum jelly.

Trans-axial computed tomography images of the affected femur were captured via onboard cone-beam computed tomography (CBCT). CBCT images were reconstructed with a slice thickness of 1 mm and imported into the computerized treatment planning system. Contouring consisted of identifying the gross tumor volume (GTV), noncancerous bone, and skin. The GTV was defined to include the entire left femur to ensure dose delivery to all possible tumor cells. For all rats, the clinical target volume (CTV) was identical to the GTV. The planning target volume (PTV) was the result of a symmetric 2-mm expansion beyond the GTV or CTV. A SRT plan consisting of 7 isocentrically placed fields was created. A multi-leaf collimator (5-mm leaf width at isocenter) was used to increase the dose conformity achieved within the tumor volumes, while preferentially sparing surrounding unaffected tissues outside the PTV. Each plan was normalized to achieve a minimum of 99% of the desired dose (36 Gy) within the GTV and a minimum of 95% of the desired dose (36 Gy) within the PTV as determined through evaluation of a dose-volume histogram.

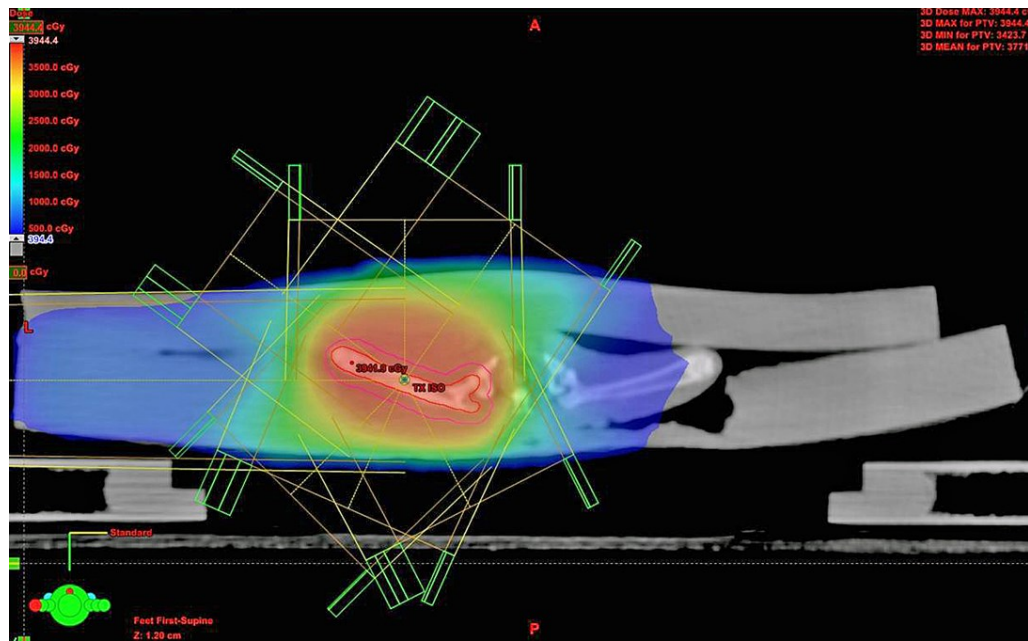


Fig. 5 Color wash showing dose distribution as well as the GTV (red line) and the 2-mm symmetrically expanded PTV (purple line).

Prior to delivery of each SRT fraction, a CBCT of the affected femur was obtained with the onboard imaging system. This CBCT was matched to the original cone-beam CT, with particular attention made to align the PTV with the affected femur. Any changes in the couch position, based on the matching process, were made to ensure precision and accuracy of SRT delivery. Each field of the SRT plan was then delivered individually.

Rats were anesthetized daily and underwent a 12 Gy fraction of SRT daily for 3 days for a total treatment dose of 36 Gy. When multiple fractions of SRT were administered, a symmetric 2-mm PTV expansion assured inclusion of the GTV through the digital matching of that day's CBCT with the original CBCT used for SRT planning. On completion of SRT each day, rats were allowed to recover from anesthesia and returned to their cages. Rats were monitored serially for their response to SRT. Quality-control testing of the linear accelerator was performed daily prior to SRT delivery.

2.9 Micro-CT

Following sacrifice on Day 70, left femurs were collected and soft tissues removed from the osteosarcoma affected limbs. The femurs were isolated and placed in 10% neutral buffered formalin for 48 hours. Then femurs were placed in 70% ethanol until micro-CT scanning. Femurs of all rats were scanned with a Scanco uCT-80 (Brüttisellen, Switzerland) at a 10-micron resolution. The region of interest for analyses included the distal femoral metaphysis spanning 3.5 millimeters beginning at the most proximal edge of the distal femoral growth plate (Fig. 6). For trabecular bone we quantified bone volume, bone mineral density, trabecular number, trabecular thickness, and trabecular separation. For cortical bone as well as whole bone analysis, we quantified bone volume and bone mineral density. Polar moments of inertia were also quantified over the region of interest as surrogate measures of bone strength.

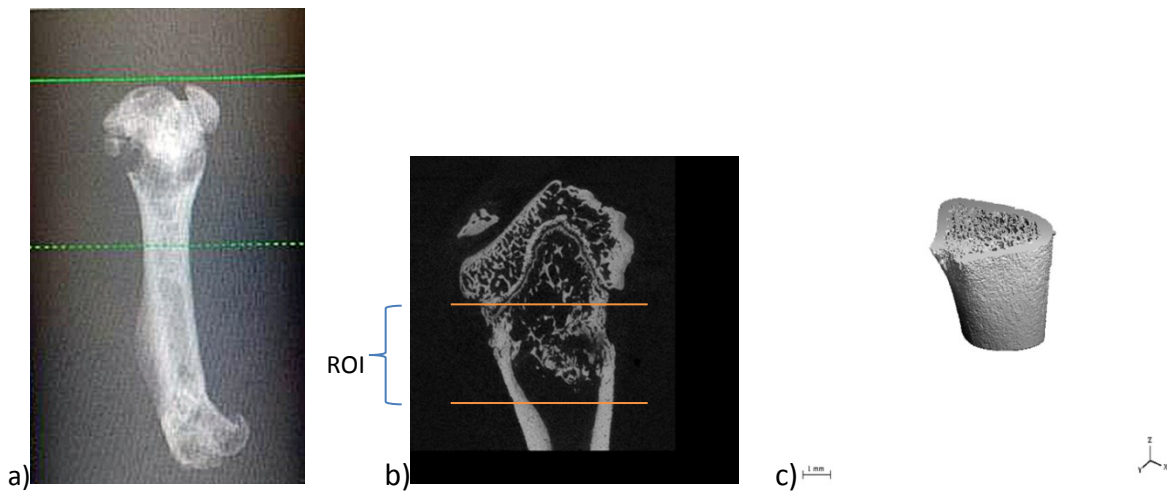


Fig. 6 a) Scanning region for micro-CT scan (tumor-burdened femora). b) Region of interest for analysis (tumor-burdened femora). c) 3-D reconstruction of region of interest (contralateral control shown, non-tumor burdened).

2.10 Histology

After micro-CT scanning, non-decalcified femurs were longitudinally sectioned in the midsagittal-craniocaudal plane and embedded in methylnmethacrylate. Serial sections were stained with hematoxylin and eosin, tartrate resistant acid phosphatase (TRAP), and Von Kossa. Unstained sections were also used to visualize fluorochrome staining (calcein) to assess double labeled surface, interlabel width, and mineral apposition rate (Appendix A Donahue Lab SOP 3-27). Total positive fluorochrome labeling was quantified as a total number of pixels as described below (Fig. 7). The calcein was administered at 12 and 3 days prior to euthanasia at a dose of 10 mg/kg given subcutaneously.

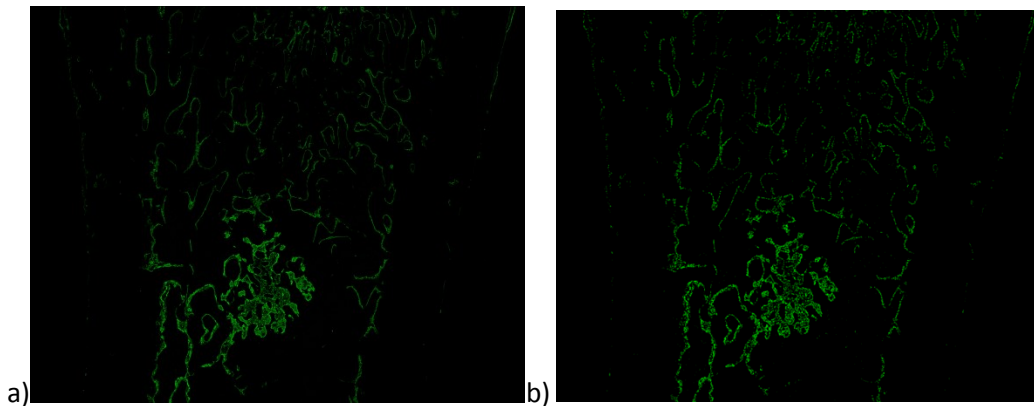


Fig. 7 a) Unedited original picture of the region of interest for sample 235. b) Edited Image 235. The editing process included removing all potential noise pixels and turning them into black to match the background. The intensities of the Calcein green were then intensified and each pixel of the image was counted as either green (+) or black (-). The pixels were then counted individually and a total number of positive pixels was determined. This gives a side by side comparison of the amount of calcein in each image.

Static histomorphometric parameters including TRAP surface, osteoclast numbers and surfaces, bone surface, bone area, osteoid surface, area and thickness were quantified with Bioquant Osteo Software (Bioquant Image Analysis, Nashville, TN, Appendix A Donahue Lab SOP 3-28, 3-25). Slides were also interpreted by an ACVP boarded pathologist for the presence of

viable osteosarcoma cells as well as interpreting percent tumor necrosis from radiation treatment.

Further qualitative assessment of the H&E slides included the location of tumor along the entire femur as well as the percentage of cortical necrosis evident in the diaphyseal cortex. Cortical bone was defined as confluent new and existing bone in the cortical line. Necrotic bone was defined as an area (greater than 20 lacunae) of cortex with greater than 50% of the lacunae lacking osteocytes.

2.11 Statistical Analysis

The micro-CT parameters, moments of inertia, radiographic severity scores and histological parameters were compared between treatment groups with ANOVA and Tukeys method for a post-hoc test (GraphPad Prism 6, GraphPad Software, San Diego, CA). Comparisons with a p-value less than 0.05 were considered significant. Transformations or non-parametric alternatives would be used when appropriate and described with the data.

Chapter 3

Results

3.1 Tumor Development

Abrams osteosarcoma cells were inoculated into the left distal metaphysis of the femur on Day 0 as described previously (2.4). A combination of imaging modalities was utilized to monitor for successful tumor inoculation. This included bioluminescence imaging, radiographs, and cone beam CT scans prior to beginning stereotactic radiation treatment. Thirty-seven of forty rats (93%) inoculated showed positive bioluminescence on days 0, 4, or 10.

Bioluminescence was used as a qualitative measure of tumor presence or absence as we experienced a number of day to day inconsistencies in regard to quantitative luciferase expression in photons/second. For example, bioluminescence that appeared positive on Day 0 may not show up at all on day 4, but reappear on day 10. One possible explanation for this could be Luciferin's inconsistent ability to penetrate deep tissues such as metaphyseal bone.

Evidence of tumor-associated osteolysis from radiographs and CT scans confirmed successful tumor inoculation in all forty rats (100%). All rats that received a radiograph severity score of 1 were confirmed via on board cone-beam CT scan for evidence of tumor-associated lysis prior to the initiation of radiation treatment.

3.2 Response to Stereotactic Radiation Therapy

Bioluminescence Imaging

Bioluminescence was used to monitor for tumor regression following stereotactic radiation treatment as well as recurrence. Thirty-four of thirty-nine (87%) lost expression by

day 25. Of the remaining five subjects four lost expression by day 32 and the last subject lost expression by day 39. One subject was removed from this total due to an early displaced fracture discovered on day 14. This subject was euthanized. Overall, all of the subjects lost expression by day 39 and thirty-eight of thirty-nine (97%) lost expression by day 32. The loss of bioluminescence is presumed to be due to the success of stereotactic radiation in causing tumor cell death. The precise timeline for cell killing is unknown as radiation-induced cell death often occurs upon future mitotic events. Our results indicate that all of our subjects lost expression within twenty-three days of the last radiation treatment.

Day 70 bioluminescence was carried out to check for significant recurrence of osteosarcoma cells. Thirty-seven of thirty-nine (95%) of the subjects showed no return of bioluminescence on the day of sacrifice. Two of thirty-nine (5%) of the subjects showed a return of bioluminescence. Of these, one was at the distal metaphysis (LPTH treatment group) and the other near the proximal region and neck of the femur (PTH treatment group) (Fig. 8).

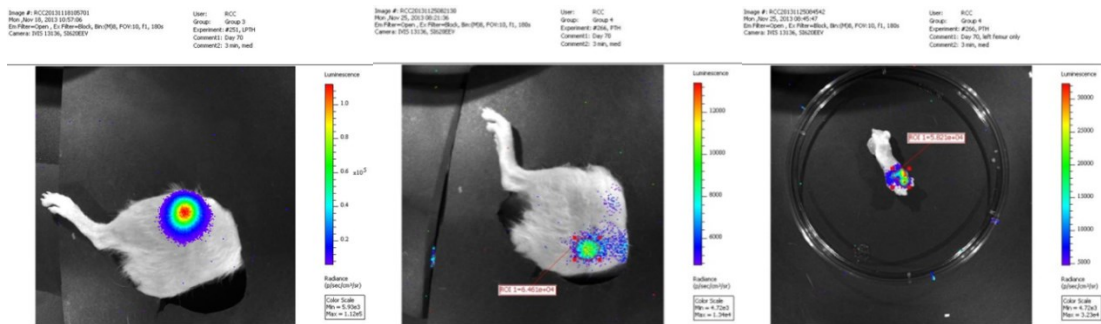


Fig. 8 Day 70 Bioluminescence suggesting recurrence in 2 of 39 subjects. Left - Subject 251 (LPTH), Middle – Subject 266 (PTH), Right – Subject 266 (PTH) harvested femur.

Radiography

Lateral radiographs were taken following the protocol previously described (2.7) on day 10 and every two weeks thereafter. The radiographs were scored by a blinded evaluator

according to the previously described scoring system (2.7). There were no significant differences found between treatment groups on any day that radiographs were taken throughout the experiment ($p > 0.84$) (Fig. 9).

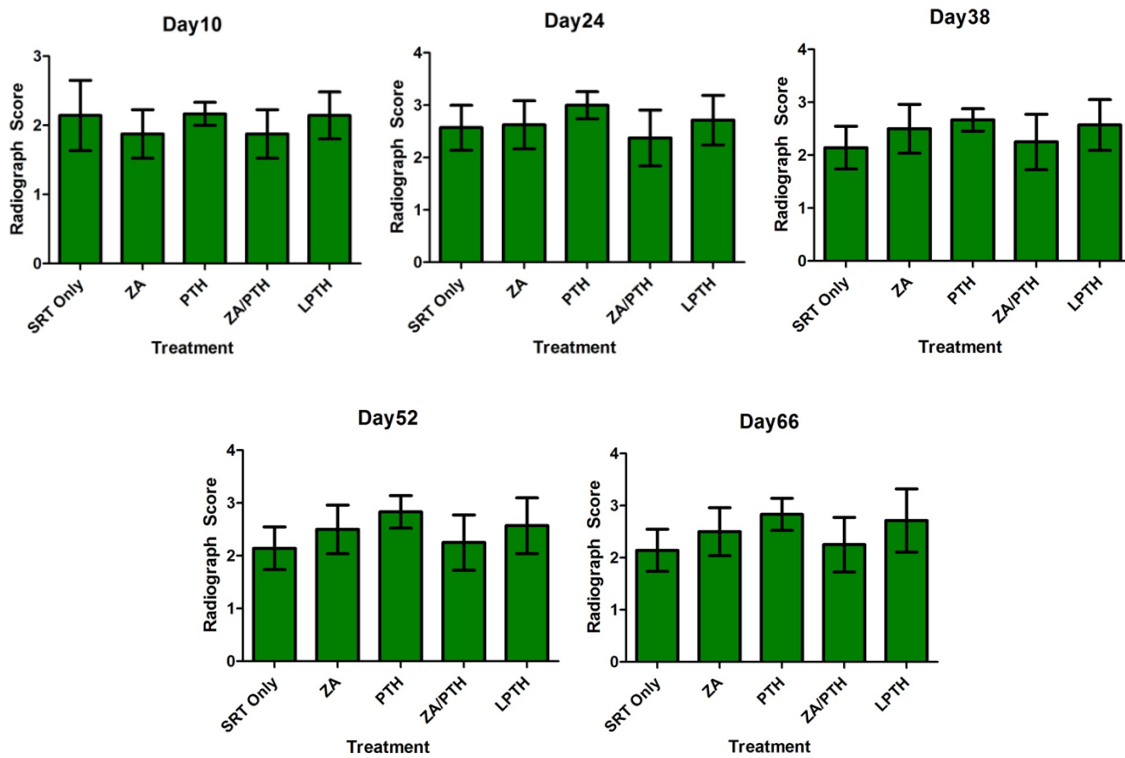


Fig. 9 Radiograph severity scoring compared between groups. Score shown as group mean +/- SE. There were no significant differences between groups on any given day ($p > 0.84$). Treatment groups are as follows: SRT only = stereotactic radiation therapy alone, ZA = zoledronic acid alone, PTH = parathyroid hormone alone, ZA/PTH = zoledronic acid and parathyroid hormone, LPTH = localized parathyroid hormone treatment alone.

Although there was no significant differences between treatment groups at any given time point, there was a significant difference from the day 10 radiograph score to day 24 ($p \leq 0.0001$). Following day 24, a pattern of decreasing severity (day 24 to 38), followed by stabilization (day 38 to 70), over the remaining duration of the study, was seen over all treatment groups.

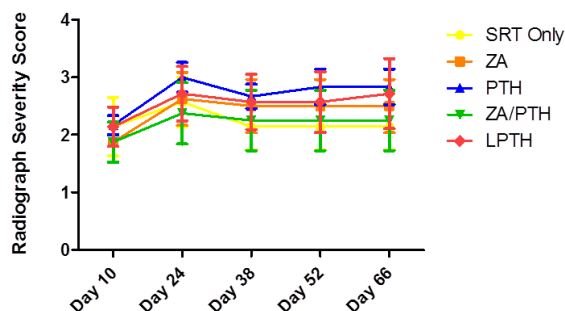


Fig. 10 Radiograph severity score over time for each treatment group. There were no significant differences between treatment groups on any given day of imaging ($p > 0.84$). There was a significant difference from Day 10 to Day 24 ($p \leq 0.0001$). Score shown as mean \pm SE. Treatment groups are as follows: SRT only = stereotactic radiation therapy alone, ZA = zoledronic acid alone, PTH = parathyroid hormone alone, ZA/PTH = zoledronic acid and parathyroid hormone, LPTH = localized parathyroid hormone treatment alone.

Fracture

A total of four subjects were euthanized due to fracture prior to the study endpoint of 70 days. These subjects were not included in the statistical analysis of other data. All subjects that fractured had high severity scores prior to and shortly after the initiation of treatment. It is likely that they were at the highest risk for fracture due to early tumor severity. Histology and bioluminescence revealed no evidence of tumor recurrence in any of the subjects that fractured. A table below describes the characteristics for each subject.

Table 1. Fracture characteristics of the four subjects with displaced fractures prior to study endpoint.

ID	Day of Fx	Location	Treatment Group	Radiograph Score (Day 10/24)	Recurrence (Y/N)
255	14	Mid-Diaphysis	N/A(prior to start)	2/N/A	N/A (prior to start of treatment)
236	38	Proximal/Near Femoral Head	SRT	3/4	N
240	67	Distal Metaphysis	PTH	2/3	N
249	52	Distal Metaphysis	PTH	2/3	N

3.3 Micro-CT

Whole Bone analysis of Distal Metaphysis – BMD, BV and pMOI

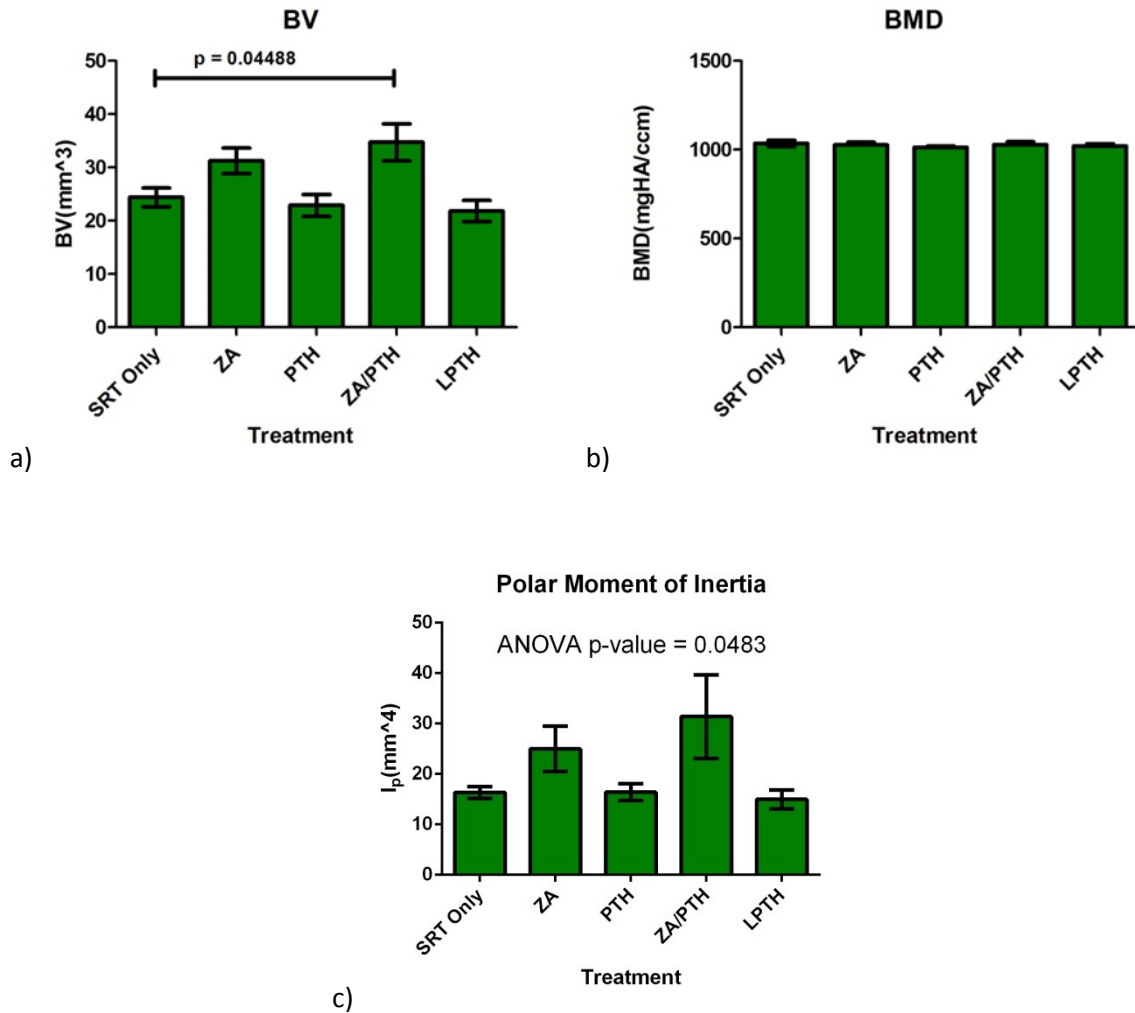


Fig. 11 Effects of radiation and adjunct therapy on bone volume (BV) (a), bone mineral density (BMD) (b) and polar moment of inertia (I_p) (c) in the distal metaphysis of tumor-burdened femora. Data represent mean (+/- SE) of raw data. Significance for polar moment of inertia calculated based on log transformed data due to differences in standard deviation. No transformations were required for bone volume or bone mineral density. Significance is noted by a connecting line above treatment groups. Treatment groups are as follows: SRT only = stereotactic radiation therapy alone, ZA = zoledronic acid alone, PTH = parathyroid hormone alone, ZA/PTH = zoledronic acid and parathyroid hormone, LPTH = localized parathyroid hormone treatment alone.

The tumor-burdened left femurs were compared between all treatment groups as described previously (2.11) and shown in Fig. 11a, b, c. Analysis over the region of interest revealed a significant increase in bone volume in the combined ZA/PTH treatment group as compared to SRT treatment alone ($p = 0.04488$). The p-value for the ZA group compared to SRT only was 0.31187. The PTH and LPTH groups compared to SRT had p values both greater than 0.95. Measurements of bone mineral density revealed no differences between groups ($p > 0.83$ for all groups compared to SRT only). Analysis of log transformed data for polar moment of inertia revealed a significant difference between groups ($p = 0.0483$) by ANOVA. Despite this, Tukey's method for multiple comparisons did not result in any significant difference in the pairwise comparisons ($p = 0.0805$).

Trabecular and Cortical Analysis

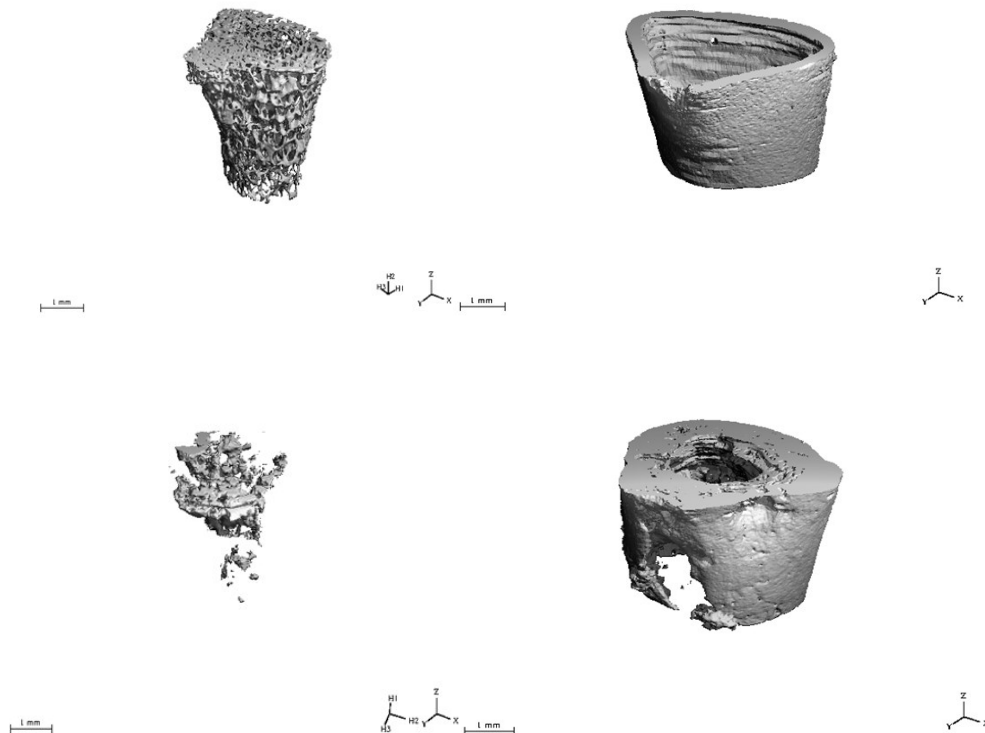


Fig. 12 Micro-Ct 3-D reconstruction of normal (top) trabecular and cortical architecture and tumor burdened (bottom) in the distal metaphysis.

In order to find a localized effect of drug therapies following radiation treatment, both trabecular and cortical compartments were evaluated for differences in microstructural properties. The trabecular and cortical compartments were defined based on what normal bone looked like on visual assessment from micro-CT. A clear distinction between true trabecular and cortical bone on many samples was made difficult due to previous tumor burden and altered ongoing bone regeneration. Analysis from the micro-CT scans revealed no significant differences between treatment groups in any of the variables quantified (Figures 13 and 14).

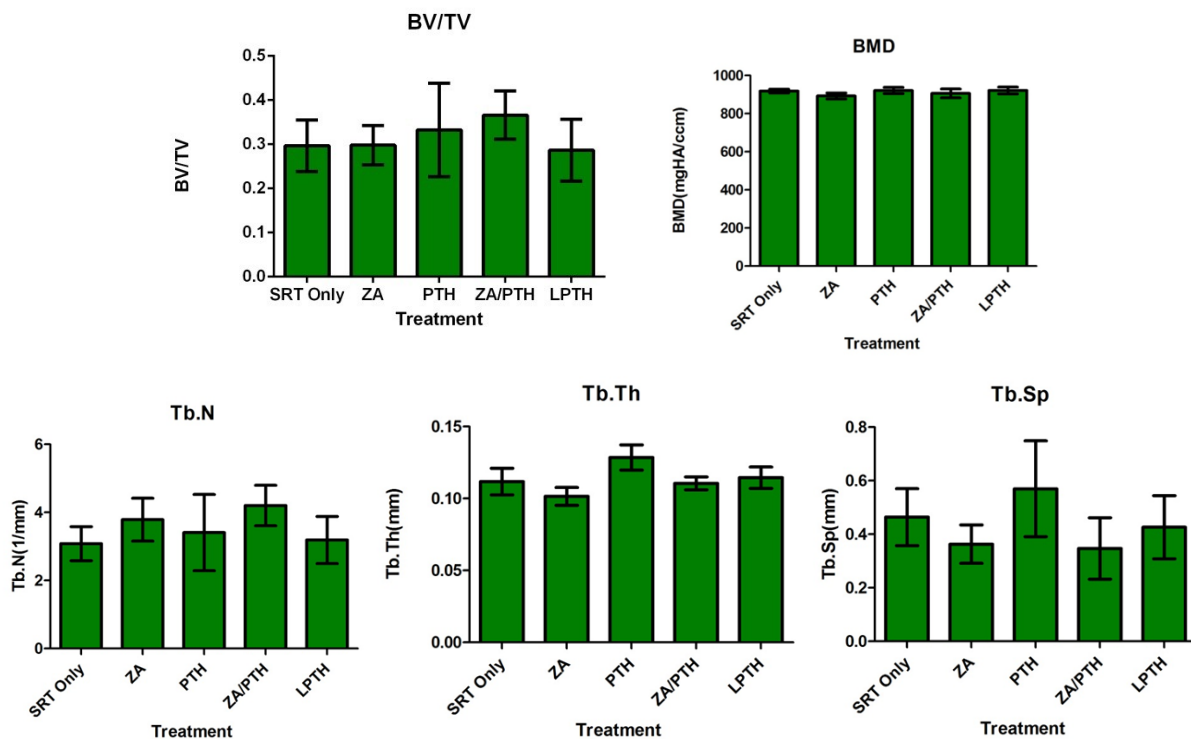


Fig. 13 Effects of radiation and adjunct therapy on trabecular bone volume, bone mineral density, number, separation and thickness in the distal metaphysis of tumor-burdened femora. Data represent mean (+/- SE) of raw data. There were no significant differences between groups ($p \geq 0.1566$).

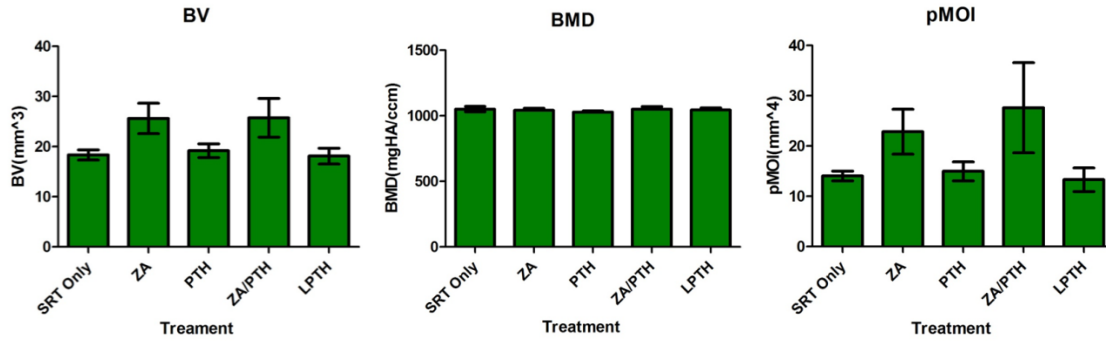


Fig. 14 Effects of radiation and adjunct therapy on cortical bone volume, bone mineral density, and polar moment of inertia in the distal metaphysis of tumor-burdened femora. Data represent mean (+/- SE) of raw data. There were no significant differences between groups ($p \geq 0.0852$).

Although there were no significant differences between groups, the trabecular analysis appeared to show a number of trends. In regard to bone volume fraction, there appeared to be a trending increase in the combined ZA/PTH treatment group ($p = 0.9088$). Similar to the data for all bone, a trend appeared with increasing trabecular number in the ZA and combined ZA/PTH treatment groups ($p = 0.7912$). Trabecular thickness was increased in only the PTH treated group, although this trend was not significant ($p = 0.1566$). Analysis of cortical bone volume compared between treatment groups revealed a similar trend to both data of all bone and trabecular regions increasing with both ZA/PTH and ZA treatment ($p = 0.0862$). A similar pattern was revealed with analysis of the polar moment of inertia although this result was also not significant ($p = 0.2097$).

Control Analysis

Contralateral femurs (non-irradiated, non-tumor-bearing) were used as controls to compare the effects of systemic treatment on normal bones. Analysis of all bone over the region of interest revealed significant increases in bone volume in the ZA treated groups ($p = 0.0149$) (Fig. 15). Comparison of bone volume between the PTH group and control for all bone

did not result in a significant difference ($p = 0.2603$). Analysis of polar moment of inertia also did not result in a significant difference although a trending increase in the ZA group was seen ($p = 0.1609$).

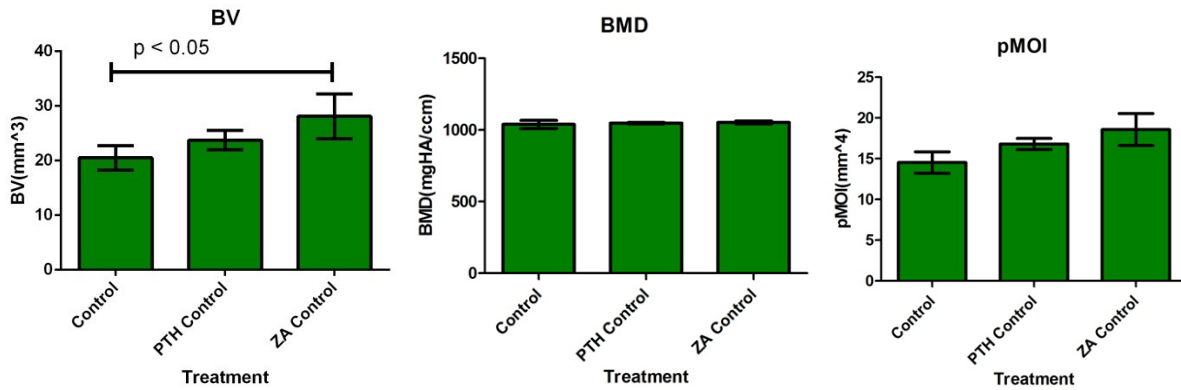


Fig. 15 Effect of PTH and ZA on microstructural properties of all bone over the region of interest in contralateral femurs representing control limbs (non-irradiated, non-tumor-bearing). Data represent mean (+/- SE) of raw data. Significance is noted by a connecting line above treatment groups. ZA treatment resulted in a significant increase in bone volume compared to control femurs ($p = 0.0149$).

Analysis of the trabecular bone of contralateral controls revealed significant increases in bone volume, trabecular number, and trabecular thickness in the ZA treated group compared to controls (Fig. 16). Systemic treatment with PTH resulted in significant increases in trabecular thickness and trabecular separation while decreasing trabecular number (Fig. 16). These results suggest the increased bone volume seen with combination therapy (ZA/PTH) for the irradiated femurs is mostly due to the ZA treatment. However, it cannot be ruled out that there is some synergistic effect of combination therapy (ZA/PTH), as this was the only group to show statistically significant difference in the irradiated tumor-burdened femurs. The analysis of the contralateral controls also reveals an unusual response to systemic PTH therapy. A number of studies have shown a very consistent effect of systemic PTH treatment which includes increased bone volume, trabecular number, trabecular thickness, and a decrease in trabecular

separation (Brouwers, van Rietbergen et al. 2009; Li, Zhou et al. 2012; Chandra, Lan et al. 2013; Vegger, Nielsen et al. 2014).

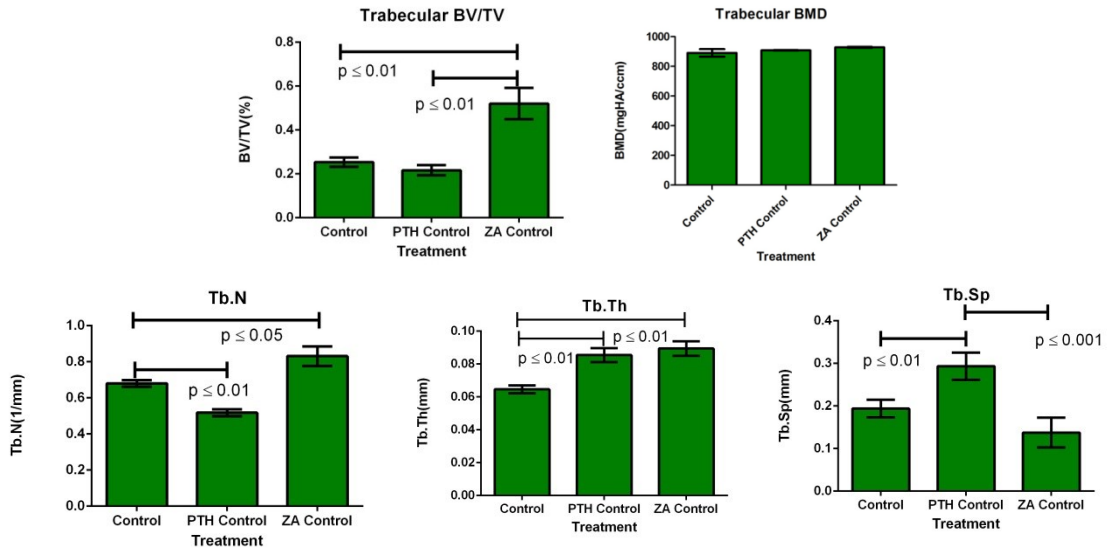


Fig. 16 Effect of PTH and ZA on microstructural properties of trabecular bone in contralateral femurs representing control limbs (non-irradiated, non-tumor-bearing). Data represent mean (+/- SE) of raw data. Significance is noted by a connecting line above treatment groups.

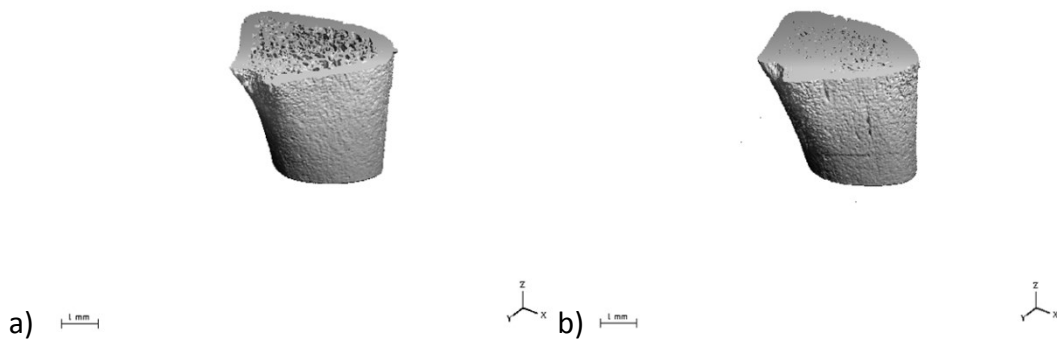


Fig. 17 Three-dimensional reconstruction of the distal metaphysis of contralateral control limbs reveals an increase in trabecular thickness, trabecular number and bone volume in the ZA treated bone (b) as compared to the no treatment control (a). Quantitative analysis corroborates these findings.

Contralateral control limbs (non-irradiated, non-tumor-burdened) were also compared to the group of tumor-burdened left femurs that were treated with only stereotactic radiation therapy. This allowed us to compare the effects of radiation and the tumor itself to normal femora. Analysis of all bone over the region of interest resulted in no significant differences ($p \geq 0.1583$) (Fig. 18). Interestingly, compartmental analysis revealed significant increases in cortical bone volume in the tumor-burdened, irradiated femurs as compared to controls ($p = 0.0370$) (Fig. 19). As expected, tumor-burdened femora had a significantly decreased trabecular number ($p = 0.0351$) and an increase in trabecular separation ($p = 0.0242$) (Fig. 19).

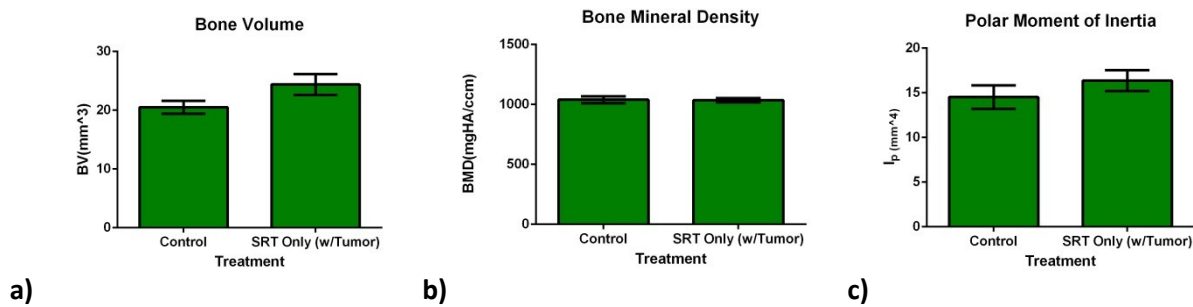


Fig. 18 Effects of radiation and tumor-burden on bone volume(a), bone mineral density(b) and polar moment of inertia(c) in the distal metaphysis compared to control femora. Data represent mean (+/- SE) of raw data. There were no significant differences between groups ($p \geq 0.1583$).

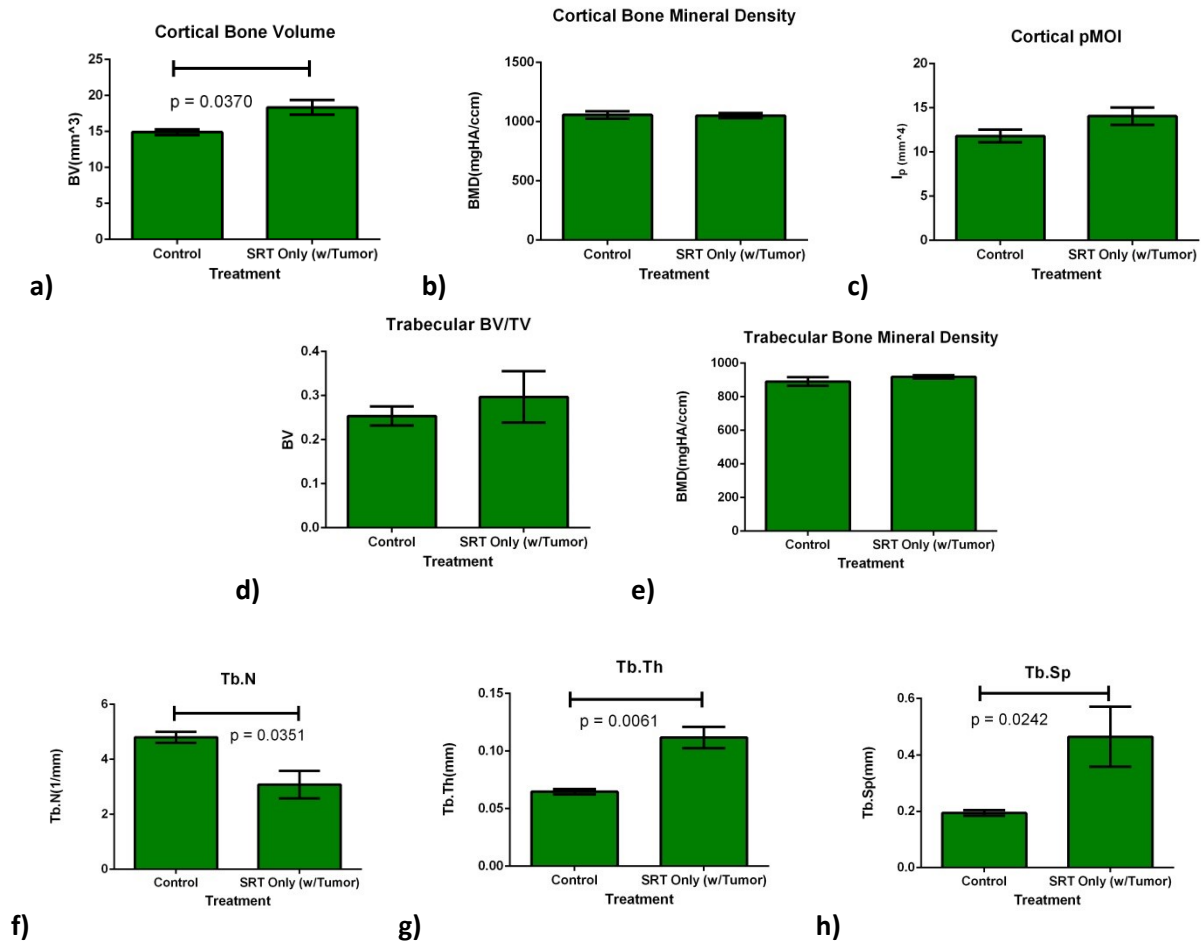


Fig. 19 Effects of radiation and tumor-burden compared to control femora. Radiation and tumor-burden resulted in significantly increased cortical bone volume (a), decreased trabecular number (f), increased trabecular thickness (g), and separation (h). Data represent mean (+/- SE) of raw data. Significance is noted by a connecting line above groups with corresponding p value. Abbreviations. pMOI = polar moment of inertia (I_p), BV/TV = bone volume/total volume, Tb.N = trabecular number, Tb.th = Trabecular thickness, Tb.Sp = Trabecular separation.

3.4 Histology

Dynamic Histomorphometry

The dynamic analysis revealed both single and double-labeled surfaces in both the trabecular and cortical bones of all subjects regardless of treatment group. This represents active mineralization occurring at the times of calcein administration on days 58 and 67 of the study. This, in and of itself, is of interest as this means that active mineralization is occurring approximately eight weeks following radiation doses of approximately 36 Gy to the femur.

Radiation has been shown to strongly suppress mineralization, however few studies have shown the effect of clinically-relevant doses of stereotactic radiation on bone mineralization (Chandra, Lan et al. 2013).

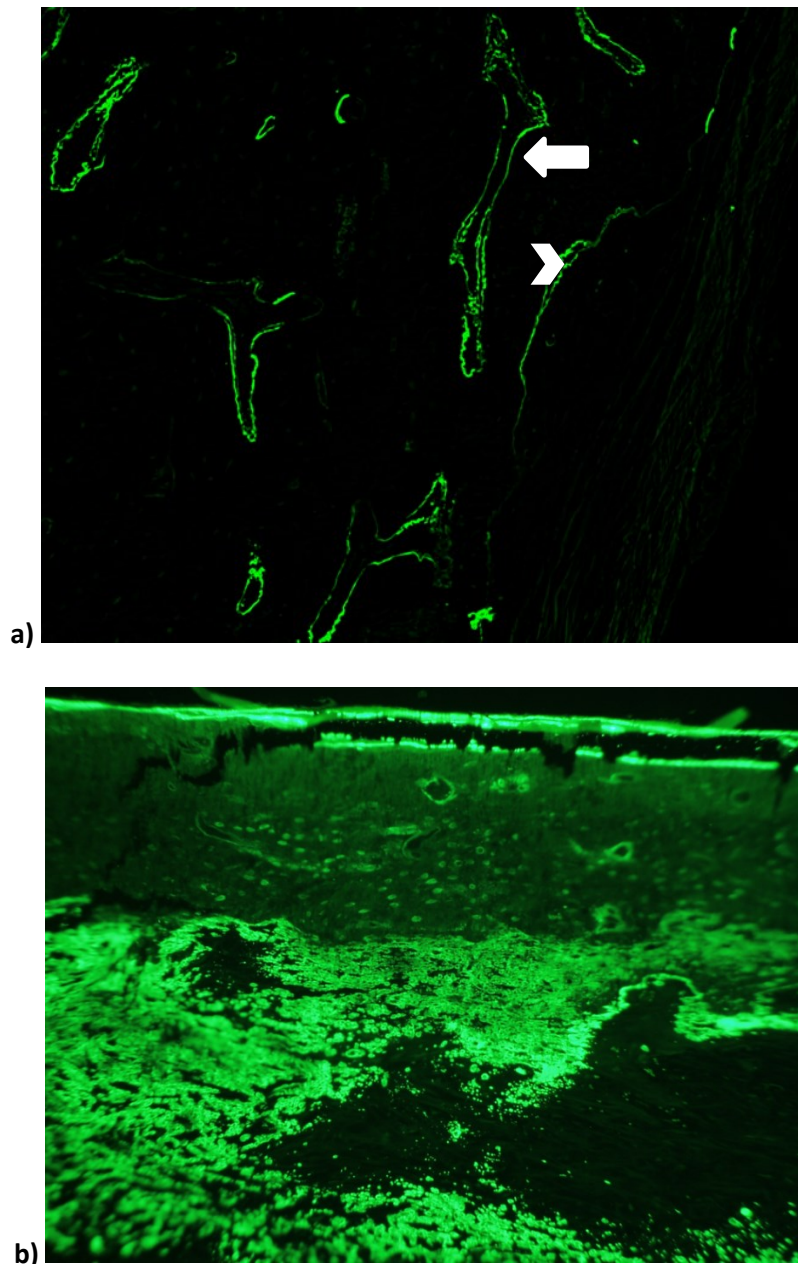


Fig. 20 Representative fluorescent micrograph illustrating single and double-labeled surfaces of both trabecular and cortical bone (a) as well as dystrophic mineralization (b) within the distal femoral metaphysis. Bone formation was examined by sequential labels with calcein in non-decalcified bone sections administered at 12 and 3 days prior to study endpoint. Single-labeled surface (arrow) and double-labeled surface (arrowhead) are highlighted (a).

Dystrophic mineralization in areas of tumor necrosis in the distal metaphyseal region of interest confounded the quantification of single-labeled surface. Thus, of the parameters typically quantified for calcein-labeled mineralization, it was deemed appropriate to only quantify double-labeled surface and inter-label width. In this work, double-labeled surface can be used interchangeably with mineralizing surface. There were no significant differences between treatment groups in regard to double-labeled surface or inter-label width ($p = 0.1504$ and 0.6891 respectively) (Fig. 22). The mineral apposition rate was calculated by dividing the average inter-label width by the time between calcein administration (9 days). Although no significant differences were found ($p = 0.6888$), the mineral apposition rate calculated is similar to control rats of other studies illustrating a normal rate of mineralization 8 weeks following stereotactic radiation therapy (Chandra, Lan et al. 2013; Jing, Cai et al. 2014). Double-labeled surface per bone surface (mineralizing surface) over the region of interest was also calculated and compared between treatment groups. No significant differences were discovered (Fig. 22) between groups (ANOVA p -value = 0.0852). It should be noted that the percentage of trabecular bone surface comprised of double-labeled surface is quite small (~1%) likely due to the combination of tumor-associated lysis and radiation effect over the region of interest.

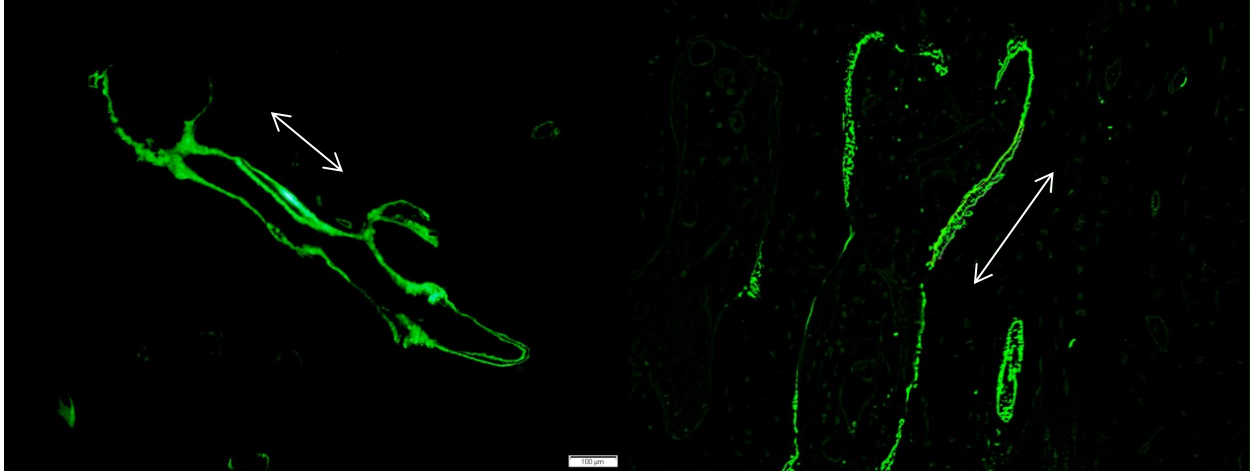


Fig. 21 Representative fluorescent micrographs illustrating double labeled surface (double arrows) of trabecular bone within the region of interest.

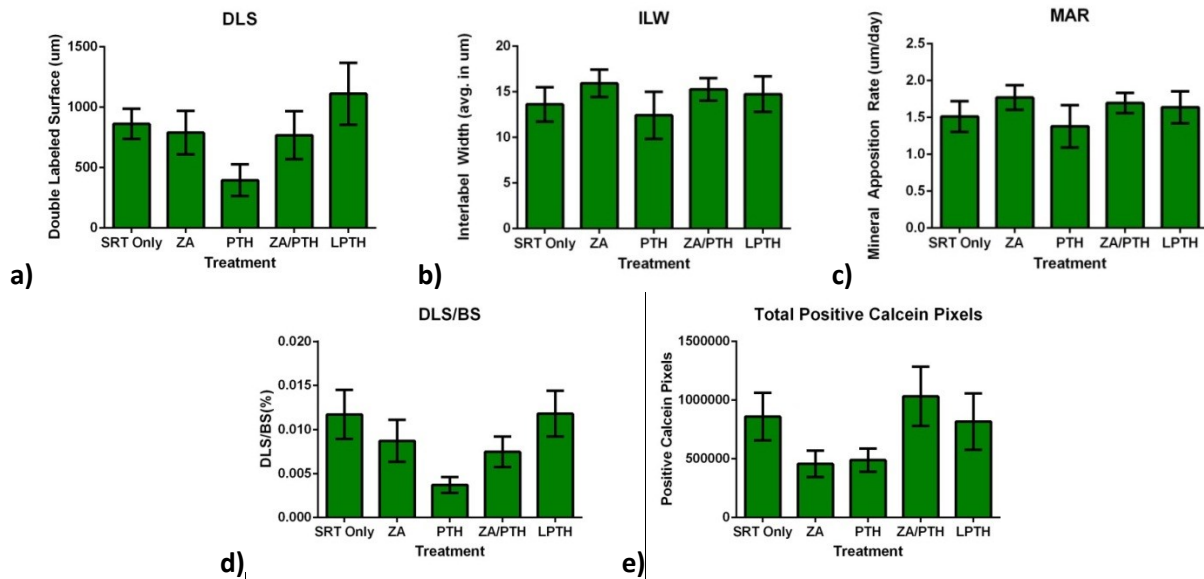


Fig. 22 Dynamic histomorphometry of trabecular bone within the region of interest. Double-labeled surface (a) and inter-label width (b) were quantified using Bioquant Osteo Software (Bioquant Image Analysis, Nashville, TN) within the region of interest. Mineral apposition rate (c) was calculated by dividing inter-label width by the time between calcein administration (9 days). Double-labeled surface was calculated as a fraction of trabecular bone surface (d). Total positive fluorescence was calculated as number of pixels as described in methods (e). There were no statistically significant differences found between any treatment groups ($p \geq 0.0852$).

Static Histomorphometry

Hematoxylin and Eosin

Longitudinal sections of left femurs from all experimental subjects were analyzed to qualitatively describe the location of osteosarcoma within the femur, check for recurrence with active osteosarcoma cells, and assess osteocyte viability in cortical bone.

The location of the previously irradiated osteosarcoma was made apparent by discrete areas of necrosis with few viable cells other than a loosely defined network of fibrous connective tissue (Fig. 23). In many samples, within these areas, were areas of dystrophic mineralization. Prior to irradiation, imaging modalities (radiographs, bioluminescence) were utilized to confirm tumor placement in the distal metaphyseal region of the left femur. Although the distal metaphysis was the most common site of lysis, other sites along the femur may have been exposed to tumor cells due to the inoculation technique (proximal to distal). Distal metaphyseal location of tumor was confirmed via histologic evaluation in 35/37 (95%) experimental subjects. Osteosarcoma cells in the diaphysis of the femur was confirmed in 33/37 (90%) of experimental subjects. The most severe lesions due to osteosarcoma were evident in the distal metaphysis (consistent with imaging) but these results illustrate the shortcomings of this model in completely depositing tumor cells in a strict well-defined location. The cells deposited in the diaphysis typically did not result in radiographically evident lysis or fracture but were confirmed present via histology. No experimental subjects exhibited osteosarcoma cells in the distal epiphysis, highlighting the tumor's inability to cross the growth plate. One subject did not show evidence of active or previous osteosarcoma over the entire femoral section, however only one plain of section was analyzed.

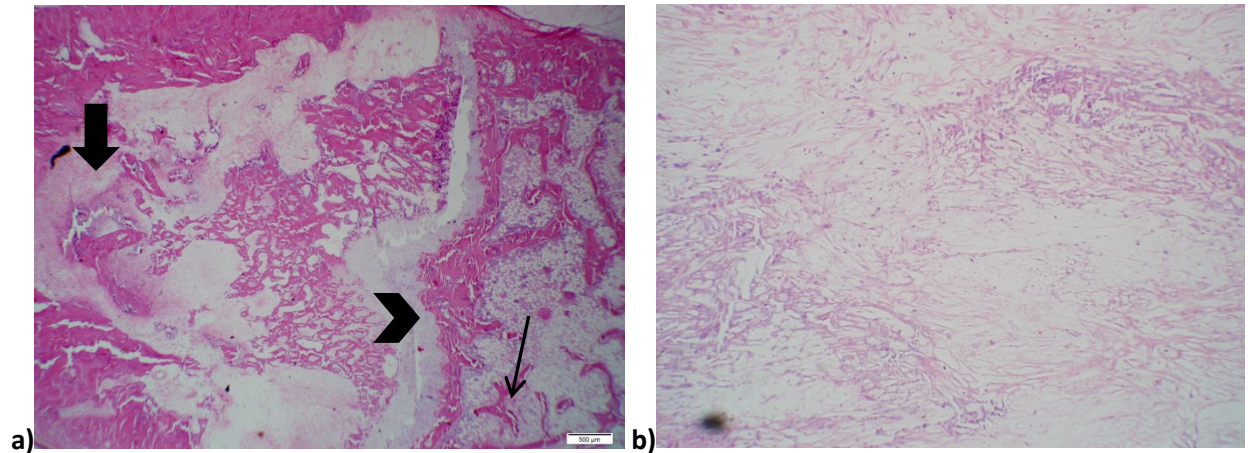


Fig. 23 Evidence of previous osteosarcoma. (H&E) a) Distal metaphysis exhibiting trabecular destruction, necrosis, and replacement fibrosis throughout regions of previous tumor burden (thick arrow). Growth plate (arrowhead) and normal trabecular bone of epiphysis (thin arrow) are highlighted. (2x) b) Closer magnification of loosely organized fibrous connective tissue and necrosis in tumor-burdened areas. (10x)

Tumor necrosis was 100% in thirty-two of thirty-six (89%) of the experimental subjects (one subject removed as no evidence of active or previous tumor was found). The overall mean percentage of tumor necrosis was 98%. Active osteosarcoma was discovered in four subjects (~10%), but exhibited an average of 85% tumor necrosis (Fig. 24). These results highlight the effectiveness of this radiation protocol totaling 36 Gy over three once-daily fractions.

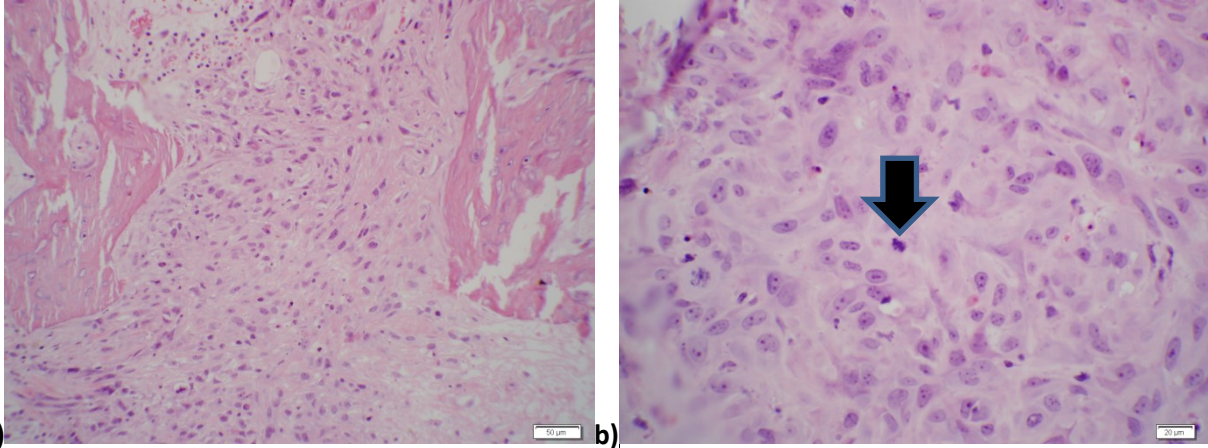


Fig. 24 Active Osteosarcoma a) Rat. Distal Metaphysis of Femur. (H&E. 20x). Replacing normal trabecular architecture are poorly differentiated neoplastic cells that are polygonal to spindle shaped with lightly eosinophilic cytoplasm. b) Rat. Distal Metaphysis of Femur. (H&E. 40x). Neoplastic cells are irregularly polygonal with indistinct cell borders and moderate amounts of cytoplasm. Nuclei contain multiple, distinct nucleoli and a mitotic figure is present (arrow).

The femurs of all experimental subjects showed typical changes in bone following irradiation. These included a reduced, but present population of hematopoietic cells, osteoclasts, osteoblasts and osteocytes. A precise timeline for survival and regeneration of marrow cells is unknown, but this work illustrates that at 8 weeks post-SRT many viable cells remain in the bone and marrow. The distal epiphysis is a prime example of this where the effect is similar to irradiated normal bone (Fig. 25).

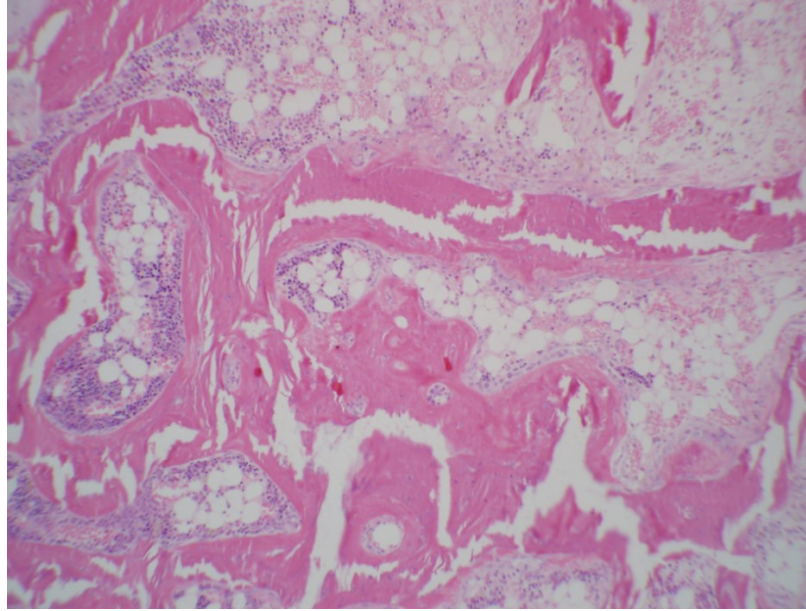


Fig. 25 Distal Femoral Epiphysis (H&E, 20x). The bone marrow of the distal epiphysis reveals normal lineage hematopoietic cells that are reduced in number.

The diaphyseal cortex showed minimal areas of necrosis as previously defined in the methods section (2.10) (Fig. 26). Nineteen of thirty-seven (51%) of the subjects had no evidence of cortical necrosis. Fifteen of thirty-seven (41%) had between 0 and 25% of cortical necrosis. Only three of thirty-seven (8%) of the subjects had 25% to 50% of cortical necrosis. These results represent a snapshot in time (8 weeks post irradiation) and areas of necrotic bone and overall cell viability may change over time due to the effects radiation treatment.

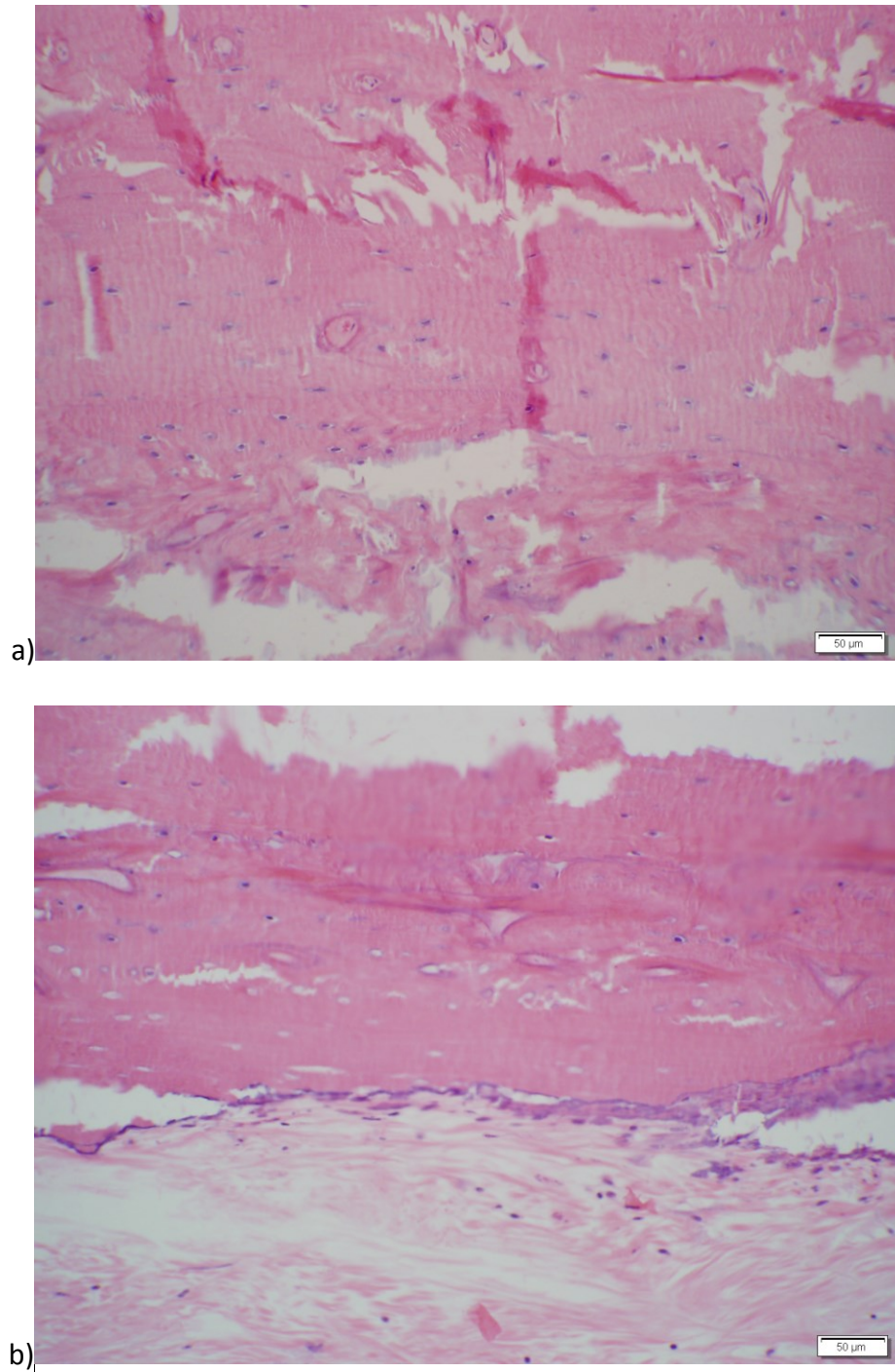


Fig. 26 The effect of stereotactic radiation therapy on cortical bone. 92% of experimental subjects showed less than 25% of the cortex having areas of necrosis. a) Cortical bone illustrating viable osteocytes filling over 80% of the lacunae (H&E, 20x). b) Cortical bone with areas exhibiting >50% of lacunae being empty representing necrotic bone (H&E, 20x).

Tartrate-Resistant Acid Phosphatase (TRAP)

TRAP stained sections were used to quantify osteoclastic activity over the region of interest. There were no significant differences between treatment groups in regard to osteoclast number ($p = 0.1658$) (Fig. 27). Osteoclast surface was significantly different between groups (ANOVA $p = 0.0219$) however pairwise comparisons were unable to detect a significant difference between groups ($p \geq 0.0761$). Analysis of total TRAP surface (Kruskall-Wallis) revealed a statistically significant decrease in the combined (ZA/PTH) treatment group compared to SRT treatment only ($p = 0.0341$). These data highlight the expected outcome with successful bisphosphonate therapy reducing osteoclast-mediated resorption.

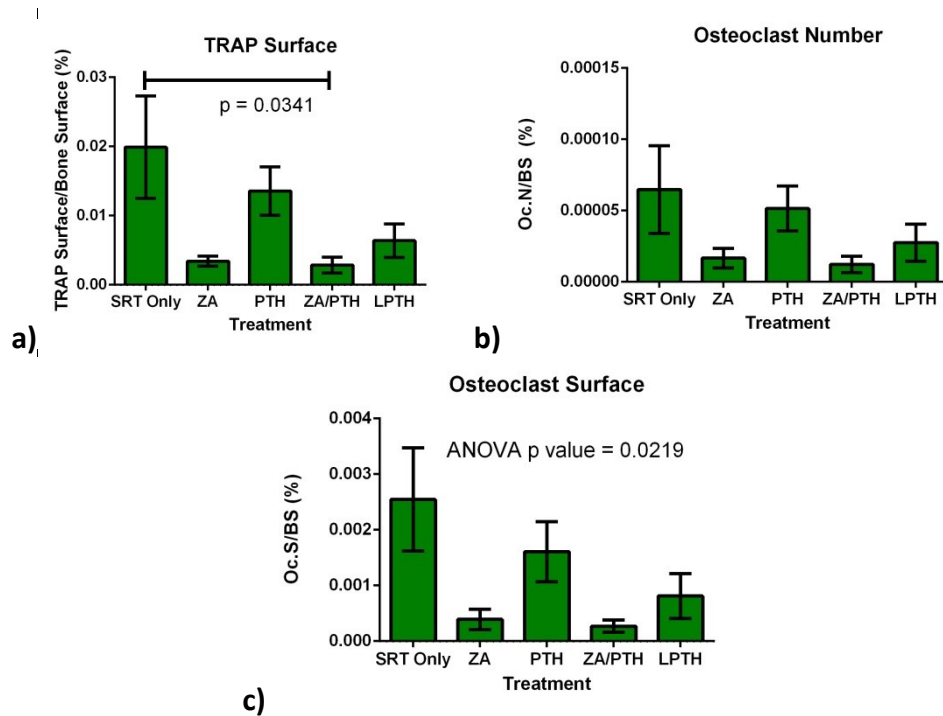
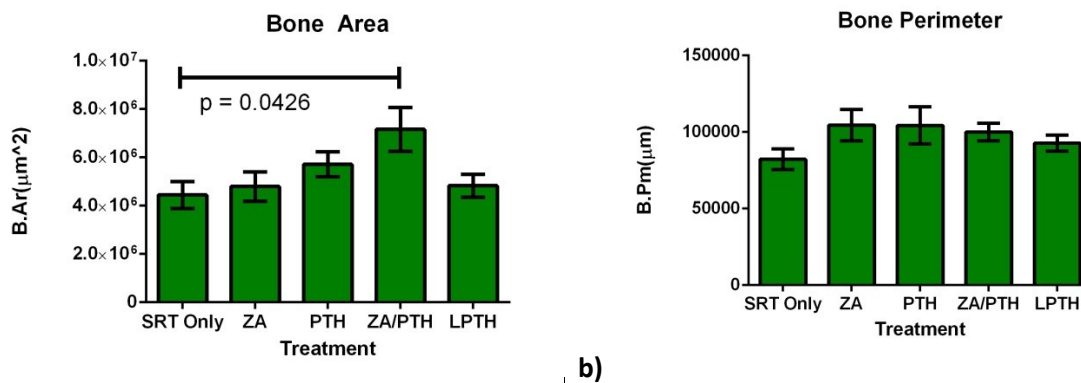


Fig. 27 Assessment of resorption over the region of interest. TRAP surface (a), osteoclast number (b), and osteoclast surface (c) were analyzed with a Kruskal Wallis test for significance. Data represent mean (+/- SE) of raw data. Significance is noted by a connecting line above groups. Analysis of TRAP surface showed a statistically significant decrease compared to SRT treatment alone ($p = 0.0341$). Analysis of osteoclast surface showed a significant difference between groups ($p = 0.0219$), however pairwise comparisons were unable to detect which groups (ZA/PTH vs SRT, $p = 0.0761$). There were no significant differences found in regard to osteoclast number ($p = 0.1658$).

Von Kossa McNeal's

Sections stained with Von Kossa McNeal's were analyzed to quantify bone mineral properties, osteoid properties, and osteoblast numbers within the trabecular bone of the region of interest. Analysis revealed a significant increase in bone area (μm^2) in the combined (ZA/PTH) treatment group compared to radiation treatment alone (Fig. 28, $p = 0.0426$). This is consistent with the three-dimensional results of all bone from the micro-CT data. There was no significant difference in bone perimeter ($p = 0.3282$). Analysis of osteoid properties revealed no significant differences in osteoid width ($p = 0.2856$), area ($p = 0.0636$), and surface ($p = 0.1029$). There were also no significant differences in osteoblast number ($p=0.1049$) (Fig. 29).



a) b)
Fig. 28 Bone mineral properties including bone area (a) and bone perimeter (b). Data represent mean (+/- SE) of raw data. Significance is noted by a connecting line above treatment groups. The combined (ZA/PTH) treatment group significantly increases bone area over the region of interest compared to SRT treatment alone ($p = 0.0426$).

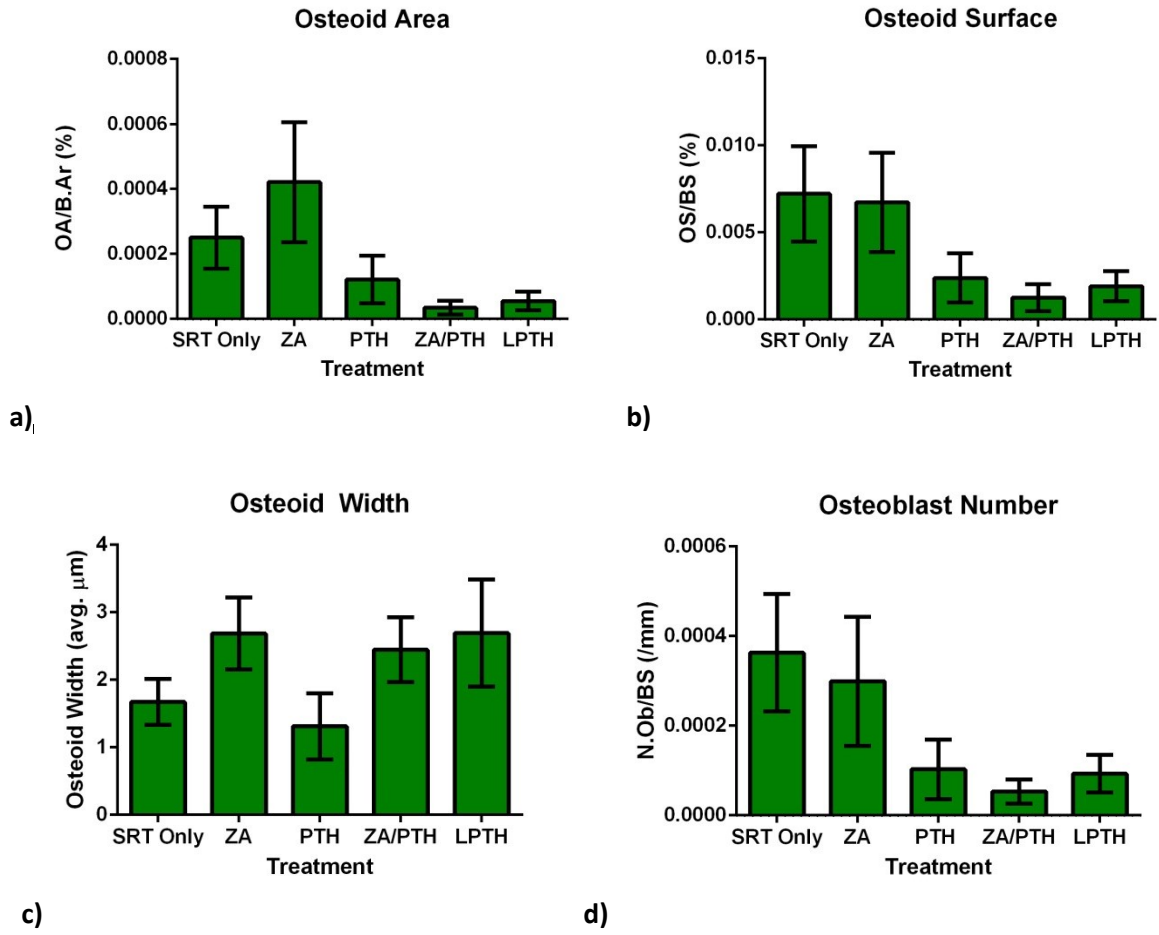


Fig. 29 Osteoid properties including osteoid area (a), osteoid surface (b), osteoid width (c), and osteoblast number (d). Data represent mean (+/- SE) of raw data. There were no significant differences between groups ($p = 0.0636$ (a), 0.1029 (b), 0.2856 (c), & 0.1049 (d)).

Chapter 4

Discussion

Stereotactic radiation therapy has been utilized clinically at Colorado State University's Flint Animal Cancer Center as a limb-sparing technique in the treatment of canine-appendicular osteosarcoma. Although median survival times achieved are similar to those of patients treated with the standard of care (amputation and adjuvant chemotherapy), there remains a high risk of pathologic fracture following radiation treatment. Using an orthotopic model of canine osteosarcoma in athymic rats, we compared four different therapeutic regimens and radiation treatment alone (SRT; SRT plus ZA; SRT plus PTH; SRT plus ZA and PTH; and SRT plus locally-delivered PTH). The treatment effect was characterized in relation to bone microarchitecture, bone quantity, bone strength as well as histological evaluation over the region of interest (distal femoral metaphysis).

The combination therapy (ZA/PTH) resulted in greater total bone volume ($p = 0.0449$) and polar moment of inertia (ANOVA p value = 0.0483) compared to SRT alone based on micro-CT analysis of bone in the region of interest (Fig. 11). Polar moment of inertia has been shown to positively correlate with bone strength in nude rats and is a useful surrogate when mechanical testing cannot be performed (Bagi, Hanson et al. 2006). Individual treatment with PTH or ZA failed to produce statistically significant differences ($p = 0.9938$ & 0.3214 respectively). Static histomorphometry also showed that the combination therapy (ZA/PTH) resulted in statistically significant increases in bone area (Fig. 28).

Due to their differing mechanisms of action, bisphosphonates (which decrease osteoclast-mediated resorption) and parathyroid hormone (a bone anabolic agent) have been studied in combination as their use may result in an additive effect improving bone architecture. Studies that have evaluated combination therapies in relation to osteoporosis have failed to show an increased benefit of this therapy (Gasser, Kneissel et al. 2000; Black, Greenspan et al. 2003; Finkelstein, Hayes et al. 2003; Samadfam, Xia et al. 2007). The benefits of combination therapy have been shown in treatment for disuse osteopenia (Vegger, Nielsen et al. 2014), fracture healing (Li, Zhou et al. 2012), and adjunct treatment following radiation therapy (Arrington, Fisher et al. 2010).

Although the combination treatment group demonstrated the most dramatic treatment effect, this appears largely due to the bisphosphonate. This becomes evident when looking at the data from control contralateral limbs. These represent essentially normal bone that is non-tumor bearing and non-irradiated across all groups. Micro-CT analysis reveals significant increases in bone volume ($p \leq 0.05$) in the ZA treatment group as compared to no treatment controls (Fig. 15). Analysis of the trabecular bone in the contralateral controls reveals a significantly increased trabecular bone volume fraction ($p \leq 0.01$), trabecular number ($p \leq 0.05$) and trabecular thickness ($p \leq 0.01$) in the ZA group (Fig. 16). Although ZA alone appears to substantially affect bone microarchitecture in both control and experimental groups, it was only combination therapy that resulted in significant improvements in the tumor-burdened, irradiated femurs.

The anabolic effect of intermittently administered PTH has been illustrated in many studies leading to FDA approval for high risk osteoporosis treatment (Neer, Arnaud et al. 2001;

Black, Greenspan et al. 2003; Greenspan, Bone et al. 2007). Bone volume fraction, trabecular number, and trabecular thickness tend to be increased with a decrease in trabecular separation (Brouwers, van Rietbergen et al. 2009; Li, Zhou et al. 2012; Chandra, Lan et al. 2013; Vegger, Nielsen et al. 2014). In our study, PTH did not result in this pattern of improved bone microarchitecture when administered on its own (Fig. 11 & 13). The micro-CT analysis of all bone over the region of interest of experimental, tumor-burdened, irradiated femurs resulted in no significant differences from radiation treatment itself (Fig. 11). Control analysis revealed no changes in whole bone or trabecular bone volume fraction (Figs. 15 & 16). Trabecular properties of contralateral controls administered systemic PTH revealed a significant decrease in trabecular number ($p \leq 0.01$) and an increased trabecular thickness ($p \leq 0.01$) and separation ($p \leq 0.01$) (Fig. 16).

The use of immunodeficient animal models for the study of intermittent PTH administration has not been widely described; only one published study could be identified that used athymic rats. In this particular study, the characteristic anabolic bone properties were elicited by PTH administration at a dose twice that used in this study and administered four times daily (as opposed to once-daily dosing) (Bagi, Hanson et al. 2006). This study aimed to illustrate the correlation between micro-CT and mechanical testing which appears to be the reasoning behind the atypically high dose used in most clinically-based rodent PTH studies in immunocompetent animals. There is some evidence supporting the role of T-cells in modulating PTH in a mouse model of hyperparathyroidism (Gao, Wu et al. 2008). It should be noted that we ensured bioactivity of our PTH with an ELISA for cAMP and the analysis from our

control limbs confirms an atypical response. Further work is necessary to elucidate the effectiveness/dose-response of PTH in immunodeficient models, specifically athymic rats.

Currently, bisphosphonates are the first line treatment for osteoporosis and are also used as palliative treatment for metastatic bone disease. Their use stems from their binding affinity for bone mineral and their ability to inhibit osteoclast-mediated bone resorption. Zoledronic acid, a potent, third-generation nitrogen-containing bisphosphonate, demonstrates the strongest inhibitory profile against osteoclasts and the strongest binding affinity in comparison to all other bisphosphonates (Russell, Watts et al. 2008). Our work demonstrated its effect with improved bone architecture in contralateral controls and a decreased TRAP surface in experimental tumor-burdened femora (Figs. 15, 16 & 25). Although, the decreased TRAP surface reflects a reduction in bone turnover there was an increase in bone volume in groups treated with ZA. This is likely due to ZA's indirect effect on the remodeling cycle through osteoclastic inhibition.

A number of recent studies have evaluated the direct and indirect anti-cancer effects of ZA as well as its ability to act as a radiosensitizing agent against tumor cells. Preclinical studies in tumor cell lines have illustrated reduced migration, invasion, adhesion, and proliferation after bisphosphonate treatment. Clinical trials have also reported a reduced risk of new cancer or recurrence in breast and colorectal cancer (Gnant and Clezardin 2012). A number of cell lines, tumoral and non-tumoral, are radiosensitized following ZA administration (Alcaraz, Olivares et al. 2013; Kijima, Koga et al. 2013). Further studies aim to work out the full mechanism of this observation.

Zoledronic acid has already been utilized for the palliative treatment of a number of canine osteolytic tumors. Fan et al. reported the use of ZA in healthy dogs (n = 6) and those exhibiting malignant osteolysis (n = 20). This study reported that ZA administration resulted in bone biologic effects, as evidenced by decreased bone resorption markers as well as subjective pain alleviation in 50% of those dogs treated for osteosarcoma. Repeated administration of ZA, at a dose of 0.25 mg/kg, was also well tolerated with no evidence of toxicity (Fan, de Lorimier et al. 2008). A single case report demonstrated successful palliation for appendicular osteosarcoma over 16 months. This dog was administered a monthly dose of 4mg that was well-tolerated, reduced pain and improved the quality of life for this large breed dog when other treatment options were not pursued (Spugnini, Vincenzi et al. 2009).

Current clinical practices at Colorado State University provide for a single dose (1 mg/kg, IV diluted in 250mls of 0.9% NaCl, administered over 2 hrs) of pamidronate, another nitrogen-containing bisphosphonate, one day prior to the initiation of stereotactic radiation therapy for local treatment of osteosarcoma. Pamidronate is relatively inexpensive and has shown some clinical success in palliation of bone osteolysis. Zoledronic acid has been shown to be superior to pamidronate in humans for the treatment of skeletal complications due to multiple myeloma and hypercalcemia of malignancy (Major, Lortholary et al. 2001; Sanfilippo 2014). In regard to multiple myeloma, ZA was associated with an increased overall survival, decreased skeletal-related events, and may be the preferred bisphosphonate in this context (Sanfilippo 2014). Our study showed improved bone quantity and estimated strength with ZA treatment 8 weeks following stereotactic radiation therapy and may similarly indicate a potential for superior outcomes with zoledronic acid versus pamidronate when treating prior to SRT. Our work also

indicates that there may be a potential benefit of continued dosing of zoledronic acid following stereotactic radiation treatment. At this time, cost may be the most important limiting factor (~24 times more expensive than pamidronate for a single dose in large breed dogs) for the use of ZA. A single dose of pamidronate for a 30kg dog costs approximately \$50 compared to \$1200 for a single 4mg (human recommended dose) dose of zoledronic acid. Further studies to compare the two bisphosphonates directly as well as determining a minimal effective dose are needed. Based on our work, using a total dose of 0.1 mg/kg and the human recommended dose (4mg, or approx.. 0.057 mg/kg in a 70 kg adult), it is likely that a reduced dose, from that already utilized in dogs, would still result in clinical effect.

Stereotactic radiotherapy was delivered successfully and achieved local tumor control in all rats with experimentally induced osteosarcoma of the distal aspect of the femur. Our study resulted in a mean percentage tumor necrosis of 98%. Active osteosarcoma was found in only four subjects, one of which was detected as recurrence by bioluminescence imaging at the study endpoint (251, LPTH group). These subjects still maintained tumor necrosis between 80-90%. A previous study of radiation therapy for dogs with osteosarcoma showed that a mean percentage tumor necrosis of $\geq 80\%$ correlates with excellent local tumor control and an increase in survival rate (Powers, Withrow et al. 1991) Short-term effects of radiation on the skin were acceptable (Grade 1, VRTOG) with none requiring treatment (LaDue and Klein 2001). Those rats that were only treated with radiation therapy showed no signs of progressive disease and their loss of luciferase activity further highlighted the success of treatment achieving local control. Previous work with this model showed that if left untreated local

progression would lead to fracture around 5 weeks post-inoculation (Schwartz, Custis et al. 2013).

While the deleterious effects of radiation on bone have been described, there is very little reported information cataloguing the effects of stereotactic radiation therapy on bone (higher dose per fraction/fewer fractions). We were able to qualitatively assess the femurs 8 weeks following radiation at study endpoint. As expected, we found a severely reduced, but present population of hematopoietic cells in the marrow cavity. Osteoblasts, osteoclasts, and osteocytes, appear subjectively reduced in number as well. Dynamic histomorphometry revealed single and double-labeling of surfaces across all treatment groups. This is of interest as there remains some level of active mineralization occurring at the study endpoint. The cortical bone remains viable to a large extent with less than 25% of the diaphyseal cortical bone exhibiting signs of necrosis in 41% of experimental subjects. 51% of subjects showed no evidence of cortical necrosis. Although radiation may cause long term effects not yet seen in this study (continued necrosis, fibrosis, vascular damage), these findings indicate a potential window of time where therapeutic interventions may be of benefit in regard to bone healing and regeneration.

There are some limitations in this study that need to be addressed. First, there was some variability in tumor severity at the initiation of treatment. Although this orthotopic model allows for control in timing, location and number of tumor cells delivered we noted variation in progression. Radiographic analysis confirmed that no groups had significantly different grades of tumor severity at the time of treatment. Despite this, in vivo micro-CT analysis may provide a more accurate assessment for standardizing tumor severity at the time of treatment. This

would allow for an individualized treatment approach relating starting severity with response to treatment. Secondly, our model successfully created tumor-associated osteolysis at the distal metaphyseal region of the femur; however, due to our inoculation technique (proximal to distal) a small number of cells were deposited at more proximal locations of the femur. This typically did not result in visible osteolysis at other locations, but the presence of tumor cells was confirmed via histologic examination. We controlled for this by including the entire femur as our gross tumor volume in radiation planning regardless if there was evidence or not of osteolysis at other locations of the femur.

Overall, the combined treatment (ZA/PTH) improved bone microarchitecture, quantity and a surrogate measure of bone strength following stereotactic radiation therapy in comparison to radiation treatment alone. These properties support a reduction in fracture risk and showed therapeutic benefit eight weeks following radiation. Our data indicate this result was largely due to zoledronic acid, a potent anti-resorptive, however we showed a beneficial effect of combined therapy. Zoledronic acid is therefore a promising therapeutic for decreasing bone pain due to lysis, improving bone microarchitecture and strength, and reducing fracture risk in canine patients undergoing stereotactic radiation therapy for the local treatment of canine-appendicular osteosarcoma. Further studies are needed to characterize its effect compared to other bisphosphonates as well as its appropriate dosing regimens to maximize effect and reduce cost. This work also illustrates the success of stereotactic radiation therapy in achieving local tumor control and a potential therapeutic window of opportunity. Longitudinal studies of the long term effect of high dose radiation on bone will be important as the clinical benefits of stereotactic radiation therapy expand its application.

References

- Akcaý, T., S. Turan, et al. (2008). "Alendronate treatment in children with osteogenesis imperfecta." Indian Pediatr **45**(2): 105-109.
- Alcaraz, M., A. Olivares, et al. (2013). "Zoledronic acid and radiation: toxicity, synergy or radiosensitization?" Clin Transl Oncol **15**(4): 300-306.
- Andrews, E. B., A. W. Gilsenan, et al. (2012). "The US postmarketing surveillance study of adult osteosarcoma and teriparatide: Study design and findings from the first 7 years." Journal of Bone and Mineral Research **27**(12): 2429-2437.
- Arcangeli, S., M. Scorsetti, et al. (2012). "Will SBRT replace conventional radiotherapy in patients with low-intermediate risk prostate cancer? A review." Crit Rev Oncol Hematol **84**(1): 101-108.
- Arrighi, I., S. Mark, et al. (2009). "Bone healing induced by local delivery of an engineered parathyroid hormone prodrug." Biomaterials **30**(9): 1763-1771.
- Arrington, S. A., E. R. Fisher, et al. (2010). "Anabolic and antiresorptive drugs improve trabecular microarchitecture and reduce fracture risk following radiation therapy." Calcif Tissue Int **87**(3): 263-272.
- Aspenberg, P. and T. Johansson (2010). "Teriparatide improves early callus formation in distal radial fractures." Acta Orthop **81**(2): 234-236.
- Bagi, C. M., N. Hanson, et al. (2006). "The use of micro-CT to evaluate cortical bone geometry and strength in nude rats: correlation with mechanical testing, pQCT and DXA." Bone **38**(1): 136-144.
- Bashutski, J. D., R. M. Eber, et al. (2010). "Teriparatide and osseous regeneration in the oral cavity." N Engl J Med **363**(25): 2396-2405.
- Baxter, N. N., E. B. Habermann, et al. (2005). "Risk of pelvic fractures in older women following pelvic irradiation." JAMA **294**(20): 2587-2593.
- Bielack, S., D. Carrle, et al. (2008). "Osteosarcoma: ESMO clinical recommendations for diagnosis, treatment and follow-up." Annals of Oncology **19**: 94-96.
- Black, D. M., S. R. Cummings, et al. (1996). "Randomised trial of effect of alendronate on risk of fracture in women with existing vertebral fractures. Fracture Intervention Trial Research Group." Lancet **348**(9041): 1535-1541.
- Black, D. M., S. L. Greenspan, et al. (2003). "The effects of parathyroid hormone and alendronate alone or in combination in postmenopausal osteoporosis." N Engl J Med **349**(13): 1207-1215.
- Broadhead, M. L., J. C. Clark, et al. (2011). "The molecular pathogenesis of osteosarcoma: a review." Sarcoma **2011**: 959248.
- Brouwers, J. E., B. van Rietbergen, et al. (2009). "Effects of PTH treatment on tibial bone of ovariectomized rats assessed by in vivo micro-CT." Osteoporos Int **20**(11): 1823-1835.
- Brown, R. K., R. R. Pelker, et al. (1991). "Postfracture irradiation effects on the biomechanical and histologic parameters of fracture healing." J Orthop Res **9**(6): 876-882.
- Chan, H. L. and L. K. McCauley (2013). "Parathyroid hormone applications in the craniofacial skeleton." J Dent Res **92**(1): 18-25.
- Chandra, A., S. Lan, et al. (2013). "PTH prevents the adverse effects of focal radiation on bone architecture in young rats." Bone **55**(2): 449-457.
- Chang, B. K. and R. D. Timmerman (2007). "Stereotactic body radiation therapy: a comprehensive review." Am J Clin Oncol **30**(6): 637-644.
- Cheng, M. L. and V. Gupta (2012). "Teriparatide - Indications beyond osteoporosis." Indian J Endocrinol Metab **16**(3): 343-348.

- Clezardin, P. (2011). "Bisphosphonates' antitumor activity: an unravelled side of a multifaceted drug class." Bone **48**(1): 71-79.
- Coetzee, M. and M. C. Kruger (2004). "Osteoprotegerin-receptor activator of nuclear factor-kappaB ligand ratio: a new approach to osteoporosis treatment?" South Med J **97**(5): 506-511.
- Conill, C., X. Tomas, et al. (2007). "Pathological femur fracture secondary to radiation therapy for soft tissue sarcoma." Clin Transl Oncol **9**(8): 537-539.
- Coomer, A., J. Farese, et al. (2009). "Radiation therapy for canine appendicular osteosarcoma." Vet Comp Oncol **7**(1): 15-27.
- Cusano, N. E., M. R. Rubin, et al. (2013). "Therapy of hypoparathyroidism with PTH(1-84): a prospective four-year investigation of efficacy and safety." J Clin Endocrinol Metab **98**(1): 137-144.
- Cusano, N. E., M. R. Rubin, et al. (2012). "Mini-review: new therapeutic options in hypoparathyroidism." Endocrine **41**(3): 410-414.
- Custis, J. (2014). Communication regarding curative-intent stereotactic radiation therapy for the treatment of canine osteosarcoma. R. Curtis. Fort Collins, CO.
- Donahue, S. W., S. A. Galley, et al. (2006). "Parathyroid hormone may maintain bone formation in hibernating black bears (*Ursus americanus*) to prevent disuse osteoporosis." J Exp Biol **209**(Pt 9): 1630-1638.
- Donahue, S. W., M. E. McGee, et al. (2006). "Hibernating bears as a model for preventing disuse osteoporosis." J Biomech **39**(8): 1480-1488.
- Drake, M. T., B. L. Clarke, et al. (2008). "Bisphosphonates: mechanism of action and role in clinical practice." Mayo Clin Proc **83**(9): 1032-1045.
- Elliott, S. P., S. L. Jarosek, et al. (2011). "Three-dimensional external beam radiotherapy for prostate cancer increases the risk of hip fracture." Cancer **117**(19): 4557-4565.
- Fan, T. M. (2010). "Animal models of osteosarcoma." Expert Rev Anticancer Ther **10**(8): 1327-1338.
- Fan, T. M., L. P. de Lorimier, et al. (2008). "The bone biologic effects of zoledronate in healthy dogs and dogs with malignant osteolysis." J Vet Intern Med **22**(2): 380-387.
- Farese, J. P., R. Milner, et al. (2004). "Stereotactic radiosurgery for treatment of osteosarcomas involving the distal portions of the limbs in dogs." J Am Vet Med Assoc **225**(10): 1567-1572, 1548.
- Federman, N., N. Bernthal, et al. (2009). "The Multidisciplinary Management of Osteosarcoma." Current Treatment Options in Oncology **10**(1-2): 82-93.
- Finkelstein, J. S., A. Hayes, et al. (2003). "The effects of parathyroid hormone, alendronate, or both in men with osteoporosis." N Engl J Med **349**(13): 1216-1226.
- Fleisch, H., R. G. Russell, et al. (1966). "Effect of pyrophosphate on hydroxyapatite and its implications in calcium homeostasis." Nature **212**(5065): 901-903.
- Flint, A. F., L. U'Ren, et al. (2004). "Overexpression of the erbB-2 proto-oncogene in canine osteosarcoma cell lines and tumors." Vet Pathol **41**(3): 291-296.
- Frith, J. C., J. Mönkkönen, et al. (1997). "Clodronate and Liposome-Encapsulated Clodronate Are Metabolized to a Toxic ATP Analog, Adenosine 5'-(β,γ -Dichloromethylene) Triphosphate, by Mammalian Cells In Vitro." Journal of Bone and Mineral Research **12**(9): 1358-1367.
- Fuerst, A., S. Derungs, et al. (2007). "Use of a parathyroid hormone peptide (PTH1-34)-enriched fibrin hydrogel for the treatment of a subchondral cystic lesion in the proximal interphalangeal joint of a warmblood filly." Journal of Veterinary Medicine Series a-Physiology Pathology Clinical Medicine **54**(2): 107-112.
- Gao, Y., X. Wu, et al. (2008). "T cells potentiate PTH-induced cortical bone loss through CD40L signaling." Cell Metab **8**(2): 132-145.
- Gasser, J. A., M. Kneissel, et al. (2000). "PTH and interactions with bisphosphonates." J Musculoskeletal Neuronal Interact **1**(1): 53-56.

- Gnant, M. and P. Clezardin (2012). "Direct and indirect anticancer activity of bisphosphonates: a brief review of published literature." Cancer Treat Rev **38**(5): 407-415.
- Gnant, M., B. Mlineritsch, et al. (2009). "Endocrine therapy plus zoledronic acid in premenopausal breast cancer." N Engl J Med **360**(7): 679-691.
- Gnant, M., B. Mlineritsch, et al. (2011). "Adjuvant endocrine therapy plus zoledronic acid in premenopausal women with early-stage breast cancer: 62-month follow-up from the ABCSG-12 randomised trial." Lancet Oncol **12**(7): 631-641.
- Gorman, E., A. M. Barger, et al. (2006). "Cutaneous metastasis of primary appendicular osteosarcoma in a dog." Vet Clin Pathol **35**(3): 358-361.
- Gray, S. K. (2012). Treatment of Osteoporosis in a Mouse Model of Duchenne Muscular Dystrophy Using Black Bear Parathyroid Hormone. Mechanical Engineering, Michigan Technological University. **Master of Science: 111.**
- Gray, S. K., M. E. McGee-Lawrence, et al. (2012). "Black bear parathyroid hormone has greater anabolic effects on trabecular bone in dystrophin-deficient mice than in wild type mice." Bone **51**(3): 578-585.
- Green, J. and P. Clezardin (2010). "The molecular basis of bisphosphonate activity: a preclinical perspective." Semin Oncol **37** **Suppl 1**: S3-11.
- Greenspan, S. L., H. G. Bone, et al. (2007). "Effect of recombinant human parathyroid hormone (1-84) on vertebral fracture and bone mineral density in postmenopausal women with osteoporosis: a randomized trial." Ann Intern Med **146**(5): 326-339.
- Hall, E. J. and A. J. Giaccia (2012). Radiobiology for the Radiologist, Wolters Kluwer Health.
- Harper, K. D., J. H. Kregel, et al. (2007). "Osteosarcoma and teriparatide?" J Bone Miner Res **22**(2): 334.
- Hess, G., A. Barlev, et al. (2012). "Cost of palliative radiation to the bone for patients with bone metastases secondary to breast or prostate cancer." Radiat Oncol **7**: 168.
- Hiraga, T., P. J. Williams, et al. (2004). "Zoledronic acid inhibits visceral metastases in the 4T1/luc mouse breast cancer model." Clin Cancer Res **10**(13): 4559-4567.
- Hodsman, A. B., D. A. Hanley, et al. (2003). "Efficacy and safety of human parathyroid hormone-(1-84) in increasing bone mineral density in postmenopausal osteoporosis." J Clin Endocrinol Metab **88**(11): 5212-5220.
- Hopewell, J. W. (2003). "Radiation-therapy effects on bone density." Med Pediatr Oncol **41**(3): 208-211.
- Hu, X., A. X. Yu, et al. (2010). "The expression and significance of IDH1 and p53 in osteosarcoma." J Exp Clin Cancer Res **29**: 43.
- Hubner, W., A. Blume, et al. (2005). "The influence of X-ray radiation on the mineral/organic matrix interaction of bone tissue: an FT-IR microscopic investigation." Int J Artif Organs **28**(1): 66-73.
- Jegoux, F., O. Malard, et al. (2010). "Radiation effects on bone healing and reconstruction: interpretation of the literature." Oral Surg Oral Med Oral Pathol Oral Radiol Endod **109**(2): 173-184.
- Jhaveri, P., B. S. Teh, et al. (2008). "Stereotactic body radiotherapy in the management of painful bone metastases." Oncology (Williston Park) **22**(7): 782-788; discussion 788-789, 796-787.
- Jing, D., J. Cai, et al. (2014). "Pulsed Electromagnetic Fields Partially Preserve Bone Mass, Microarchitecture, and Strength by Promoting Bone Formation in Hindlimb-Suspended Rats." J Bone Miner Res.
- Jolette, J., C. E. Wilker, et al. (2006). "Defining a noncarcinogenic dose of recombinant human parathyroid hormone 1-84 in a 2-year study in Fischer 344 rats." Toxicol Pathol **34**(7): 929-940.
- Jung, R. E., D. L. Cochran, et al. (2007). "The effect of matrix bound parathyroid hormone on bone regeneration." Clin Oral Implants Res **18**(3): 319-325.
- Kang, S. Y., S. S. Deshpande, et al. (2013). "Parathyroid hormone reverses radiation induced hypovascularity in a murine model of distraction osteogenesis." Bone **56**(1): 9-15.

- Kavanagh, B. D. and R. D. Timmerman (2005). Stereotactic Body Radiation Therapy, Lippincott Williams & Wilkins.
- Kemper, M. (2003). "Screeningversuch zur Optimierung synthetischer und fibriner Hydrogele als dreidimensionale Tragersubstanz für Bone Morphogenetic Protein, Transforming Growth Factor Beta und Parathormon zur Beschleunigung der Knochenheilung. Dissertation."
- Kijima, T., F. Koga, et al. (2013). "Zoledronic acid sensitizes renal cell carcinoma cells to radiation by downregulating STAT1." PLoS One **8**(5): e64615.
- Koh, A. J., C. M. Novince, et al. (2011). "An irradiation-altered bone marrow microenvironment impacts anabolic actions of PTH." Endocrinology **152**(12): 4525-4536.
- Ladue, T. and M. K. Klein (2001). "Toxicity criteria of the veterinary radiation therapy oncology group." Vet Radiol Ultrasound **42**(5): 475-476.
- Lane, A., M. Black, et al. (2012). "Toxicity and efficacy of a novel doxorubicin and carboplatin chemotherapy protocol for the treatment of canine appendicular osteosarcoma following limb amputation." Aust Vet J **90**(3): 69-74.
- Li, Y. F., C. C. Zhou, et al. (2012). "The effects of combined human parathyroid hormone (1-34) and zoledronic acid treatment on fracture healing in osteoporotic rats." Osteoporos Int **23**(4): 1463-1474.
- Liberman, U. A., S. R. Weiss, et al. (1995). "Effect of oral alendronate on bone mineral density and the incidence of fractures in postmenopausal osteoporosis. The Alendronate Phase III Osteoporosis Treatment Study Group." N Engl J Med **333**(22): 1437-1443.
- Linz, U. (2012). Ion Beam Therapy: Fundamentals, Technology, Clinical Applications, Springer Berlin Heidelberg.
- Longhi, A., A. Pasini, et al. (2005). "Height as a risk factor for osteosarcoma." Journal of Pediatric Hematology/Oncology **27**(6): 314-318.
- MacEwen, E. G., J. Kutzke, et al. (2003). "c-Met tyrosine kinase receptor expression and function in human and canine osteosarcoma cells." Clin Exp Metastasis **20**(5): 421-430.
- Major, P., A. Lortholary, et al. (2001). "Zoledronic acid is superior to pamidronate in the treatment of hypercalcemia of malignancy: a pooled analysis of two randomized, controlled clinical trials." Journal of Clinical Oncology **19**(2): 558-567.
- McGee-Lawrence, M. E., H. V. Carey, et al. (2008). "Mammalian hibernation as a model of disuse osteoporosis: the effects of physical inactivity on bone metabolism, structure, and strength." Am J Physiol Regul Integr Comp Physiol **295**(6): R1999-2014.
- McGee-Lawrence, M. E., S. J. Wojda, et al. (2009). "Six months of disuse during hibernation does not increase intracortical porosity or decrease cortical bone geometry, strength, or mineralization in black bear (*Ursus americanus*) femurs." J Biomech **42**(10): 1378-1383.
- McGee-Lawrence, M. E., S. J. Wojda, et al. (2009). "Grizzly bears (*Ursus arctos horribilis*) and black bears (*Ursus americanus*) prevent trabecular bone loss during disuse (hibernation)." Bone **45**(6): 1186-1191.
- Mitchell, M. J. and P. M. Logan (1998). "Radiation-induced changes in bone." Radiographics **18**(5): 1125-1136; quiz 1242-1123.
- Morello, E., M. Martano, et al. (2011). "Biology, diagnosis and treatment of canine appendicular osteosarcoma: similarities and differences with human osteosarcoma." Vet J **189**(3): 268-277.
- Mueller, F., B. Fuchs, et al. (2007). "Comparative biology of human and canine osteosarcoma." Anticancer Res **27**(1A): 155-164.
- Neer, R. M., C. D. Arnaud, et al. (2001). "Effect of parathyroid hormone (1-34) on fractures and bone mineral density in postmenopausal women with osteoporosis." N Engl J Med **344**(19): 1434-1441.

- Neuprez, A. and J. Y. Reginster (2008). "Bone-forming agents in the management of osteoporosis." Best Pract Res Clin Endocrinol Metab **22**(5): 869-883.
- Ng, A. J., A. J. Mutsaers, et al. (2012). "Genetically engineered mouse models and human osteosarcoma." Clin Sarcoma Res **2**(1): 19.
- O'Donoghue, L. E., J. P. Rivest, et al. (2011). "Polymerase chain reaction-based species verification and microsatellite analysis for canine cell line validation." J Vet Diagn Invest **23**(4): 780-785.
- O'Loughlin, P. F., M. E. Cunningham, et al. (2009). "Parathyroid hormone (1-34) augments spinal fusion, fusion mass volume, and fusion mass quality in a rabbit spinal fusion model." Spine (Phila Pa 1976) **34**(2): 121-130.
- Pallan, S., M. O. Rahman, et al. (2012). "Diagnosis and management of primary hyperparathyroidism." BMJ **344**: e1013.
- Powers, B. E., S. J. Withrow, et al. (1991). "Percent tumor necrosis as a predictor of treatment response in canine osteosarcoma." Cancer **67**(1): 126-134.
- Ritter, J. and S. S. Bielack (2010). "Osteosarcoma." Ann Oncol **21 Suppl 7**: vii320-325.
- Rosen, C. J., Drezner M.K., Mulder, J.E. (2013). "Parathyroid Hormone Therapy for Osteoporosis." from <http://www.uptodate.com/contents/parathyroid-hormone-therapy-for-osteoporosis>.
- Rubery, P. T. and S. V. Bukata (2010). "Teriparatide may accelerate healing in delayed unions of type III odontoid fractures: a report of 3 cases." J Spinal Disord Tech **23**(2): 151-155.
- Rubin, M. R., F. Cosman, et al. (2002). "The anabolic effects of parathyroid hormone." Osteoporos Int **13**(4): 267-277.
- Russell, R. G. (2006). "Bisphosphonates: from bench to bedside." Ann N Y Acad Sci **1068**: 367-401.
- Russell, R. G., N. B. Watts, et al. (2008). "Mechanisms of action of bisphosphonates: similarities and differences and their potential influence on clinical efficacy." Osteoporos Int **19**(6): 733-759.
- Russell, R. G., Z. Xia, et al. (2007). "Bisphosphonates: an update on mechanisms of action and how these relate to clinical efficacy." Ann N Y Acad Sci **1117**: 209-257.
- Russinoff, S., S. Miran, et al. (2011). "Osteosarcoma cells differentiate into phenotypes from all three dermal layers." Clin Orthop Relat Res **469**(10): 2895-2904.
- Samadfam, R., Q. Xia, et al. (2007). "Pretreatment with anticatabolic agents blunts but does not eliminate the skeletal anabolic response to parathyroid hormone in oophorectomized mice." Endocrinology **148**(6): 2778-2787.
- Sanfilippo, K. G., B. Luo, S. Weilbaecher, K. Tomasson, M. Vij, R. Colditz, G. Carson, K. (2014). "Comparative Effectiveness on Survival of Zoledronic Acid versus Pamidronate in Multiple Myeloma." Leukemia and Lymphoma.
- Schaln-Jantti, C., E. Mornet, et al. (2010). "Parathyroid hormone treatment improves pain and fracture healing in adult hypophosphatasia." J Clin Endocrinol Metab **95**(12): 5174-5179.
- Schwartz, A. L., J. T. Custis, et al. (2013). "Orthotopic model of canine osteosarcoma in athymic rats for evaluation of stereotactic radiotherapy." Am J Vet Res **74**(3): 452-458.
- Schwartz, A. 2013. Mesenchymel Stem Cell Rescue for Bone Formation Following Stereotactic Radiotherapy for Osteosarcoma. Biomedical Engineering. Colorado State University. **Dissertation: 46.**
- Shaheen, M., B. M. Deheshi, et al. (2006). "Prognosis of radiation-induced bone sarcoma is similar to primary osteosarcoma." Clin Orthop Relat Res **450**: 76-81.
- Siclari, V. A. and L. Qin (2010). "Targeting the osteosarcoma cancer stem cell." J Orthop Surg Res **5**: 78.
- Sottnik, J. L., D. L. Duval, et al. (2010). "An orthotopic, postsurgical model of luciferase transfected murine osteosarcoma with spontaneous metastasis." Clin Exp Metastasis **27**(3): 151-160.
- Spugnini, E. P., B. Vincenzi, et al. (2009). "Zoledronic acid for the treatment of appendicular osteosarcoma in a dog." J Small Anim Pract **50**(1): 44-46.

- Stone, H. B., C. N. Coleman, et al. (2003). "Effects of radiation on normal tissue: consequences and mechanisms." Lancet Oncol **4**(9): 529-536.
- Subbiah, V., V. S. Madsen, et al. (2010). "Of mice and men: divergent risks of teriparatide-induced osteosarcoma." Osteoporos Int **21**(6): 1041-1045.
- Takata, S. and N. Yasui (2001). "Disuse osteoporosis." J Med Invest **48**(3-4): 147-156.
- Vahle, J. L., G. G. Long, et al. (2004). "Bone neoplasms in F344 rats given teriparatide [rhPTH(1-34)] are dependent on duration of treatment and dose." Toxicol Pathol **32**(4): 426-438.
- Vahle, J. L., M. Sato, et al. (2002). "Skeletal changes in rats given daily subcutaneous injections of recombinant human parathyroid hormone (1-34) for 2 years and relevance to human safety." Toxicol Pathol **30**(3): 312-321.
- Vegger, J. B., E. S. Nielsen, et al. (2014). "Additive effect of PTH (1-34) and zoledronate in the prevention of disuse osteopenia in rats." Bone.
- Vigorita, V. J., Ed. (2008). Orthopaedic Pathology. Philadelphia, PA, USA., Lippincott, Williams, and Wilkins.
- Winer, K. K., J. A. Yanovski, et al. (1996). "Synthetic human parathyroid hormone 1-34 vs calcitriol and calcium in the treatment of hypoparathyroidism." JAMA **276**(8): 631-636.
- Winer, K. K., J. A. Yanovski, et al. (1998). "A randomized, cross-over trial of once-daily versus twice-daily parathyroid hormone 1-34 in treatment of hypoparathyroidism." J Clin Endocrinol Metab **83**(10): 3480-3486.
- Winter, M. C., I. Holen, et al. (2008). "Exploring the anti-tumour activity of bisphosphonates in early breast cancer." Cancer Treat Rev **34**(5): 453-475.
- Withrow, S. J. and C. Khanna (2009). "Bridging the gap between experimental animals and humans in osteosarcoma." Cancer Treat Res **152**: 439-446.
- Withrow, S. J. and R. M. Wilkins (2010). "Cross talk from pets to people: translational osteosarcoma treatments." ILAR J **51**(3): 208-213.

Appendix I

SOPs

5-11: SOP- Abrams OSA

Protocol Used by: Sara Gookin

Time to Complete: 30-60 minutes/day

Supplies Required	Supplier and Catalog Number	Storage Conditions	Location
Minimum Essential Media 1X with Earle's Salt and L-glutamine	Cellgro (Fisher) 10-010-CV	4°C	Fridge
Antibiotic Penn-Strep? (ask Laura)	VWR 45000-652		Fridge
MEM essential amino acids (50X)	Cellgro (Fisher) 25-030-CI	4°C	Fridge
MEM non-essential amino acids (100X)	Gibco 11140-050	4°C	Fridge
Sodium Bicarbonate 7.5%	Cellgro (Fisher) 25-035-CI	4°C	Fridge
FBS (Characterized)	VWR 16777-014	4°C	-20°C

Additional Supplies Required:

Pipet Aid (Hood)
Centrifuge
CO₂ incubator at 37°C
Serological Pipettes (5, 10, 25 mL)

Sterile media bottle (100 ml, 250 ml, 1000 ml)
 15 and/or 50 ml Centrifuge Tubes (BD Falcon)
 Corning TC Flask (#430641)

General Notes:

- All materials used must be sterile.
- Warm all solutions except PBS in a water bath to 37°C prior to use.
- Grow cells to 70-80% confluent before splitting. It is important not to allow cells to be too over or under confluent.

Procedure:

1. Growing Cells

- Perform all steps in a laminar flow hood
- Prepare Growth Media

%	Item	Amount for 500mL
	MEM 1X with Earle's Salt and L-glutamine	430mL
10%	Fetal Bovine Serum	50mL
1%	Anitibiotic-Antimycotic (100X)	5mL
0.5%	MEM essential amino acids (50X)	5mL
1%	MEM Non-essential amino acids (100X)	5mL
0.075%	Sodium Bicarbonate 7.5%	5mL

- Sterile Filter after mixing everything together
- Keep at 4°C for about a month

2. Thaw Cells

- a. Wear eye protection, if cryogenic vials have not been tightly sealed they may contain liquid nitrogen and this may cause bursting. Also, wear ultra-low temp gloves.
- b. Remove vial
- c. Place immediately in 37°C water bath and allow to thaw completely ~2min
- d. Spray vial with 70% EtOH and place in biosafety cabinet
- e. Transfer cells to culture dish
- f. Add media gradually
 - i. 15mL media to a T75
- g. Place in 37°C + 5%CO₂ Incubator

3. Growing Cells

- a. From Frozen Stock: grow O/N and replace media within 24hours (Feed Cells)
- b. If confluent, split cells

4. Split Cells

- a. Remove media
- b. Wash with 5mL PBS
- c. Add 2mL Trypsin-EDTA
- d. Let sit for 5min, check with microscope to see if all the cells detached
- e. Add 4mL Growth Media to deactivate Trypsin
- f. Transfer to a 14mL Falcon Tube
 - i. Remove 50µL to epp for counting cells
- g. Centrifuge 1200rpm, 5-10min, RT
- h. Remove Supernatant
- i. Split accordingly

5. Cell Count

- a. Invitrogen Countess Cell Counter
 - i. Mix 50µL Trypan Blue + 50µL Cells (not sterile) in epp
 1. 0.4% Trypan Blue
 - ii. Open cell counting chamber
 - iii. Add 10µL of mixture to side A & B on chamber
 1. Pipette up and down to make sure mixture is equally distributed

- iv. Insert slide chamber into the Countess Cell Counter
 - v. Adjust Focus
 - vi. Count Cells
- b. Hemocytometer
- i. Affix cover slip
 - ii. Mix equal volumes of 0.4% Trypan Blue and Cells
 - 1. 50µl Trypan Blue + 50µl Cells
 - iii. Load 10µl into each side of Hemocytometer
 - iv. Count Cells
 - 1. Four outer corners: take the average of those cells $(A+B+C+D)/4$
 - v. Average x Dilution Factor (2, because 1:1 dilution with trypan) x 10,000 = cells/ml
6. Repeat growth, counting and splitting of cells
- a. Confluency should be 70-80% before splitting

7. Freeze Cells

- a. Freeze Media

%	Item	Amount for 10mL
45%	MEM 1X w/Earle's salt and L-glutamine	22.5mL
45%	FBS	22.5mL
10%	DMSO	5mL

- b. Centrifuge Cells
 - i. 1200rpm, 10', RT
- c. Remove Media
- d. Resuspend Pellet in Freeze Media
 - i. Depends on how many cells
 - ii. Want 1-2million cells/cryovial
 - iii. Write the cell line, passage number, date and your initials on the cryogenic tube
- e. Place in Nalgene Mr. Frosty

- i. Directions for Mr. Frosty are in Lab
 - ii. Place in -80°C Over Night
- f. Remove Mr. Frosty and Transfer to Liquid Nitrogen Tank for Long Term Storage

IF LUCIFERASE EXPRESSING

1. Add D-Luciferin to cells (want 150mg/ml)
 - a. T75 – add $75\mu\text{L}$
 - b. T25 – add $25\mu\text{L}$
2. Let sit for 10min before imaging
3. Imaging System
 - a. Open
 - i. Administrator (No Password)
 - b. Initialize
 - c. Field of View –
 - i. A: For T25 or T75 flask
 - ii. B: For T125 or larger
 - d. Start with AUTO or 1:00min exposure
 - e. If no glow, increase the time
 - f. If too much glow, decrease the time
 - g. Binning: Medium
 - h. Temperature Bar: should be green before you are able to image
 - i. DON'T open the door unless it Reads IDLE
 - i. Ready
 - j. Acquire
 - k. Yes, on pop up screen (background problem)
 - i. Wait for the 1min exposure and results will pop up on the screen

9-11: bbPTH Reconstitution for Rat's

Protocol Used by:

Supplies Required	Supplier and Catalog Number	Storage Conditions	Location
0.9% Sodium Chloride	Central Supplies	RT	Laura's Lab
bbPTH		-80°C	Freezer
Filter 0.2µm		RT	
HCl		RT	Chemical Cabinet
Insulin Syringe	309301	RT	Drawer
Rat's			
Eppendorfs 1.5ml		RT	
Falcon Tubes 50ml		RT	

General Notes:

- Administer Injections at the same time each day
- Record individual injections
 - Bent Needles
 - Volume administered in two partial doses
- Keep reconstituted bbPTH on ICE – bring ice bucket to mouse room
- Use Laura's Mouse Scale to weigh rat's once a week

Acidic Saline (50ml's)

0.9% NaCl + 0.001N HCl

1. Measure out 50ml's of 0.9% Sodium Chloride
 - a. 0.9% Sodium Chloride = 0.154M NaCl
2. Sterile Filter (0.2 μ m) in Biosafety Cabinet
3. Add 0.001N HCl to 50ml's of 0.9% Sodium Chloride in Biosafety Cabinet
 - a. HCl: 12.1N
 - b. $(50\text{ml})(0.001\text{N}) = (X)(12.1\text{N})$
 $X = 0.0041\text{ml}$ or 4.1 μ l

Black Bear PTH

Lyophilized from PBS

01/05/2011

0.566mg

9444.7g/mol

Reconstitute

1. Reconstitute the bbPTH to a concentration of 1mg/ml
 - a. $566\mu\text{g}/566\mu\text{l}$ acidic saline = $1\mu\text{g}/\mu\text{l}$ = 1mg/ml
2. Remove bbPTH from -80°C
3. Let thaw at RT for 15min
4. Centrifuge vial to collect the lyophilized powder to the bottom of the tube
5. *In Biosafety cabinet* for remaining steps
6. Add 566 μ l of Sterile acidic saline to vial containing 566 μ g of bbPTH
 - a. Vortex
 - b. Centrifuge
7. Transfer 100 μ l of the reconstituted bbPTH Sol'n into five Sterile 1.5ml epps
 - a. 100 μ l = 100 μ g
8. Immediately freeze aliquots of bbPTH Sol'n at -80°C

Animal Dose

Dose: 100 μ g/kg

*Keep everything on ICE

1. Remove aliquoted bbPTH (1mg/ml) from -80°C
 - a. Allow to thaw on ice
 - b. Centrifuge before opening
2. Dilute bbPTH to a concentration of 0.1µg/µl solution of bbPTH

*100µl bbPTH (1mg/ml) + 900µl acidic saline = 0.1µg/µl

3. Add 900µl of acidic saline to our aliquoted 100µl of bbPTH (1mg/ml)
 - a. Mix/vortex
4. Rat Dose
$$\frac{100\mu\text{g}}{\text{kg}} \times \frac{(\text{Rat})\text{kg}}{0.1\mu\text{g}} \times \frac{\mu\text{l}}{1} = \mu\text{l Injection Amount}$$
5. Weigh the Rat's once a week and recalculate the injection amount (ml) for each mouse
6. Examples

ID	Weight (kg)	Injection Amount(µl)
95	0.125	125
63	0.140	140

7. Fill Insulin Syringes with calculated amount of bbPTH
8. Inject bbPTH Subcutaneously

Vetrigel

*2 people necessary

1. Anesthetize Rat
2. Shave
3. Clean (3 hibiclens + 3 70% EtOH)
4. Ryan places first needle on both Rat's
5. Run Heparin through 2nd Needle's
6. Place 2nd Needle's
7. Vetrigel
 - a. Use Liquid syringe **A** to reconstitute bbPTH 1-84
 - i. Remove 2 vials of bbPTH 1-84 from -80°C

- ii. Thaw at RT for 15min
- iii. Centrifuge
- iv. Attach a needle to syringe A and resuspend PTH
- v. Centrifuge vials before placing back in syringe A

Dose: 100 μ g

$(566\mu\text{g} \times 2 \text{ Vials}) / 500\mu\text{l} = 2.264\mu\text{l}/\mu\text{l}$

100 μ g = 44 μ l

- b. Connect Syringe A to B
- c. Push all of liquid into powder and slowly mix Back and Fourth
Mixing Time
0'' – Begin slowly
30'' – Transition slow to fast
60'' – DONE (~30 Cycles)

*Leave in Syringe A

- d. Two drops in sterile Petri Dish
- e. Two Syringes with Needles

Load: 0.1ml of Vetrigel in each syringe

- f. Remove Needle from syringe's
- g. Connect to Rat with Needle
- h. Inject Slowly

9-12: ZA Reconstitution for Rat's

Protocol Used by:

Supplies Required	Supplier and Catalog Number	Storage Conditions	Location
0.9% Sodium Chloride	Central Supplies	RT	Laura's Lab
bbPTH		-80°C	Freezer
Filter 0.2µm		RT	
HCl		RT	Chemical Cabinet
Insulin Syringe	309301	RT	Drawer
Rat's			
Eppendorfs 1.5ml		RT	
Falcon Tubes 50ml		RT	

General Notes:

- Administer Injections at the same time, once weekly
- Record individual injections
 - Bent Needles
 - Volume administered in two partial doses
- Keep reconstituted ZA on ICE – bring ice bucket to mouse room
- Use Laura's Mouse Scale to weigh rat's once a week

Zoledronic acid (Zometa)

Lyophilized

10mg

Reconstitute the ZA to a concentration of 2 mg/ml

$$10\text{mg}/5\text{ml} = 2\text{mg}/\text{ml}$$

1. Remove ZA from Sara's Drawer
2. Centrifuge vial to collect the lyophilized powder to the bottom of the tube
3. *In Biosafety cabinet* for remaining steps
4. Add 5ml's of Sterile saline to 10mg of ZA
5. Transfer 50 μ l of the reconstituted ZA into 100 Sterile 0.6 ml epps
6. Immediately freeze aliquots of ZA at -20°C

Animal Dose

Dose: 12.5 μ g/kg

*Keep everything on ICE?

1. Remove aliquoted ZA(2mg/ml) from -20°C
 - g. Allow to thaw on ice
 - h. Centrifuge before opening
2. Dilute ZA to a concentration of 0.01 μ g/ μ l
3. Add 50 μ l of 0.9% saline to the 2mg/ml 50 μ l ZA aliquot (from the -80°C) = **1mg/ml**
 - a. Mix/vortex
4. Add 50 μ l of 1mg/ml ZA to 450 μ l 0.9% saline = **0.1mg/ml**
 - a. Mix/vortex
5. Add 400 μ l of 0.1mg/ml ZA to 3.6ml 0.9% saline = **0.01mg/ml** = 0.01 μ g/ μ l
 - a. Mix/vortex
6. Rat Dose

$$\frac{12.5\mu\text{g}}{\text{kg}} \times \frac{(\text{Rat})\text{kg}}{1} \times \frac{\mu\text{l}}{0.01\mu\text{g}} = \mu\text{l Injection Amount}$$

7. Weigh the Rat's once a week and recalculate the injection amount (μ l) for each rat
8. Examples

ID	Weight (kg)	Injection Amount(μ l)
95	0.125	156
63	0.140	175

9. Fill Insulin Syringes with calculated amount of ZA
 10. Inject ZA Subcutaneously
- 2mg/ml \rightarrow 2X diluted = 1mg/ml
1mg/ml \rightarrow 10X diluted = 0.1mg/ml
0.1mg/ml \rightarrow 10X diluted = 0.01mg/ml

9-19: SOP – Osteosarcoma Cell Injections into Distal Femoral Metaphysis of Nude Rats

Protocol used by: Ryan Curtis

Cell Culture work done following SOP – Abrams OSA 5-11 by Sara Gookin

Materials

22g 1.5 inch needles

1ml luer lock syringes

Surgical scrub - 70% ethanol and Chlorhexadine solution

Cultured Abram's OSA Luc + cells (0.2 ml of MEM with cells at a conc. of 1×10^6 cells per 50 ul) per rat

Isoflurane

Sterile Surgical Gloves

Nude Rats

Heating Pad

Rodent Anesthesia unit

Procedure

1. Prepare procedure area as needed to include heating pad, surgical drapes, towels etc.
2. Prep enough cells as needed using SOP – Abrams OSA 5-11 by Sara Gookin. Per individual rat you will use 0.2 ml of MEM with a concentration of 1×10^6 cells per 50ul drawn up in a 1 ml syringe.
3. Anesthetize rat using 5% Isoflurane in an induction chamber.
4. Place rat on surgical table in right lateral recumbency (right leg down) while maintaining general anesthesia with 2-3% Isoflurane.
5. Give Buprenorphine SR-Lab (0.8 to 1 mg/kg) SQ once ~15 minutes prior to procedure for nearly 72 hours of pain control. Apply sterile lubricant to eyes prior to procedure.
6. Clip area over left femur followed by surgical prep (three times interchanging from chlorhexadine then 70% ethanol).
7. Insert a 22g 1.5 inch needle into the left femur at the level of the trochanteric fossa and advance distally through the medullary cavity until the desired injection site (distal femoral metaphysis).
8. Once placed, 0.2 ml of MEM at 1×10^6 OSA cells per 50ul can be drawn up into a 1 ml luer lock syringe. The cells in MEM should be imaged to test for luciferase expression prior to injection. Then place a new 22g 1.5 inch needle on that syringe before letting stand upright (needle down) for three minutes. This allows for clumping of cells and improved tumor cell uptake.
9. Following 3 minutes, remove the first placed needle from the femur as this needle cannot be used as it is typically clogged by a bone core.
10. Now insert the 2nd needle (attached to filled syringe with cells) through the already drilled hole in the proximal femur to advance distally to desired injection site (distal femoral metaphysis).
11. Once placed, inject 0.1 ml of cells into site slowly to prevent embolism.
12. Remove the needle and syringe slowly, then discard into sharps container.
13. Repeat procedure for each rat needing Abrams OSA Luc + inoculation.



Fig. 1 – Proper placement of a 22g 1.5 inch needle prior to OSA cell inoculation into the distal femoral metaphysis.

Notes:

22g x 1.5 needle + syringe – the empty needle holds 50 μ l, so when you attach the new needle and place it (2nd needle placed) you have to inject 100 μ l to account for the void space.

3-27. Bioquant Fluorescent Labeled Bones (Cortical and Trabecular)

Protocol used by: Alison Doherty and Danielle Roteliuk

Time to complete/image: 5-15min

Supplies required:

BioQuant

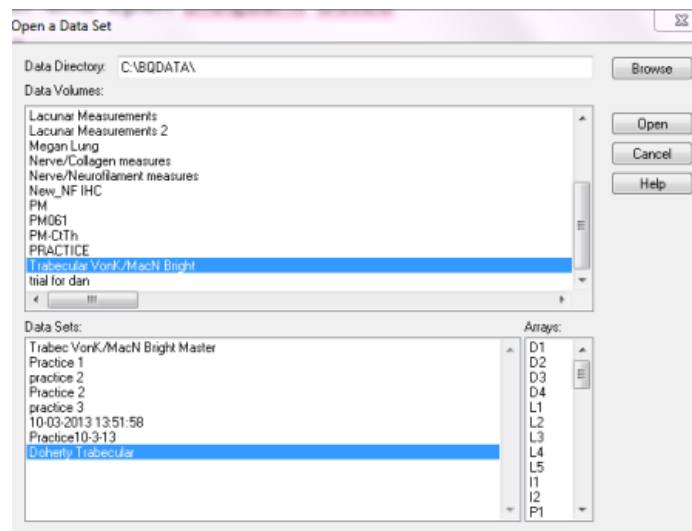
10x objective images of fluorescent-labeled bone slides

General Notes:

- Analysis of single label, double label, interlabel width

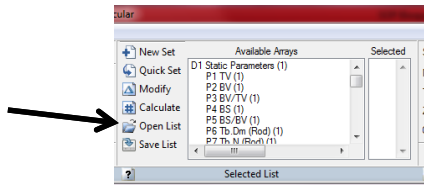
Procedure:

1. Start computer and open Bioquant Osteo
2. Open Data set
 - a. File folder
 - b. “Open Data Set”
 - i. Data Directory: C:\BQDATA\
 - ii. Data Volume: Doherty
 - iii. Data Set: Doherty ** This will change with each sample: Create Quick Set!

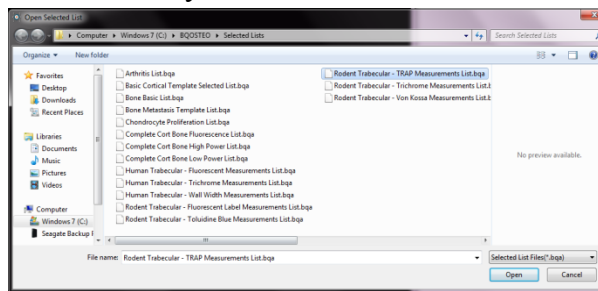


- c. Click “Open”

3. In “Selected List” window, click “Open List”

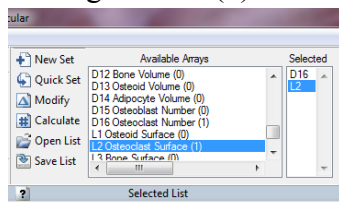


- a. Select correct list under:
 - i. Computer
 - ii. Windows 7 (C:)
 - iii. BQOSTEO
 - iv. Selected Lists
 - v. Doherty Cortical Fluorescent...



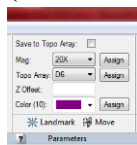
4. In “Selected List” window, under “Available Arrays,” double click the following to move them over to the “Selected” column*

- a. L5 Double Label (0)
- b. I2 Interlabel width (0)
- c. L6 Single Label (0)

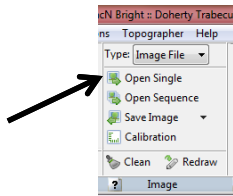


*To remove an array from column, double click the array under “selected” column

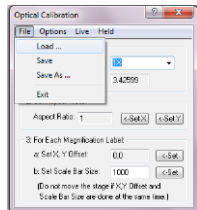
5. In “Parameters” window, check that 10x is selected for magnification, and that D4 is selected for Topo Array for each of the selected arrays. The assign button will lock that (theoretically) in place.



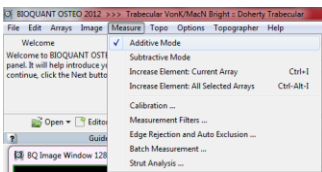
6. Open your image:
 - a. In the “Image” window, click “Open Single”



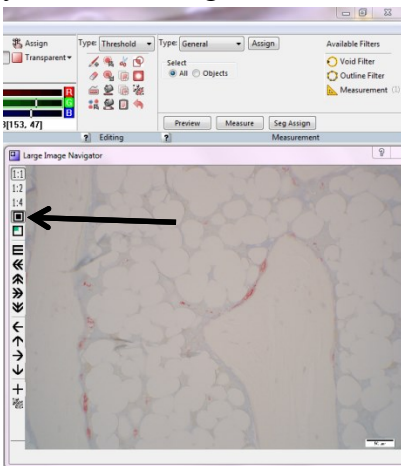
- b. Find your image of choice and open
7. In “Image” window, click the “Calibration” button
 - a. In the “Optical Calibration” window, under “File,” click “Load”



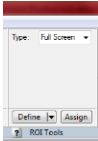
- b. Select:
 - i. Computer
 - ii. Windows 7 (C:)
 - iii. BQOSTEO\Calibration Backup
 - iv. 9-9-13_NikonScope.cal
- c. Click “Open,” then close the “Optical Calibration” window
8. Double check, in the “Parameters” window, that 10x is selected for magnification, and that D4 is selected for Topo Array
9. Ensure that “Additive Mode” is checked under “Measure”



10. In the “Large Image Navigator” window, click the Shrink/Expand Image button so that your whole image is visible in the image box (not zoomed in)



11. In the “ROI Tools” window, select “Full Screen” under “Type,” then click “Define”



12. For measuring double labels: In the “Selected List” window, click to highlight “L5” under “Selected”

13. In the “Measurement” window, make sure that:

- a. dLs is selected
- b. I2 is the width variable
- c. L5 is the surface variable
- d. The box is checked for “spacebar to end”

14. Click the “Draw 1” button

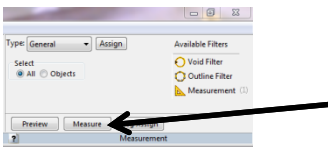
- a. This will take the cursor into the image box
- b. Use the “Z” key to zoom in and out
- c. Left click at the start of the outer label (so on endocortical surfaces this will be the closest label to the medullary cavity, on the periosteal surface this will be the label closest to the soft tissues) and continue clicking along the length of the outer double label.
- d. Spacebar to stop when you reach the end of the label

15. Click the “Draw 2” button

- a. Repeat the steps in 14 only on the inner label
- b. Make sure that the outer label is longer than the inner label, otherwise you will get aberrant width measurements!
- c. Spacebar to leave the box

16. The two lines should now be connected by various interlabel measurements (interlabel width)

17. In the “Measurement” window, click “Measure”: a number should appear under L5 and I2 in the “Raw Data” window



18. For measuring Single labels: In the “Selected List” window, click to highlight “L6” under “Selected”

19. Make sure that the Topo array is set to full screen and defined

20. In the “Measurement” window, make sure that:

- a. Manual is selected
- b. The box is checked for “spacebar to end”

21. Click measure

- a. This will take the cursor into the image box
- b. Use the “Z” key to zoom in and out
- c. Left click at the start of the label and continue clicking to trace the label
- d. Right click to end tracing that label and start a new single label in the image
- e. Spacebar to exit the image window and to measure the single label lengths...this is additive!**

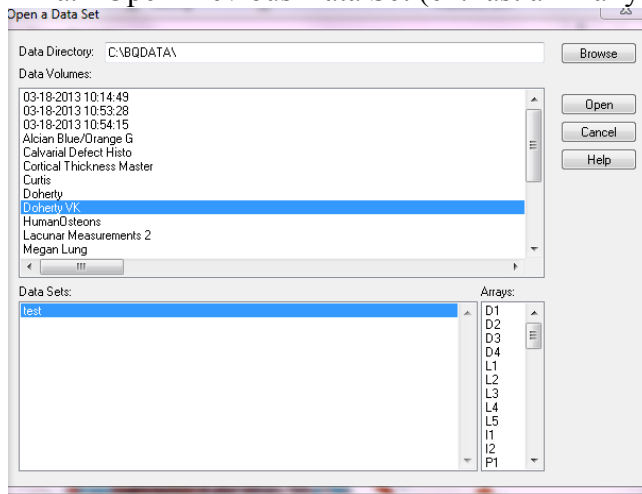
**Note: For each new image, hit Ctrl+Alt+i to add rows to the raw data table. Hit Ctrl+i to add just one new data cell. For each image, make sure that you record the single labels separately by clicking on the L6 data cell corresponding to the image you are measuring (i.e. image 3, make sure you are in the L6 column, row 3)

22. Save Data and move to excel file

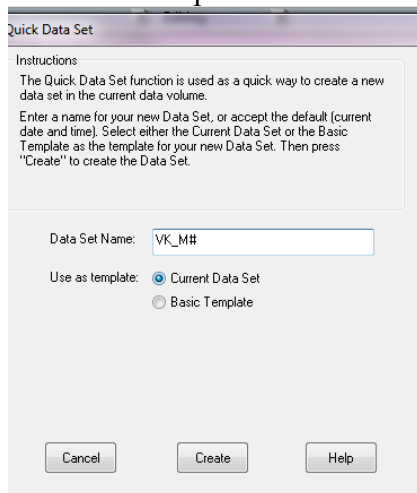
- a. File folder: Save Data
- b. File folder: Data Manager:
 - i. Desktop: My Computer: Windows 7 (C:): scroll to Doherty
 - ii. Click “export Raw Data”
 - iii. Drag each quick set to window, then click “to clipboard”
- c. Open Excel
 - i. On keyboard, hit “Ctrl” “V” to paste data table
 - ii. Check that pasted data matches your data
 - iii. Save the Excel file
- d. You can also copy data quickly by going to Edit: Copy Data: All or selected array
 - i. Open Excell and hit “Ctrl” “V” to paste data table

3-25. SOP – Marmot trabecular Von Kossa

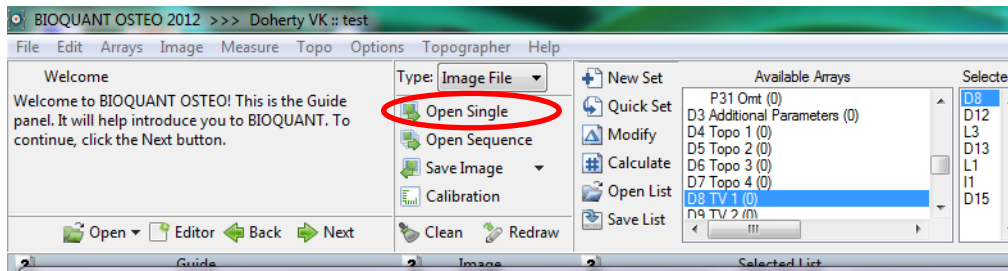
1. Open BIOQUANT OSTEOP 2012
2. **File -> Open Data Set**
3. Data Volumes: Doherty VK (or Curtis VK)
 - a. Open Previous Data Set (ex: last animal you collected data)



4. **File -> Quick Data Set**
5. Data Set Name: VK_M#
 - *Make a new one for each animal
 - a. VK : Von Kossa
 - b. M: Marmot
 - c. #: Sample ID

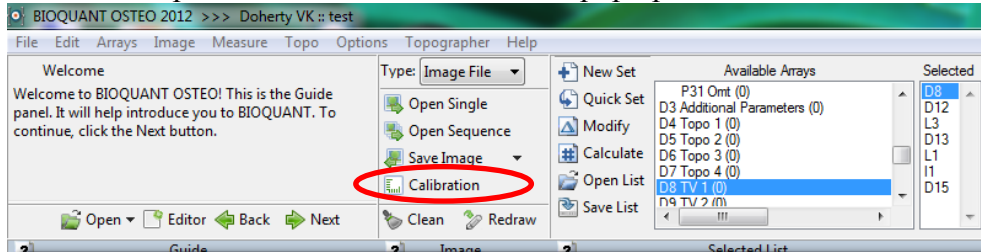


6. **Open Single Image**

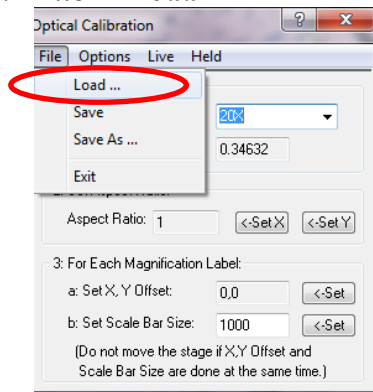


7. **Calibration**

a. An Optical Calibration Window will pop up



b. **File -> Load**



c. 3-3-14_Slide Scanner.cal

* This is for images taken on the slide scanner in pathology (DMC)

d. Exit out of the Optical Calibration Window

8. Open List (in the Selected List area)

a. An *Open Selected List* Window will pop up

b. Select **Doherty Trabecular VK.bqa**

c. Open

d. Selected Arrays will automatically be selected

D8: Tissue Volume (μm^2)

D12: Bone Volume (μm^2)

L3: Bone Surface (μ)

D13: Osteoid Volume (μm^2)

L1: Osteoid Surface (μ)

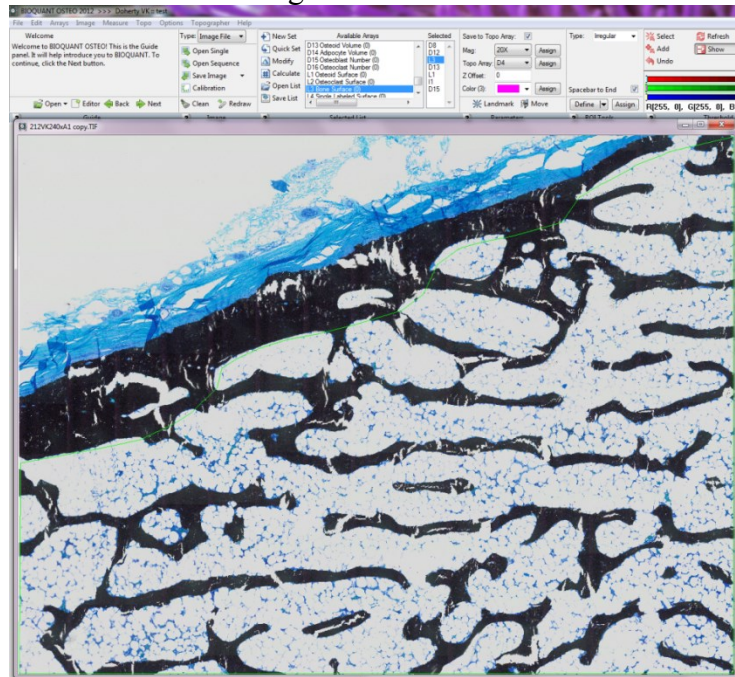
I1: Osteoid Thickness (μ)

D15: Osteoblast Number

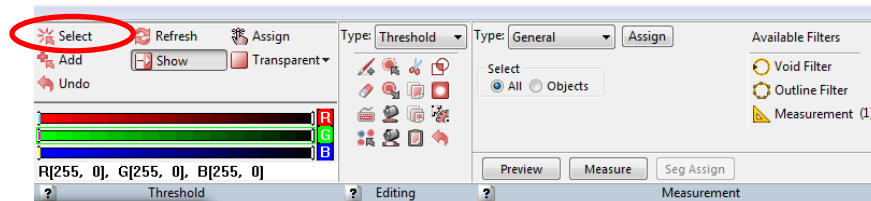
9. Select **L3**

a. This will give you data for D8, D12 and L3

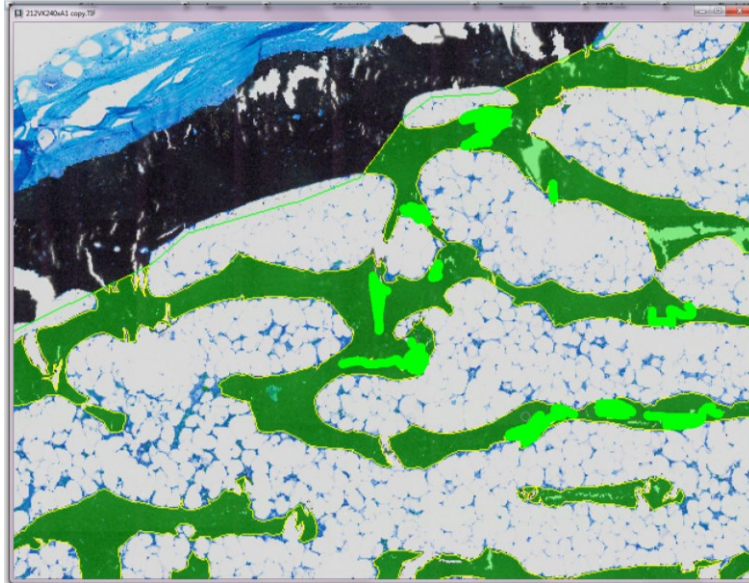
- b. Under **Parameter**
 - i. Make **sure Save to Topo Array** is checked in the Parameters area
 - ii. Select the Magnification the image was taken at
Mag: 40x
 - iii. Topo Array: D4
 - iv. Z Offset: NOTHING
- c. Under **ROI Tools**
 - i. Type: **Irregular**
 - ii. Check **Spacebar to End**
 - iii. Draw Region of Interest
***Exclude Cortices Edge**



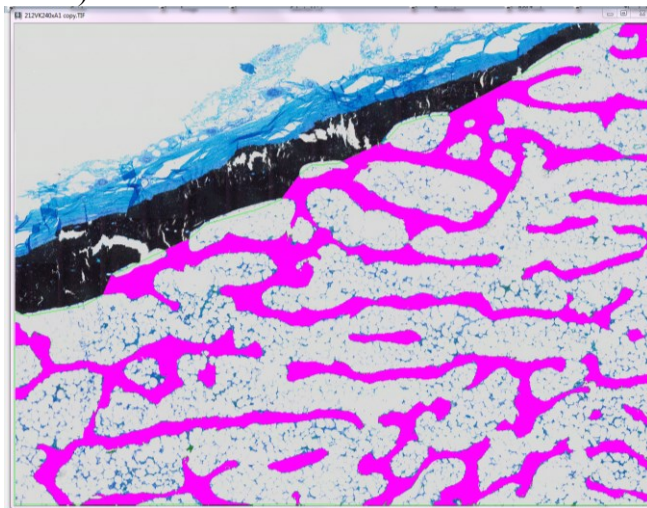
- d. Under **Threshold**
 - i. Select



- ii. Threshold the Bone = All of the BLACK
- iii. Fill in all of the holes in the bone with either the paint bucket (if lines connect so you don't fill in the entire white region) or with the paint brush



- iv. When you are satisfied that all the bone is selected -> **Preview** (to double check) -> **Measure**



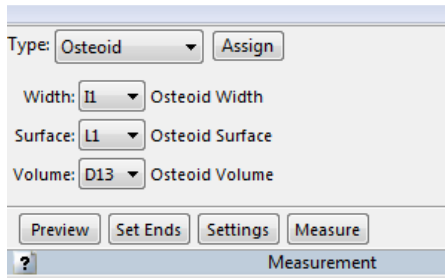
- v. Values for D8, D12 and L3 will be measured

Raw Data: All Selected Arrays						
	D8	D12	L3	D13	L1	I1
1	8865199.32	2256981.50	68862.07			

- vi.

10. Select **D13**

- Width: I1 (Osteoid Width)
- Surface: L1 (Osteoid Surface)
- Volume: D13 (Osteoid Volume)



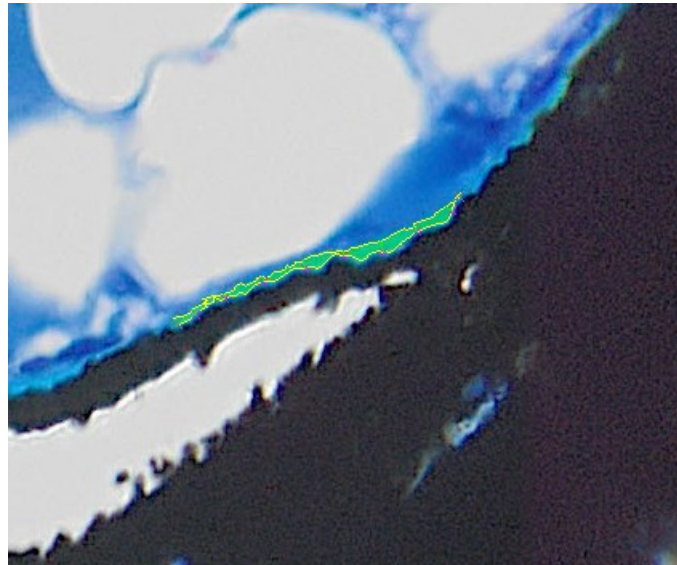
- a. In the Large Image Navigator Window -> Zoom 1:1 (so you can see the osteoid)
- b. Use the **Course Move** buttons to move the window



*You will have zero overlap with the course move buttons

*Use the **Fine Move** buttons to move it slightly to make an osteoid more in the middle

- c. Once you Find Osteoid
 - i. Threshold -> Select osteoid
 - *Use the paint brush to add more to the selection or the eraser to remove non-osteoid
 - ii. Happy with Selected Osteoid
 - iii. **Preview**
 - iv. Cursor will automatically enter Window
 - v. Highlight osteoid
 - vi. Cursor will automatically exit window
 - vii. **Set Ends** -> place an 'x' at each end of the osteoid
 - viii. **Measure**



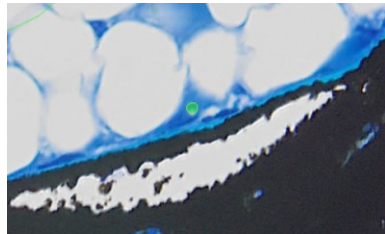
- ix. Values for D13, L1 and I1 will be measured

	D8	D12	L3	D13	L1	I1	D15
1	8865199.32	2256981.50	68862.07	30.89	38.88	0.95	
2				29.69	39.46	0.73	

- x. Under D13 -> Ctrl+I to make a new line
 - * For ONLY D13
 - *L1 and I1 automatically fill in the next line when you measure the next osteoid
 - *D13 is additive so it will continue to add to the same line unless you tell it not to (by adding a line with Ctrl+I)
- xi. **BEFORE** moving onto the next section on the image measure D15

11. Select D15

- a. DO AT THE SAME TIME YOU FIND OSTEOID... after you measure osteoid, measure D15 before moving on to the next section in the image
- b. **ALWAYS**
 - i. ROI Tools
 - ii. Type: Full Screen
 - iii. Define
- c. In **Editing**, Select Paint Brush
- d. Make the size of the paint brush half the size of the osteoblast
- e. Make a dot on the osteoblast



- f. Measure
 - *Measures the number of osteoblasts you selected
- g. Ctrl + I for D15 to make a new line
- h. Return to D13
 - i. Ctrl + I for D13 to create a new line
 - *this only creates a new line for D13, **NOT** L1 and I1 (they are not additive and will automatically create a new line)
 - ii. Continue scanning image until you find the next osteoid and repeat Steps #10 and #11
 - *Once you select D13 (full screen) and find the next osteoid, Click **Preview** and the same threshold that was used for the previous osteoid should automatically appear, You can use this or you can start from scratch and select a NEW threshold

12. Moving on to the next image in the same sample

*Marmots have around 4 images per animal

- a. Ctrl+I for D8, D12 and L3 and D13 and D15

	D8	D12	L3	D13	L1	I1	D15
1	3391427....	1050389....	22870.77	68.12	64.96	1.58	1.00
2	0.00	0.00	0.00	127.59	153.23	0.79	6.00
3	0.00	0.00	0.00	136.91	106.86	1.27	6.00
4	0.00	0.00	0.00	297.64	131.34	2.94	4.00
5	0.00	0.00	0.00	55.29	35.53	2.24	1.00
6	0.00	0.00	0.00	105.35	94.65	1.25	3.00
7	0.00	0.00	0.00	5.29	14.88	0.44	1.00
8	0.00	0.00	0.00	68.93	80.65	1.19	3.00
9	0.00	0.00	0.00	88.38	74.47	1.33	4.00
10	0.00	0.00	0.00	225.94	124.01	2.38	5.00
11	0.00	0.00	0.00	164.70	119.35	1.80	2.00
12	0.00	0.00	0.00	214.28	93.13	3.45	2.00
13	0.00	0.00	0.00	144.45	132.45	1.28	7.00
14	0.00	0.00	0.00	93.15	61.03	1.92	4.00
15	0.00	0.00	0.00	30.65	26.30	1.86	1.00
16	0.00	0.00	0.00	20.73	33.16	0.68	2.00
17	0.00	0.00	0.00	76.45	81.70	1.13	3.00
18	0.00	0.00	0.00	51.96	34.85	2.26	1.00
19	0.00	0.00	0.00	116.53	112.13	1.26	8.00
20	0.00	0.00	0.00	235.23	121.67	2.30	4.00
21	0.00	0.00	0.00	140.72	118.92	1.44	5.00
22	0.00	0.00	0.00	128.04	95.26	1.34	2.00
23	0.00	0.00	0.00	69.77	70.59	1.03	3.00
24	0.00	0.00	0.00	44.83	62.50	0.59	4.00
25	0.00	0.00	0.00	0.00			0.00

- b. Open Single image

i. Verify overlap with last image so you aren't counting the same thing

- c. Repeat steps #9-12

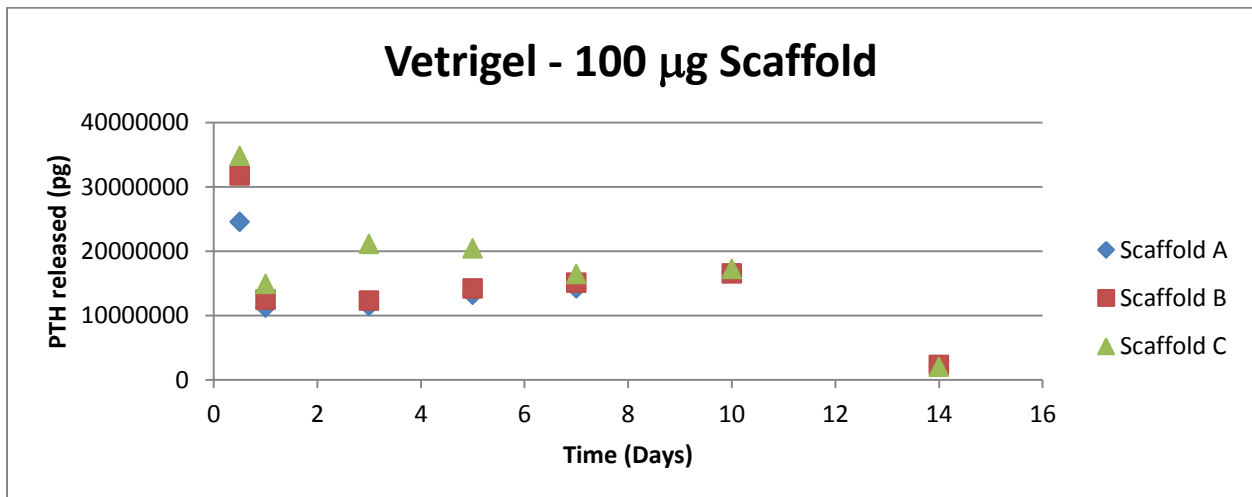
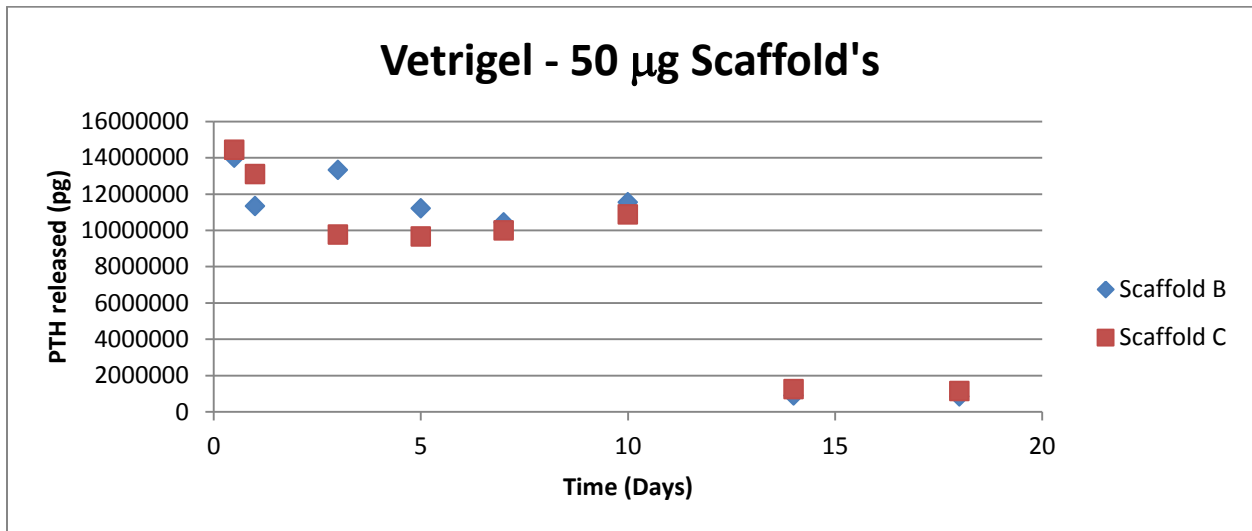
TIPS

- Ctrl + I in *Raw Data* box makes a second row (only selected array, ex. D8)
- Ctrl + Alt + I in *Raw Data* box makes entire new row in all arrays (D8, D12, L3, ect...)
- Right click to get out of the image box
- Keyboard functions when in the image box
 - Z – ZOOM (can only zoom twice before going back to original)
 - B – when on erase or fill -> B automatically switches to Draw
 - M – when in draw or erase -> M switches to fill
 - D – toggles between highlighted threshold and no threshold
 - Helps you see what is under the threshold
- Threshold -> Draw a circle and then fill and everything in the circle will be highlighted

Appendix II

bbPTH Release Profile in Vetrigel

bbPTH (Vehicle, 50 μ g, 100 μ g) was loaded into Vetrigel and 44ul blobs were placed in 6-well plates. After solidification, sterile PBS was placed into the well and incubated at 37°C containing 5% CO₂. The PBS was collected and replaced on Days 0.5, 1, 3, 7, 10, 14 and 18. A canine intact PTH ELISA (Immutopics International, San Clemente, CA), using bbPTH as standards, was used to determine the bbPTH levels released throughout the duration of the experiment. The data collected by the ELISA was used to calculate the amount of bbPTH needed to treat cells in the following experiment.



50µg Scaffold	Average(B&C)	stdev	Cumulative(B&C)	% Release	% stdev
0				0	0
0.5	14211111	314270	14211111	28	0.629
1	12211111	1257079	26422222	53	2.514
3	11544444	2514157	37966667	76	5.028
5	10433333	1099944	48400000	97	2.200
7	10211111	314270	58611111	117	0.629
10	11211111	471405	69822222	140	0.943
14	1065556	251416	70887778	142	0.503
18	993333	212132	71881111	144	0.424
sum	71881111				

100µg Scaffold	Average(A&B&C)	stdev	Cumulative(A&B)	% Release	% stdev
0				0	0.00
0.5	30359259	5254432	30359259	30	5.25
1	12840741	1866975	43200000	43	1.87
3	14951852	5342970	58151852	58	5.34
5	15951852	3913152	74103704	74	3.91
7	15248148	1118494	89351852	89	1.12
10	16840741	339450	106192593	106	0.34
14	2102593	170813	108295185	108	0.17
sum	108295185				

